SSC PC-034
103 PAGES

A Proposal for Research and Development to

Design and Build a New High Resolution Fiber Tower Electromagnetic and Hadronic Calorimeter for SSC Application

University of Florida

Paul Avery, Julie Harmon, James Walker, Andy White, and John Yelton

University of Sherbrooke

Christain Carrier and Roger Lecomte

RCA

Robert McIntyre

Oak Ridge National Laboratory

Gary Alley, Martin Bauer, Barbara Bishop, Hugh Brashear, Tony Gabriel and Mark Rennich

TABLE OF CONTENTS

APPENDICES

Appendix 1

I. 'An Electromagnetic Calorimeter with Wavelength Shifting Fiber Readout.' B. Loehr, S. Weissenrieder, F. Barreiro, and E. Ros, DESY 86-072, FTUAM-EP-86-04 (July 1986).

II. 'A Scintillator-Lead Photon Calorimeter Using Optical Fiber Readout Systems.' H. Fessler, P. Freund, J. Gebauer, K. M. Glas, K. P. Pretzl, P. Seyboth, J. Severlein, and J. C. Thevenin, MPI-PAE/Exp.El. 149 (February 1985).

A Proposal for Research and Development to

Design and Build a New High Resolution Fiber Tower Electromagnetic and Hadronic Calorimeter for SSC Application

ABSTRACT

The purpose of this proposal is to design and build a lead/scintillator calorimeter which is ideally suited to operation at the Superconducting Supercollider (SSC). It is based on two recent revolutionary developments in detector technology. The first of these is the development of new plastic scintillator which is one hundred times more resistant to degradation by radiation than previous scintillator. The second revolution concerns the development of new solid state photodetectors with a speed, sensivitity, noise level, dynamic range, stability and cost which makes them especially suited for calorimetry readout devices. In addition, they are immune to magnetic fields.

The design of the calorimeter is optimized to achieve minimal readout area consistent with adequate photoelectron production in the solid state devices. The result of this optimization is very good energy resolution, minimal dead space due to readout material, and minimal area, and therefore, cost of solid state readout devices.

Our objective is to produce the fastest, most hermetic, high resolution, compensation calorimeter in the most economical way possible.

From an engineering point of view, the purpose of this proposal is to design and build a lead/scintillator calorimeter based on the fiber tower calorimeter (FITCAL) concept which is large enough to contain hadronic showers and to test its operation in all respects. This subsystem program has three major design, test, and construction parts to meet these objectives: Part I) design and construct an electromagnetic calorimeter; Part II) design and construct a nine component hadronic calorimeter based on the learning curve of Part I, and Part III) design a FITCAL calorimeter for SSC application. During these major phases, testing and research and development will continue in several other areas needing additional attention.

We request full support for this extremely promising new approach to calorimetry at the SSC.

I. Introduction

A. Objectives

The objectives of the proposed program are to verify the calorimeter measurement capabilities and the engineering design concept for the fiber tower calorimeter (FITCAL). We will accomplish this in a phased development program which will culminate in the fabrication and beam testing of a full–scale prototype assembly. The proposed program begins with a series of small–scale light collection and component design studies. In the second phase of the program, individual longitudinal tower segments will be built and tested. Phase three will build on the earlier developments and a complete prototypical tower will be constructed. In the final phase of the proposed program, we will design and test a segment of a full–scale FITCAL SSC detector. This subsystem will be used in beam tests to verify the proposed calorimeter design and engineering studies.

B. Background

The use of precise calorimetric measurements of jet energies angles, and types is expected to be of great importance in all experiments at the Superconducting Supercollider (SSC). The signatures of new physics are anticipated to include identification and measurements of jets, electrons, photons, and missing energy. All of these measurements depend upon calorimetry. At high energies, calorimetric measurements of these quantities are superior to other known methods. For example, in calorimetry, the relative energy resolution improves as $1/\sqrt{E}$, in magnetic measurement, the resolution deteriorates like E. In addition, in calorimetry the depth for containment of energy increases only as lnE which results in relatively compact detectors even at the energy of the SSC. Finally, since measurements of jets will be crucial, the similar response of calorimeters to charged and neutral hadrons or electromagnetic particles is essential, and fortunately, straight forward to achieve.

The performance criteria for successful calorimetry have been studied and identified at numerous SSC workshops. They include:

1. Excellent hermiticity.
2. Adequate shower containment in depth.
3. Adequate lateral and longitudinal segmentation.
4. Fast time response.
5. Adequate compensation.
6. Radiation hardness.
7. Tower geometry.
8. Ease of calibration.

Quantitative specification of some of these criteria have been made at SSC workshops for calorimetry at a luminosity of 10^{33} cm^2sec^{-1}. The technique of calorimetry we propose meets all of the above requirements.

The efforts in this proposal are directed at designing, building and testing a prototype lead/scintillator calorimeter suitable for operation at the SSC. The calorimeter operation will be simulated with a Monte Carlo program which will aid in the design, and the

evaluation of the results. The lead to scintillator ratio will be varied calculationally and experimentally to achieve optimum compensation. The response of the calorimeter to hadrons and electrons over a wide range of energies will be investigated. Finally, the construction techniques for this type of calorimeter will be developed in a manner suitable for mass production and cost minimization.

There are two recent revolutionary developments which have made the proposed technique extremely attractive. First, the University of Florida group has developed new plastic and new dyes which together have much higher resistance to degradation by radiation than previous plastic scintillator. Light output and attenuation length is expected to be rather uniform up to 10^7 rads. Secondly, new solid state photodetectors, such as the Rockwell solid state photomultipliers (SSPM), and the new RCA avalanche photodiodes (APD), show great promise as scintillation light detectors suitable for calorimetry at the SSC. The calorimeter design which we propose here is particularly well suited to these solid state photodetectors as compared to other prototype designs submitted to the SSC because of the very small readout area of fibers in our design. This minimizes readout costs. In particular, our area of readout is at least a factor of 25 smaller than any other design.

At the same time, we have measured using conventional phototubes adequate light collection efficiency such that only a finite, but acceptable deterioration of energy resolution occurs. Therefore, the combination of high quantum efficiency, fast operation, low power consumption, and operation in a high magnetic field makes the use of these new solid state photodetectors with the new scintillator a technique which should be aggressively explored at this time. We believe that the FITCAL design which embodies these two evolutionary developments is optimized for minimum overall system cost.

II. Initial Considerations

A. Calorimetry with Lead and Scintillator

The energy resolution of hadrons measured by a calorimeter[1] has contributions from sampling fluctuations, which are reduced if the sampling frequency is increased, and contributions due to the large fluctuations between the different components of hadronic showers (i.e., electromagnetic, hadronic, low energy neutrons, nuclear binding energy, etc.). The energy resolution may be written:

$$\frac{\sigma}{E} = \frac{a}{\sqrt{E}} + b \ ,$$

where the two terms are related to the above two mechanisms, respectively. The constant term, b, can be written[2] as

$$b = b_o \left[\left(\frac{e}{h} \right)_{intr} - 1 \right] \ ,$$

where $\left(\frac{e}{h}\right)_{intr}$ is the average detector response to an electron compared to the purely hadronic components of a hadron shower. If $\left(\frac{e}{h}\right)_{intr} \neq 1$, fluctuations in the fraction of

energy going into the electromagnetic component in a hadron shower leads to several undesirable and related detector characteristics:

1. The hadronic energy resolution is impaired at all energies,
2. The second term, b, can be dominant at high energy and be larger even than the expected calibration error. Thus, if $\frac{e}{h} - 1 > 0.1$, then $b \geq 1.5\%$, and
3. The resolution will not scale as $E^{-1/2}$.

In an experiment, one does not measure $\left(\frac{e}{h}\right)_{intr}$, but rather the relation between the average calorimeter signals for an electron and a hadron of the same energy, $\frac{e}{h}$, the latter being due to a mixture between the electromagnetic and hadronic components of the shower. Since this mixture is energy dependent, $\frac{e}{h}$ varies with energy, whereas $\left(\frac{e}{h}\right)_{intr}$ is a constant depending on the calorimeter only. Figure II.1 shows the relationship between $\frac{e}{h}$ and $\left(\frac{e}{h}\right)_{intr}$ based on a Monte Carlo simulation[2] of hadronic showers in a calorimeter. It is apparent that a well designed calorimeter has $\left(\frac{e}{h}\right)_{intr} = 1$, and therefore, this leads to $\frac{e}{h} = 1$ at all energies (approximately). This is especially important due to the very large number of low energy (less than 10 GeV) pions in very high energy jets. Until recently, the ratio, $\frac{e}{h}$ close to one, has been achieved only in sampling calorimeters using depleted uranium as absorber and plastic scintillator as detector. Some time ago, Brau and Gabriel[1] suggested that, 'compensation, $\left(\frac{e}{h}\right) = 1$, could also possibly be achieved using lead and scintillator,' albeit with a different ratio of thickness. The optimum ratio of lead to scintillator thickness is expected to be between 3 and 5.

This expectation was verified[3] with a sampling calorimeter consisting of 10 mm thick lead plates and 2.5 mm thick scintillator sheets. In the energy range 3-75 GeV, the energy resolution was measured to be 23% $\sqrt{E}$ for electrons and 44% $\sqrt{E}$ for hadrons. For energies above 10 GeV, the ratio e/h was 1.05± 0.04. This result gives strong support to this proposal based on lead and scintillator. We will study the resolution with detailed Monte Carlo simulation and experimentally to determine how the energy resolution and e/h varies with 1) the lead to scintillator thickness ratio, 2) the absolute thickness of these materials, and 3) how to extend good compensation down to energies of order 1 GeV.

Thanks to the relatively large ratio (4:1) of lead to scintillator thickness, compared to 1:1 for Uranium and scintillator, the average nuclear interaction length for the two types of compensating calorimeters are essentially the same. Thus, the proposed calorimeter is as compact as possible.

B. Compensation as a Function of Time

The important ratio, e/h, is also affected by the signal integration time. It is likely that this ratio approaches its asymptotic value faster in the case of lead than the uranium absorber. This should be the case, since the fission occurring in Uranium increases the fraction of energy carried by slow neutrons. Detailed simulation of this effect has not been carried out. We propose to measure the ratio, e/h, as a function of signal integration time and compare the results with simulated data.

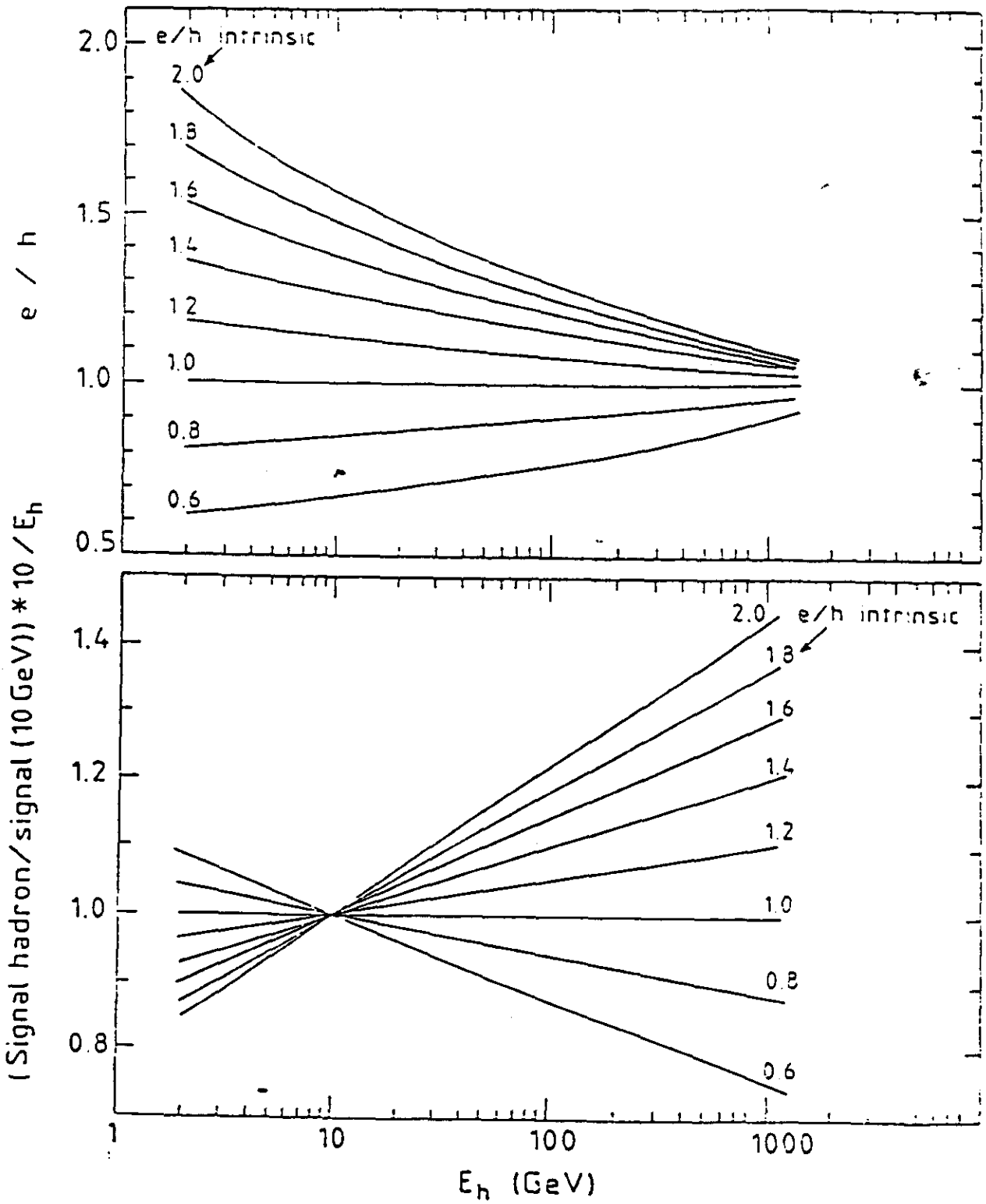

Relationship Between *e/h* intrinsic and *e/h* as a Function of Hadronic Energy
FIGURE II.1

C. Radiation Level with Lead Absorber

The flux of slow neutrons produced by hadron interactions in a lead sampling calorimeter is expected to be several times lower than in the case of Uranium. Since these neutrons are the major source of radiation damage in the plastic scintillator and photosensitive devices used in the hadronic part of the calorimeter, it is advantageous to use lead as the absorber.

D. Cost Comparison of Lead and Uranium

A recent preliminary cost comparison[4] has been made for the use of lead and uranium in an SSC calorimeter. Based on the experience of constructing the uranium calorimeter for ZEUS, the uranium cost is broken down as follows:

Depleted Uranium Billet	=	\$ 1.58/lb
Roll/Shear/Punch	=	\$ 7.71/lb
Clad with Stainless Steel	=	\$ 2.62/lb
Total Cost:	=	\$11.91/lb

On the other hand, lead plate cost is estimated as follows:

Lead Plate Cost	=	\$ 0.80/lb
Numerically controlled cutting/hole production and button addition	=	\$ 2.00/lb
Total Cost:	=	\$ 2.80/lb

Cladding of the lead with aluminum which has been considered, can slightly increase the above cost number.

A generic SSC calorimeter[5], including barrel plus endcaps, may weigh about 5,000 tons. Hence, the absorber costs are expected to be:

Uranium Calorimeter	=	\$120M
Lead Calorimeter	=	\$ 30M

In conclusion, there is an overwhelming cost advantage to the use of lead and this choice also reduces radiation levels to photosensitive readout devices.

E. The Choice of Scintillator

We have chosen plastic scintillator as a readout medium for several important reasons. These are:

1. **Compensation:** It has been experimentally demonstrated at least once that the combination of lead and scintillator can give full compensation.
2. **Energy Resolution:** The experimental hadronic energy resolution[3] of 44% / $\sqrt{E}$ with 10 mm lead plates promises 30% / $\sqrt{E}$ with the 4 mm lead

plates which are envisaged in this proposal. The corresponding electromagnetic energy resolution based on data with 4 mm lead thickness is expected to be $15\% / \sqrt{E}$.

3. Fast Time Response: We expect to readout the energy of the event in 10-20 nsec. This has to be compared to a typical figure of 200-400 nsec integration time for liquid argon. This short readout time for scintillator permits separation of events from different beam crossings which occur every 16 nsec. In the case of electromagnetic showers all the energy is collected within 10 nsec. Slow neutrons produced in hadronic cascades create a tail in the time response, however, we expect 85% of the total hadronic energy to be detected within 20 nsec. Integration beyond that time will be performed for full compensation and energy resolution checks.

4. Hermiticity: A greater degree of hermiticity can be achieved with the use of scintillator than liquid argon. Our mechanical design contains less than 2% dead spaced plus cracks. Monte Carlo studies[6] have indicated that at this level of hermiticity missing transverse energy is probably dominated by neutrino production by heavy quarks[6].

5. Radiation Hardness: There have been recent developments[7] in the use of siloxane as the base for plastic scintillators and in associated dyes. This new type of plastic scintillator shows no degradation (at the 5% level) up to 10^7 rads exposure. Much further work remains to be done to implement this technology on the scale required for the SSC. A company is in the process of licensing this technology and has received initial financing to develop the technology. (Calorimetry based on this scintillator should be stable for ten years of SSC operation down to about 10^o polar angle. At smaller angles, the scintillator can be changed on an appropriate schedule.

6. Calibration: There will be a very large number of produced Z_o's which will provide the most powerful on-line calibration for the electromagnetic caorimetry. A similar tool for calibrating the hadronic calorimetry does not exist. It is essential to have a means of calibrating the 10,000 or so channels in the calorimeter to about $\pm 1\%$ in a routine manner. Both CDF and UA2 have obtained an absolute energy calibration of better than 1 1/2% using embedded radioactive sources. A similar technique will be developed in this case.

For all of the above reasons, we are proposing the detailed study of a lead/scintillator prototype calorimeter suitable for operation at the SSC.

F. Description of Conceptual Design of a Fiber Tower Calorimeter (FITCAL)

1. General Tower Concept and Advantages Over Other Approaches

The basic idea of FITCAL is to use scintillator plates interspersed with lead plates and readout the emitted light with wavelength shifting fibers oriented parallel to the incident particles. A schematic drawing of a FITCAL 'tower' is shown in Figure II.2. The above design concept may be compared to two others, known as Spaghetti Calorimetry (SPACAL) and ZEUS Calorimetry (ZEUSCAL), respectively. SPACAL employs a very large number of scintillating fibers (25/ cm^2) running parallel to the incident particles. ZEUSCAL uses scintillating plates interspersed with metal absorber plates and light is readout using wavelength shifting plates running parallel to the incident particles. The principal advantages of FITCAL are:

a. Channeling is reduced by a factor of 100 compared to SPACAL. Tails of resolution functions are thereby greatly reduced.

b. Projective geometry is easily achieved compared to SPACAL and yet FITCAL still preserves the ability to calibrate all fibers and maintain the optimum absorber to scintillator thickness throughout the calorimeter.

c. Longitudinal segmentation is able to be implemented for the purpose of powerful e/π separation. This feature is difficult to achieve with SPACAL due to the very large number of fibers.

d. Lateral segmentation in the electromagnetic section of the calorimeter to about 2 cm (typical of the diameter of an electromagnetic shower) can easily be achieved in FITCAL. This feature is important for identifying and measuring single electrons or photons within a jet and providing powerful e/π separation. ZEUSCAL has difficulty in achieving this high level of lateral segmentation without excessive spatial nonuniformities. In an attempt to address this deficiency with ZEUSCAL, it is possible to use a separate, high transverse spatial resolution detector. For example, one may use silicon at the peak of the electromagnetic shower. There are two disadvantages to this remedial action. First, it means the incorporation of an additional detector technology with all the attendant complications and additional cost (a preliminary estimate[5] has been made at \$15M). Secondly, this approach does not give an accurate measurement of the energy profile associated with the excellent transverse segmentation which is provided by FITCAl. This feature is important for optimal e/π separation and electron identification in the midst of a jet.

e. Cost minimization of the system. An important advantage of the FITCAL design is in minimization of the readout area consistent with adequate light output to reduce the area of solid state readout devices, and hence, the system cost.

FITCAL – DETAILED STRUCTURE

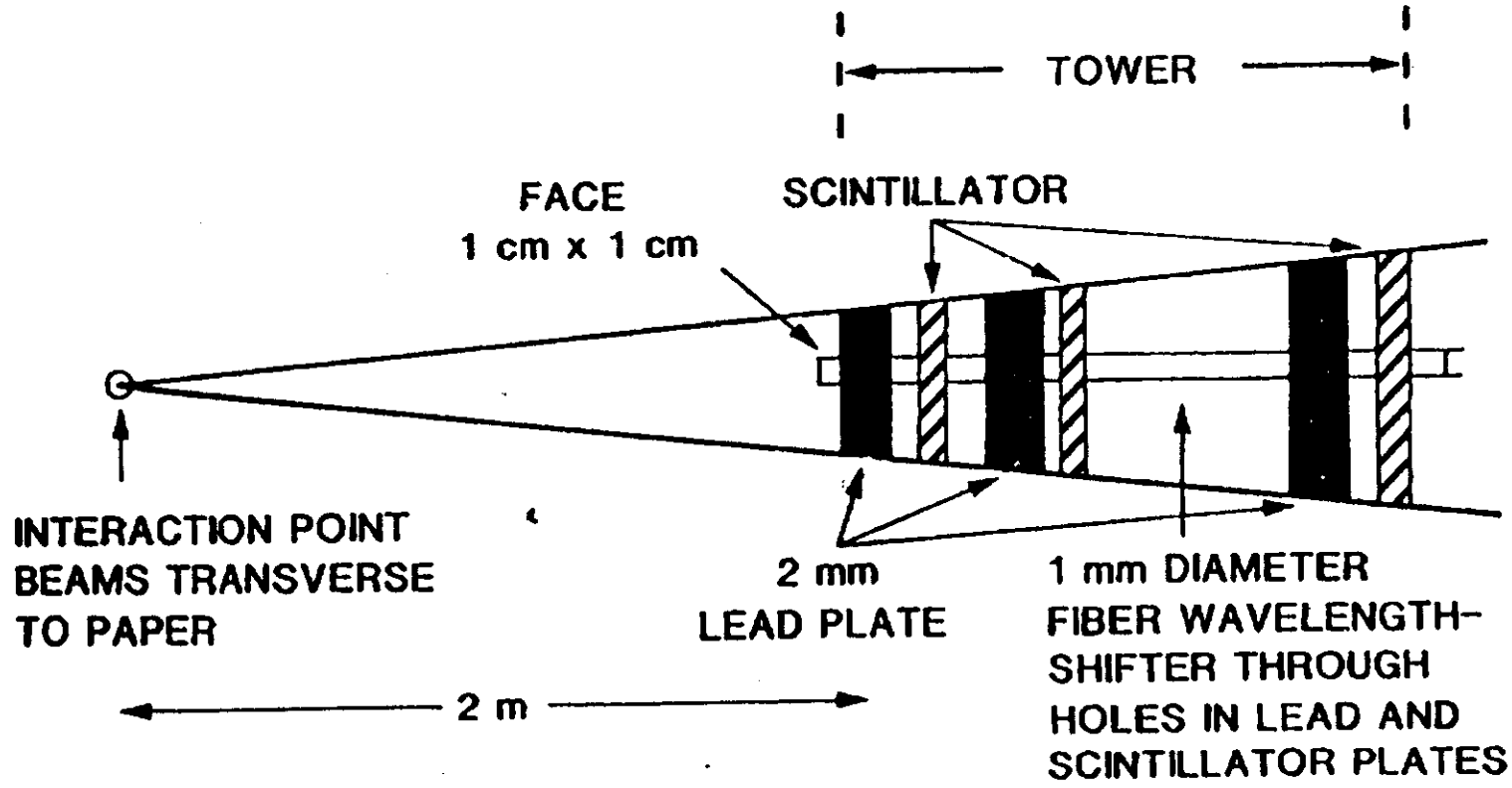

Schematic Drawing of a FITCAL 'Tower'
FIGURE II.2

For these reasons, we believe that the general concept of FITCAL offers substantial advantages over alternative implementations of metal/scintillator calorimetry at the SSC.

2. Prototype Dimensional Considerations

In this prototype proposal, we propose exploring the limits of the hadronic energy resolution function $\frac{\sigma}{E} = 30\%/\sqrt{E}$ implying about + 1% resolution at 1 TeV, and develop a calibration reliability of about + 1%. To minimize uncertainties associated with lack of energy containment, we require a calorimeter with 12 nuclear absorption lengths to contain 98% of the 1 TeV hadron energy[8]. Therefore, the proposed prototype calorimeter will be 12λ in thickness. In this way, a rigorous test of the simulation program and, the basic performance of the calorimeter, will be achieved. It is quite likely, however, that the calorimeter designed for the SSC may be somewhat shorter. This is because a 1 TeV jet's highest momentum particle has a most probable momentum of about 200 GeV, and the number distribution is down an order of magnitude at 600 GeV. Thus, for the same level of energy containment, a jet requires somewhat less thickness of calorimeter than a single hadron of the same energy.

A final choice of calorimeter thickness for an SSC detector will depend on many factors in the overall optimization procedure. However, the philosophy for prototype development which we have described above should give the most reliable procedure for final detector design consideration.

a. Transverse Containment

Similar considerations apply to transverse energy containment and again we propose to achieve the 98% level. Detailed calculations will be performed to reliably determine the transverse calorimeter dimensions, however, we expect them to be approximately 48 x 48 cm^2.

b. Longitudinal Segmentation

A detailed Monte Carlo simulation will be performed to investigate the dependence of the calorimeter physics capabilities on the number of longitudinal segments into which it is divided. Previous studies have shown that two segments in the hadronic part is adequate and at least two is required in the electromagnetic section. Pion/electron separation will be fully simulated and studied as a function of longitudinal segmentation. The preliminary design includes a total of four segmentations through the length of the calorimeter.

c. Transverse Segmentation

Fine transverse segmentation is mandatory for the high multiplicities at the superconducting supercollider. The 1986 Snow Mass Calorimeter Group conducted a study of the physics capabilities as a function of transverse segmentation in the range Δy x $\Delta\phi$ from 0.01 x 0.01 to 0.05 x 0.05. Surprisingly, no threshold effects were found, although finer segmentation

was clearly better. It is also true that with a segmentation of 0.01 x 0.01, which corresponds to 2 x 2 cm^2 at a calorimeter distance of 2m from the interaction point, the transverse size of an electromagnetic shower will be comparable to the segmentation.

It would seem, therefore, that identification of electrons in jets is optimally achieved with a segmentation of about 2 cm x 2 cm at the front face of the calorimeter. Detailed physics simulation will be performed to further justify this choice. With this segmentation, there will be enough energy sharing with adjacent towers to provide position resolution of the order of 1/10 of the tower size, or about $\pm$ 2 mm. This segmentation will occur in the first electromagnetic section and increase to 4 x 4 cm^2 in the second electromagnetic section. The hadronic transverse segmentation is chosen preliminarily as 8 x 8 cm^2 in each of the two longitudinal sections. In this way, the transverse shape of a high energy jet, which will cover typically 6 x 6 towers, will be well measured to allow a study of jet shapes and effective masses. Again, detailed physics simulations will be performed to explore the calorimeter capabilities versus transverse segmentation before a final choice of dimensions is chosen.

G. Fiber Tower Calorimetry in Presently Conceived SSC Detectors

Present discussions on potential SSC detectors have focused on the following conceptual designs.

1. Air core toroid for muon detection and no magnetic field in the region of the calorimeter. The FITCAL calorimeter will fit naturally into such a detector.

2. 'Small' solenoid inside a calorimeter. The return flux can be carried by iron outside the calorimeter. Again, FITCAL will work in a straight forward way with this approach.

3. 'Large' solenoid with high field (> 20kG) which is only just larger than the calorimeter. In this case, FITCAL must be designed with photosensitive devices which can operate at these high fields. This clearly represents a challenge, which may not be achievable with existing photomultiplier devices, but certainly will with solid state devices.

4. 'Jumbo' solenoid with low field, ($\approx$ 7.5kG) which has a radius much larger than the calorimeter. In this case, FITCAL can certainly be readout successfully with existing fast multi-anode photomultipliers and solid state devices.

5. Special purpose beauty detector which may only require an electromagnetic FITCAL. This would be a possible application of the FITCAL technology.

6. A particularly attractive possibility is the use of a single technology for particle tracking and calorimetry. This could be achieved with a scintillating fiber

tracker with solid state device readout and a FITCAL design also using solid state readout. The FITCAL approach is probably the most suited of the different scintillating calorimeters to this type of readout, since the readout is by a relatively small number of fibers. In the case of spaghetti calorimetry, there are a large number of fibers, and in a ZEUS type design, there is a large area of wavelength shifter plates. Because of their large area of readout, they are less appropriate for solid state technology. The single technology of radiation hardened scintillator, plus solid state readout with total immunity to magnetic fields opens the door wide to placing a solenoidal coil outside the calorimeter. This removes the presence of several radiation lengths of material (solenoid coil) for electrons at intermediate angles with the small coil approach. A single technology approach should offer major savings in manpower and dollars by focusing activity in a unified way. This possibility will be carefully explored early in the development.

In summary, there is a broad range of applicability of the research and development into FITCAL which we are proposing. It appears that the technology can be successfully applied to the majority of presently conceived full scale SSC detectors.

H. Results and Design Considerations from the Existing FITCAL Program

1. Radiation Hard Scintillator Development

One year ago, approval was given to proceed to design and build an 8 x 8 cm^2 x 30 cm long prototype electromagnetic calorimeter based on the FITCAL design. The research and development associated with that effort forms the technical basis for several key elements of this proposal.

A major effort has been expended at the University of Florida over the last two years to develop a plastic scintillator which provides a stable light output up to radiation exposure of several 10^7 rads. This effort has been successful and corresponds to a factor of one hundred improvement over commercial plastic scintillators. Figure II.3 shows the measured stability of light output versus radiation exposure. The absolute light yield is comparable to commercial scintillator. This technology is in the course of being licensed by the University of Florida to Nanoptics, Inc. for full scale commercialization. Other companies are also developing radiation hard scintillators and competitive bidding procedures will be followed to obtain the most desirable scintillator.

In the case of FITCAL, the scintillator plates are being designed to emit light at about 450 nm. This wavelength is long enough to assure excellent radiation resistance of the polysiloxane matrix. The wavelength shifting fiber will absorb light at 450nm and emit at 525 nm. The latter wavelength will permit a long light attenuation length with extreme resistance to radiation degradation of light transmission in the polysiloxane fiber core. Appendix 2 describes the proposed sub-contract to produce the siloxane plate and fiber required for this proposal. We anticipate initial construction of the proposed FITCAL prototype with commercially available plastic scintillator. Later, polysiloxane scintillator

RELATIVE LIGHT OUTPUT

Irradiation in Argon

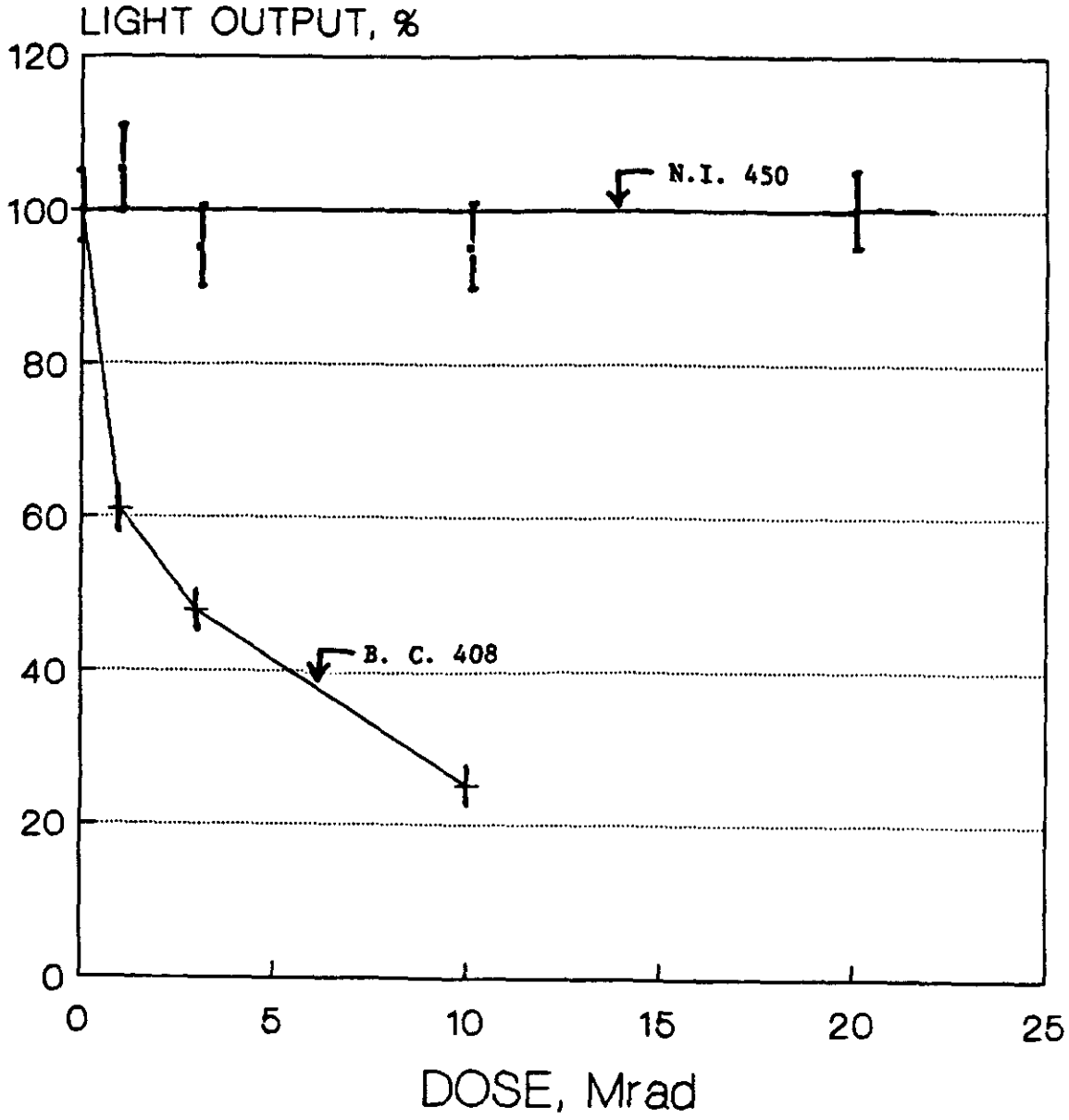

N.I. 450 - Nanoptics, Inc. scintillator emitting at 450 n.m. ; 1.5 cm^3

B.C. 408 - Bicron Corp. scintillator emitting at 408 n.m. ; 1.5 cm^3

Fig. II.3

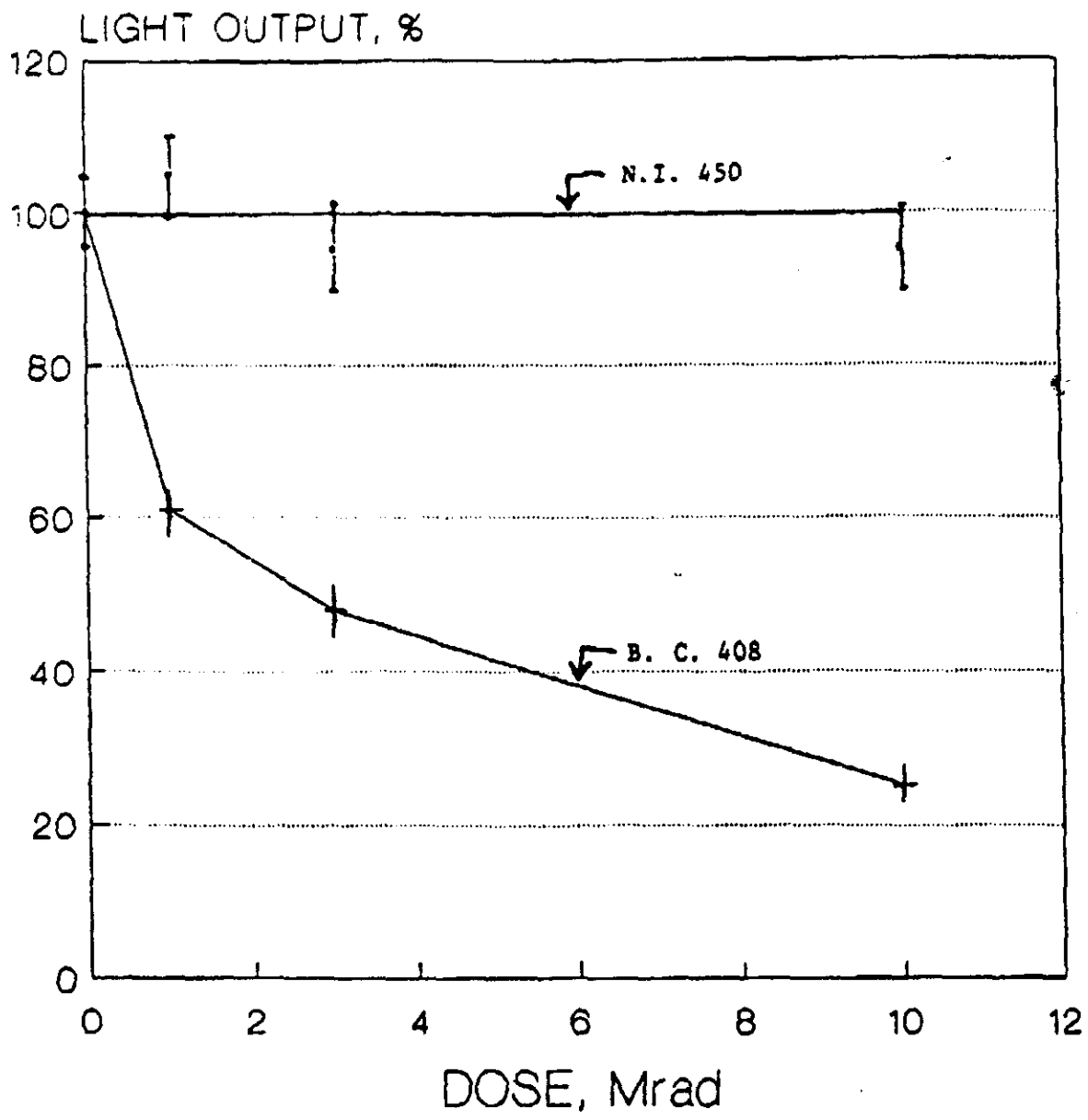

N.I. 450 - Nanoptics, Inc. scintillator emitting at 450 n.m.

B.C. 408 - Bicron Corp. scintillator emitting at 408 n.m.

Light Output Yield for Various Scintillating Materials as a Function of Dose
FIGURE II.3

plate and fiber will be used when it becomes available from Nanoptics, Inc. on a time scale specified in Appendix 2.

2. Measurement of Absolute Light Yield

a. Philosophy

The design philosophy of FITCAL is to achieve an adequate light yield, so as to not substantially impair the energy resolution, and at the same time, minimize the area of readout of wave length shifting material. This minimizes the cost of the solid state readout system. It should be emphasized that our primary thrust in FITCAL development is solid state readout since this permits operation of the calorimeter in an arbitrary high magnetic field. A second advantage of minimized readout area is reduced device capacity, higher bandwidth of the device, and lower dark current noise. A third advantage is minimizing cracks and dead space from shifter material, therefore, there is a high priority in minimizing readout area for system optimization. Other SSC calorimeter system proposals do not seem to have recognized the great importance of this parameter in system design. The specific design criterion which we have adopted at this stage is:

'The contribution to electromagnetic energy resolution through sampling fluctuations should not be exceeded by the contribution from photoelectron statistics. A similar criterion can be applied to the hadronic section of the calorimeter.'

We will show from our measurements and from comparison with measurements performed on similar calorimeter designs in the past, that the design we propose meets this criterion. Furthermore, there is sufficient flexibility in the design to vary the number of readout fibers per unit area to more closely adhere to the criterion, if desired.

b. Measurement

A 2 cm x 2 cm x 1 mm thick scintillator plate, polished on all sides had a 1.5 mm diameter hole drilled in its center. The hole was not polished. This plate represents the proposed fundamental unit in the electromagnetic calorimeter. A 1 mm diameter wavelength shifting fiber traversed the hole in the plate and at the end of its 20 cm length was optically coupled to an RCA 8850 PMT. The set up and associated wavelengths of light are shown in the Figure II.4.

A 3 mm x 3 mm wide beam of electrons from a strontium 90 source was defined by two small scintillation counters operated in coincidence as shown in the Figure II.5. A 0.8 mm thick plate of aluminum was placed in the beam to ensure the passage of energetic electrons through the 2 cm x 2 cm test scintillator plate. Coincident events in the beam counter opened a gate to permit pulses from the test counter to be analyzed in the pulse height analyzer. Random coincidence events between beam counters was small. The test counter distribution is shown in the Figure II.6. The large peak corresponds to single photoelectrons and two and even three photoelectron events could be distinguished.

The ratio of test counter events ($\geq$ 1 photoelectron) to coincidence events was found to be 0.4. Approximate tests to ensure the validity of this result were performed. These included measurement of test counter random rate, removal of wavelength shifting fiber, removal of 2 x 2 cm^2 scintillating plate, but leaving the fiber present, ensuring that only

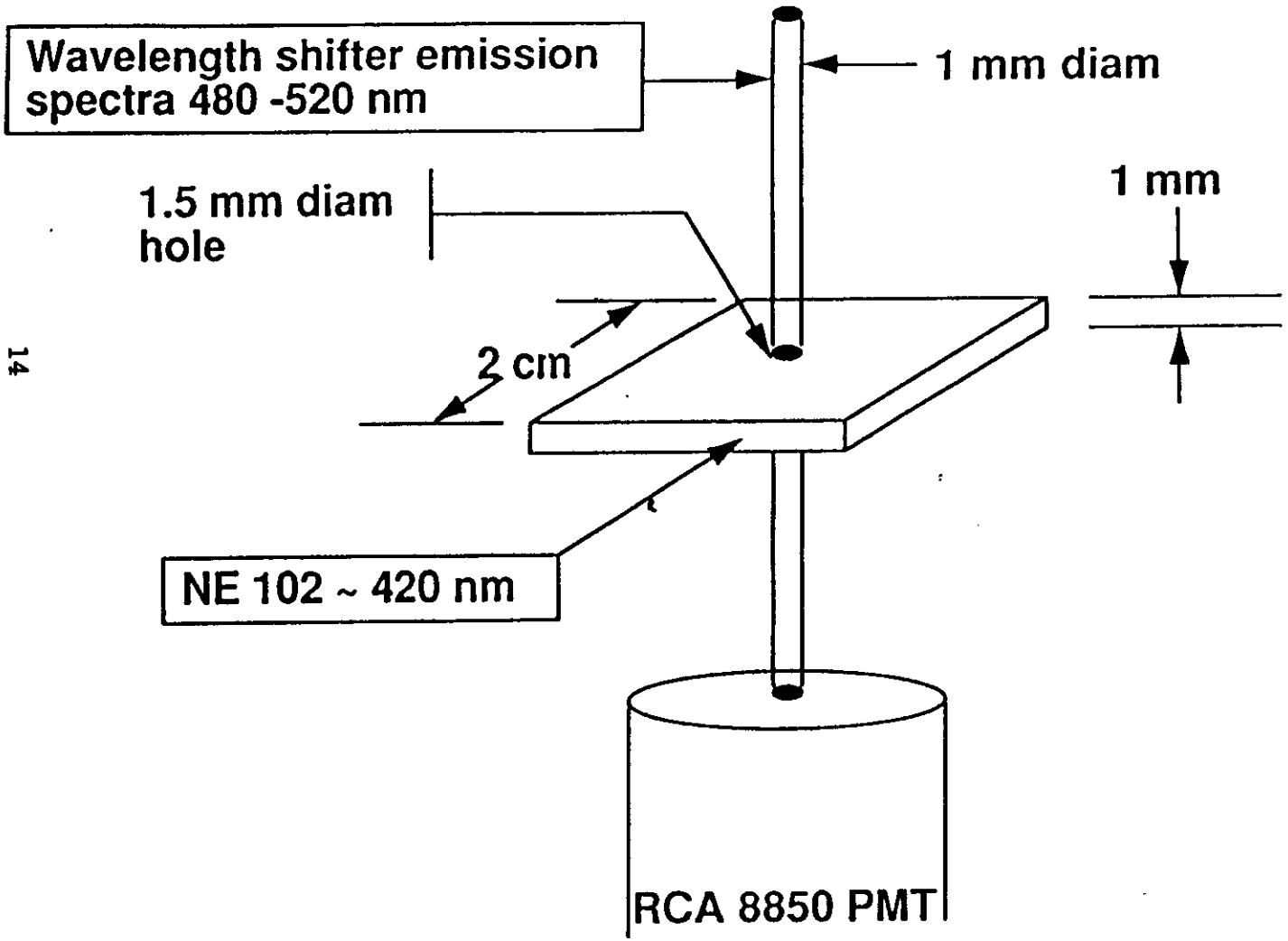

FITCAL Plastic Scintillator and Wavelength Shifter/Light Guide Configuration

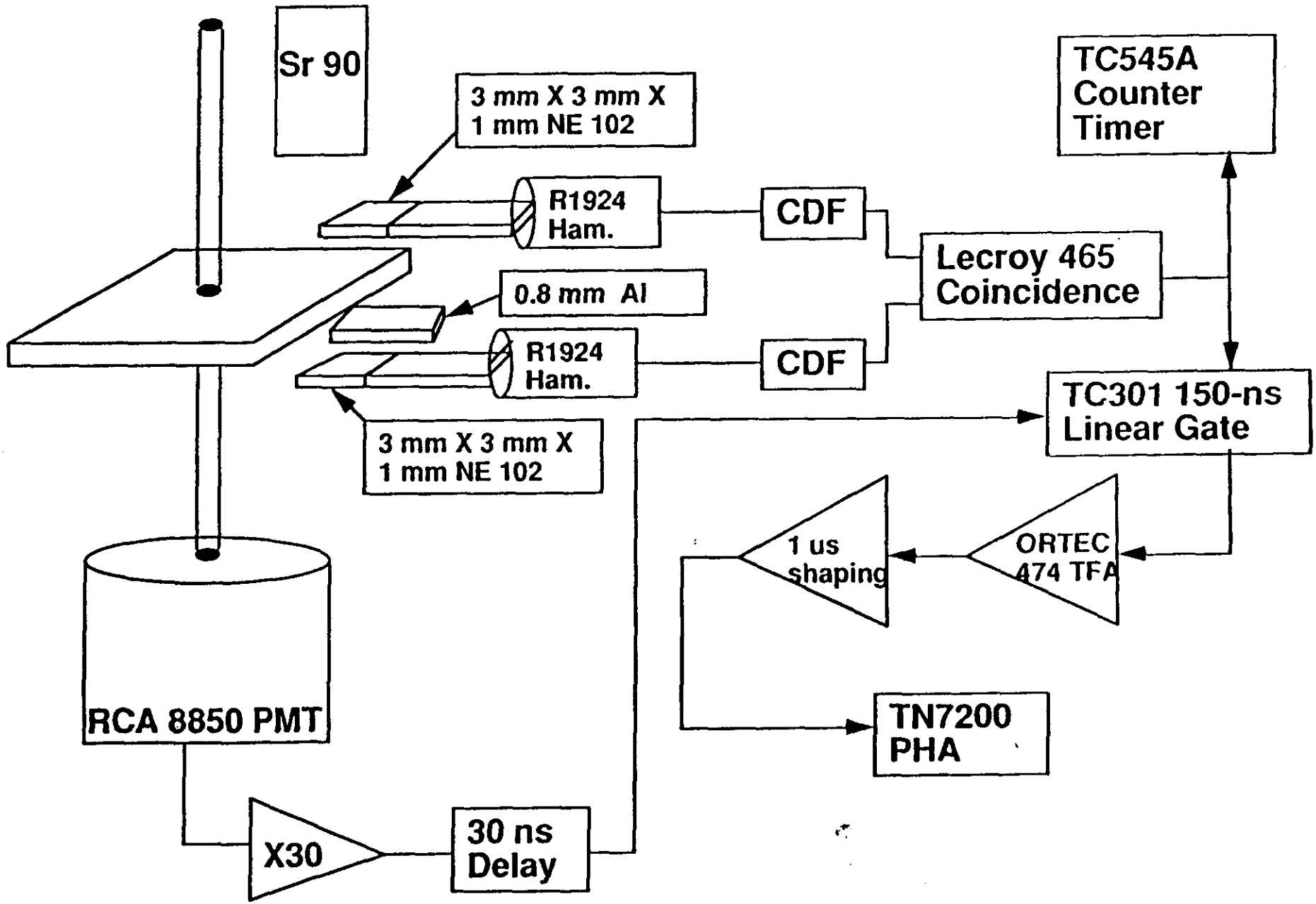

ORNL FITCAL Electronics Setup
FIGURE II.5

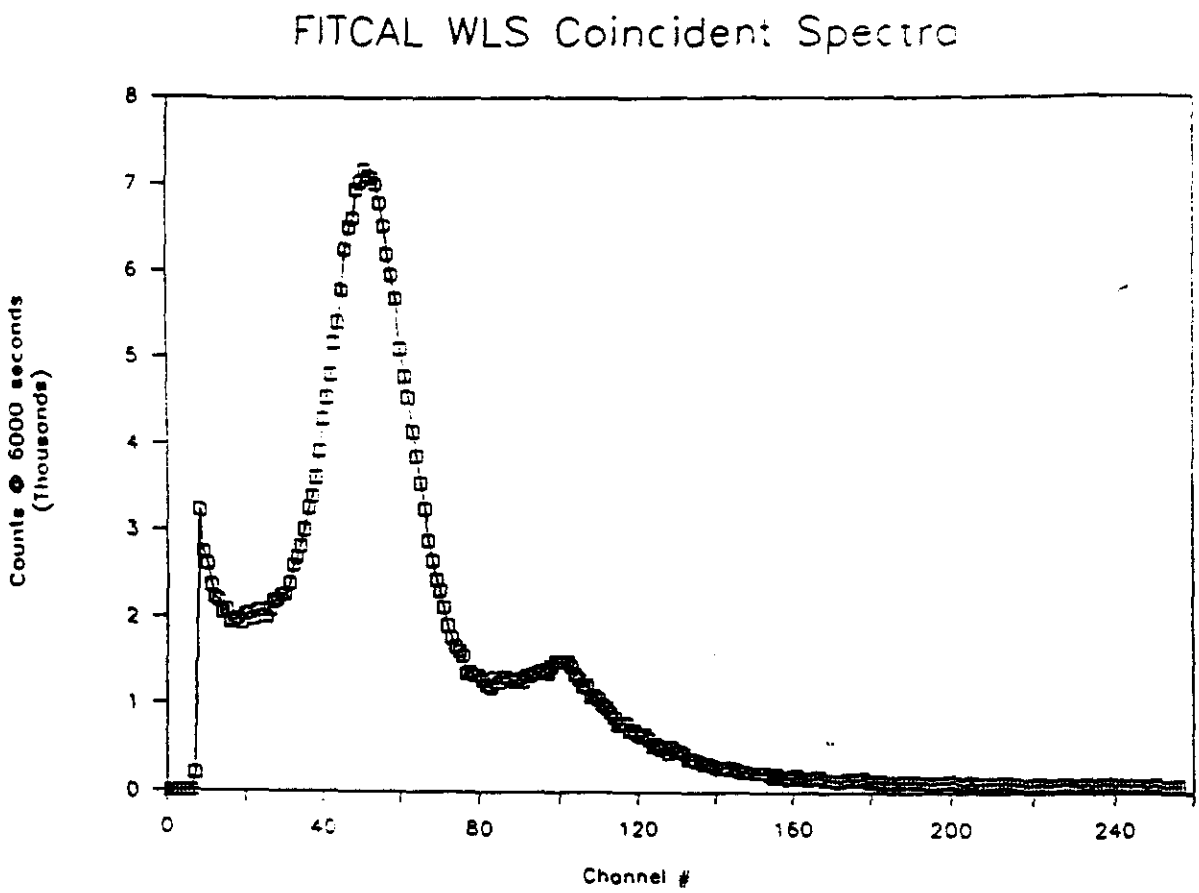

Pulse Height Distrubtion Due to Tagged Electrons
FIGURE II.6

light from the wavelength shifting fiber struck the cathode of the test photomultiplier, and the position of the source was varied to change the counting rate.

All tests were supportive of the conclusion that the FITCAL scintillator plate gave 0.4 photoelectrons per electron traversal. We plan to do further measurements which will include:

1. Uniformity of scintillator plate response.
2. Change of photoelectron yield as a function of hole polish, edge of plate polish, edge of plate reflection coefficient, etc.

c. Comparison with Previous Measurement

To our knowledge two previous electromagnetic calorimeters have been constructed with a very similar design to that proposed here, FITCAL. Since the issue of light collection efficiency, spatial uniformity, energy resolution, etc. were studied carefully in these previous prototypes we felt it was worthwhile to attach the publications resulting from these measurements as Appendix 1. Our measurements are in very good agreement with the results of these previous studies. Since the issue of light collection efficiency in the FITCAL design has been of some concern in the past, it is essential to recognize that there is little doubt in the validity of the result at this stage. Table II.1 summarizes a comparison of the results from the two previous calorimeter prototypes and our own measurement. It can be seen that we anticipate:

1. Electromagnetic Energy Resolution:

$$\frac{\sigma}{E} = 0.01 + 0.14/\sqrt{E(GeV)} \ ,$$

with approximately equal contributions from sampling fluctuations and photoelectron statistics.

2. Adequate spatial uniformity to achieve the above energy resolution averaged over the entire detector area.

The system design we have proposed, therefore, meets the objectives of uniform compensation (4 to 1 ratio of Pb to scintillator) throughout the entire length of the calorimeter, adequate light collection efficiency, and finally, minimal area of readout to minimize the cost of solid state readout. Overall system preliminary optimization has been achieved.

In the unlikely event that our development work with solid state devices rules out their use in their use in this application, the system can be re–optimized for the use of multi–anode photomultipliers. A photocathode with maximum response at 550 nm would be used to provide $\geq$ 20% quantum efficiency (compared to the non-optimized 15% quantum efficiency photomultiplier used in the test measurement.

Secondly, the number of fibers would be increased by a factor of 4 to 1 fibers per cm^2. This is still a factor of 25 fewer fibers per cm^2 than the spaghetti calorimeter design. We conservatively estimate this change will double the light yield. With these two changes, the

	Distance Between Fibers (cm)	Scint. Plate Thickness/rad. length of Pb (0.6 cm)	Number Photo-electrons/MIP/ mm Scint. Plate Thickness	Number Photo-electrons/MIP/ mm with 80% QE Solid State Photodetector	Number Photo-electrons/GeV	Energy Resolution	Maximum Variation of Pulse Height for 5 GeV electrons (on fiber to max. dist. from fiber)*
DESY	4.7	1.5	0.3		700; Model A 1700; Model B	$0.04+0.13/\sqrt{E\text{GeV}}$ $0.086/\sqrt{E\text{GeV}}$	± 25%
MAX Planck Institute	2.6	1.5	0.26		229	$0.014+0.1/\sqrt{E(\text{GeV})}$	± 10% (at 0° beam incidence; ± 8% (at 3° beam incidence)
Present Proposal to SSC	2.0	0.15	0.4 (measured with PM at 15% QE and 20 cm long read out fiber	1.05 (expected allowing for a factor of 2 attenuation in 1-2 m fiber read out	105 from scaling the measurements above (approx. 1000:1) and the ratio of sc. plate thicknesses	$0.1/\sqrt{E}$ from samp. fl.* $0.1/\sqrt{E}$ from p.e. statistics giving a total of $0.01+0.14/\sqrt{E(\text{GeV})}$ (expected)	± 7% (expected); ± 5% (expected at 3° beam incidence

*The uniformity is expected to improve at higher electron energy. This is because the diameter of the electron shower grows logarithmically with energy thereby producing a more uniform spatial distribution. We expect the 5% "on fiber" non uniformity to drop to 3% at 100 GeV. In addition, since this effect exists for only about 10% of the active area of the calorimeter the contribution to a constant term in the energy resolution is small ≈1% and acceptable (as in the case of the Max Planck calorimeter).

Table II.1

expected number of photoelectrons per GeV will become 53 and will contribute a factor of $0.14/\sqrt{E(GeV)}$ to the energy resolution. This will result in an estimated electromagnetic energy resolution of $0.01 + 0.17/\sqrt{E(GeV)}$. This is still an acceptable resolution, adequate to perform the physics anticipated at the SSC.

3. Photo Detector Read-Out

As part of this proposal, we intend investigating the relative merits of the two broad classes of photosensitive detectors.

a. Vacuum Photosensitive Devices

i. Some general design criteria for a desirable photodetector are:

The photocathode area should be large enough to accommodate a minimum of 16 each 1 mm fibers for multi-channel operation in the case of electromagnetic calorimetry and single channel operation in the case of hadronic calorimetry.

This may imply (due to cost considerations) two different types of devices for the two types of calorimetry.

ii. The multi-alkali photocathode should have good quantum efficiency ($\geq$ 20%) in the 500-600 mm range.

iii. The intrinsic rise and fall time of the device should be $\leq$ 2 nsec and pulse height should have fallen to less than 1% after 12 nsec.

iv. The device should have the sensitivity to detect signals in the range 50 to 100,000 photon flux at the photocathode.

v. The device output should be linear through the signal range specified in 4 above.

vi. The device should be radiation hard such that there is less than 10% change in response for a total exposure of 10^7 rads.

vii. The device should be minimally sensitive to magnetic fields.

viii. The cost per channel should be $\leq$ \$30.

ix. The device should be as compact as possible.

These design criteria were discussed with Burle Industries, Inc. and they have submitted a proposal to the SSC generic detector program to do the research and development necessary to produce such a device.

Hamamatsu produces a variety of multi-anode photomultipliers. Some of these are of the proximity focus type with high immunity to magnetic fields. Philips produces multi-anode photomultipliers with similar properties. There are two options for locating the photosensitive devices. They may be located at each of the longitudinal segments, or they may be at the back of the entire calorimeter if the light from each segment is piped out to the back. Cerenkov light produced in a glass envelope of the photosensitive

device (if it has one) by particles in the shower can give spurious signals. Dr. W. Selove, University of Pennsylvania, explored this problem and solved it with a specially fabricated photomultiplier in which the photocathode material was deposited on a thin film separate from the glass envelope. In addition, he used the photomultipliers facing in the same direction as the incident particles in the shower. To minimize the effect of Cerenkov light, it is clearly desirable to locate the photomultipliers at the back of the calorimeter. However, this introduces small cracks in the calorimeter for light piping purposes. Maintenance would be easier having the photo devices at the back of the calorimeter. In summary, the relative advantages of these two options have to be explored early in the development of this program.

All of the above devices, and others, will be studied to ascertain the extent to which they meet the design criteria. It is quite likely that the optimum solution depends upon the general design of the SSC detector for which FITCAL calorimetry is being used. For this reason, it is essential to thoroughly investigate the range of possible solutions to photo detector readout.

b. Solid State Devices

In the above discussion, we have concentrated on conventional vacuum photomultipliers. However, in the last two years a revolution has occurred in the development of solid state photodetectors (SSPD). These two developments were the solid state photomultipliers (SSPM)and the avalanche photodiode (APD). Our special interest in these devices is that they can operate in high magnetic fields.

1. Solid State Photomultipliers (SSPM) by Rockwell International:
   This is a solid state device capable of counting single photons[10] with an electronic gain of 5×10^4. It has very high rate capability and can be fabricated in a variety of configurations. The linear dynamic range should be extremely good and is only limited by the lateral spread of the Geiger saturated avalanche.[11] Since this should be about 6 μm in diameter, we expect full saturation of output at an input current of 3×10^4 photo electrons on a 1 mm diameter SSPM. A reasonable linear dynamic range can, therefore, be estimated to be 3×10^3 and this could be increased by coupling a 1 mm fiber to a larger area SSPM. Since the dynamic range is not important in the use of the SSPM's in tracking applications, we intend to work with the SCIFI tracking group and Rockwell to explore this particular aspect of their operation. The radiation resistance of SSPM is of primary importance and we intend to investigate this further.

   Cryogenic operation of SSPM is necessary for adequately low noise. Since the heat capacity is low, helium gas can be used. Micro transfer tubes (about 1 mm diameter vacuum insulated tubes and 2 m long) have been developed and extensively used in the area of milli and microkelvin research. Since the University of Florida has the largest microkelvin research laboratory in the world, we can rapidly transfer this technology to our application. In summary, we propose an aggressive investigation of the suitability of the SSPM revolution to our FITCAL design.

2. <u>The Avalanche Photodiode (APD)</u> by RCA: The silicon photodiode has been tested in the past[12] with disappointing results because the APD's went into breakdown before producing stable gains. This problem has now been resolved, and recent studies by us[13] have shown that stable operation can be achieved with the new RCA devices. Their characteristics make them particularly suited to FITCAL operation.

   Their typical properties relevant to FITCAL are:

   a. 1 mm diameter up to 4 x 4 mm^2. The smaller size suitable for individual electromagnetic towers while the larger size is suitable for integration of the signal from the 4 x 4 array of fibers from an 8 x 8 cm^2 hadronic tower.

   b. Total insensitivy to magnetic fields.

   c. Low power consumption (0.1 Watt) making their location at each longitudinal segment within the calorimeter a possibility. However, due to the large pulses produced in the device by traversal of shower particles through the avalanche region of the device, it will be essential to locate all of the APD's at the back of the calorimeter. Light from each longitudinal section of the calorimeter can be light piped to the back of the calorimeter using nondoped plastic optical fibers. Because of the very small readout area of FITCAL compared to other proposals, the fraction of 'crack' area will be minimal. Connections between wavelength shifting fibers and undoped fibers can be made efficiently and inexpensively.

   d. Good matching of spectral response to wavelength shifted light of $\geq$ 500 nm.

   e. High quantum efficiency of about 80% at $\geq$ 500 nm.

   f. Intrinsic high bandwidth capability.

   g. The gain of the APD's are in the range of 50 to 200.

   h. We have measured the linear dynamic range of the APD to be at least 1000.

A test on the operation of an APD as a scintillation photo sensitive device was performed. A 5 x 5 mm^2 APD had its bare sensitive area optically coupled with silicon grease to a 4 x 4 x 4 mm^3 Cesium Iodide crystal. Various gamma and x-ray sources with energies from 5.9 KeV to 1.33 MeV were applied to the crystal. The temperature variation of the APD was maintained at less than 1° C. A typical spectrum for Am^{241} is shown in Figure II.7. It can be seen that x-rays of 14-20 KeV can be well resolved. In fact, x-rays of 5.9 KeV can be resolved clearly above the noise. We have measured the APD noise to be less than 10 r.m.s. electrons for a 4 x 4 mm device operating under conditions suitable for calorimetry at the SSC. The noise will be significantly less than this for a 1 mm x 1 mm APD suitable for electromagnetic calorimetry.

A development type, C30905, APD has a simplified coupling to a fiber of 1.0 mm diameter, spectral response from 400 to 1,100 nm, a pulse rise and fall time of 0.5 nsec and

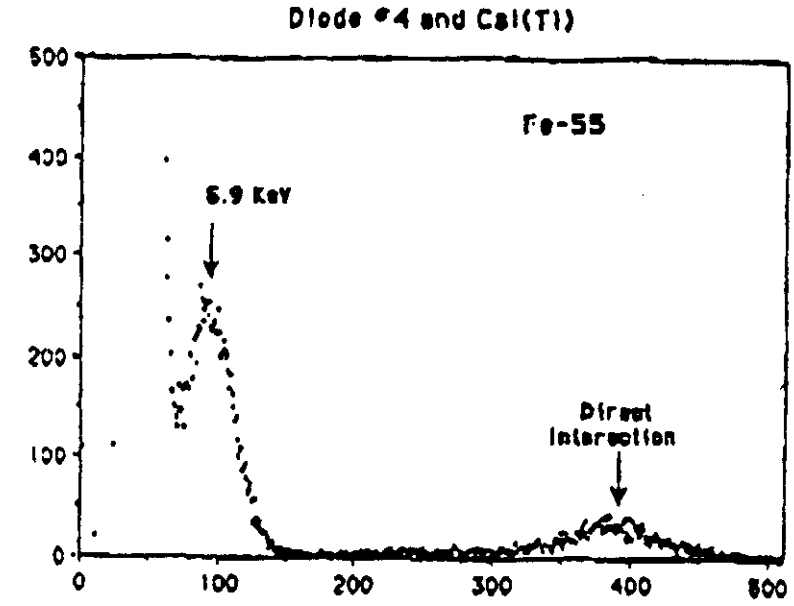

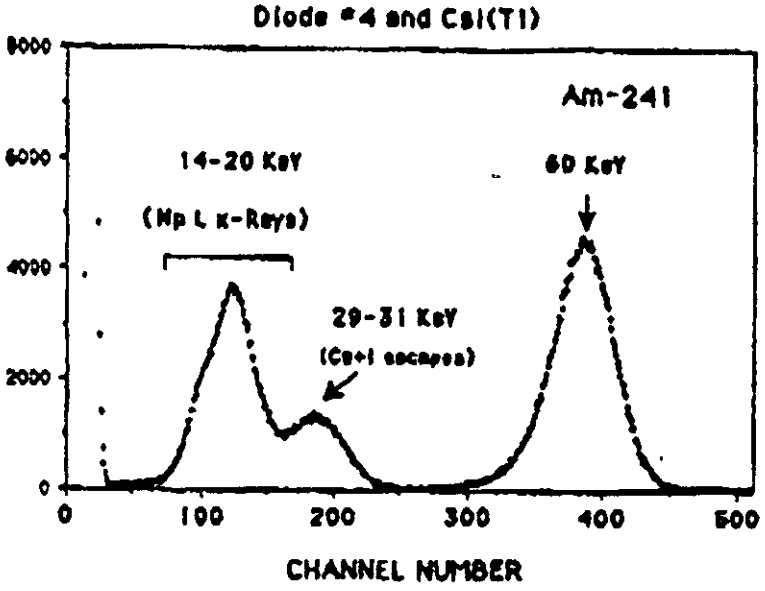

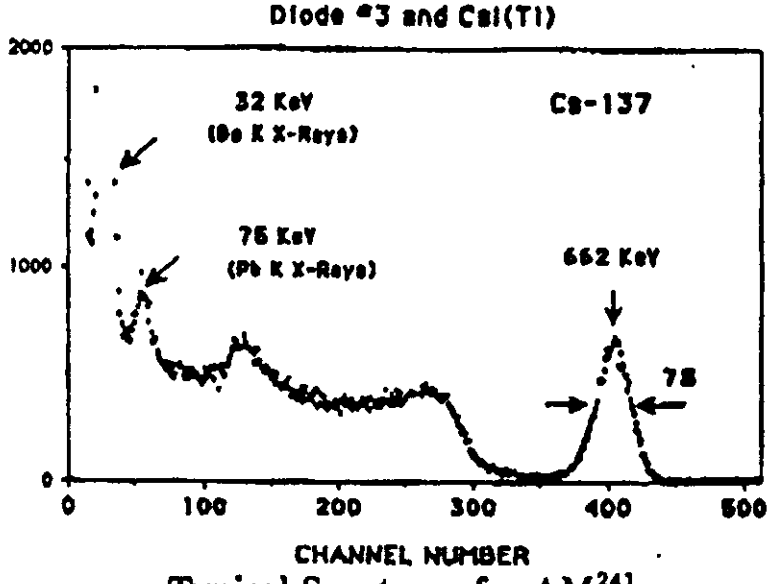

Typical Spectrum for AM^{241}
FIGURE II.7

wide operating temperature of -40° C to +70° C. We have measured the gain stability of this APD for one year and found it to be better than ±5%. A charge sensitive preamplifier is included in the package. The RCA estimated price for these devices in the quantities needed for an SSC FITCAL detector is $25.00. A series of tests is beginning now on these devices.

III. Engineering

A. Engineering Development Program

This is a proposal to design and build a calorimeter, based on the FITCAL concept, which is large enough to contain showers and test its operation in all respects. The prototype program has three major design and construction phases to meet these objectives:

Phase I. (1990) Electromagnetic Calorimeter

An electromagnetic calorimeter, 16 cm x 16 cm in area and 34 cm in depth will be built. It will have two longitudinal segments which will be read–out separately. The calorimeter will be composed of individual towers, each 2 cm x 2 cm in area. This corresponds to 128 individual read–out channels, each with 1 mm diameter sensitive area.

The objective of this phase of the program is to engage many of the design and construction problems with a small, but significant objectives. This calorimeter will be adequate to be fully tested to ensure that the design meets all the device objectives or modified appropriately before proceeding to the next step.

Phase II. (1991) Full Length Electromagnetic and Hadronic Calorimeter (A FITCAL Module)

A full length fiber tower calorimeter (FITCAL), 16 cm x 16 cm x 284.44 cm in length will be constructed (Figure III.1). It will use the Phase I electromagnetic calorimeter followed by a hadronic calorimeter segmented longitudinally into two sections. The two hadronic sections will be composed of 4 towers each 8 cm x 8 cm in area. This corresponds to 8 individual read–out channels, each 4 mm x 4 mm (composed of 16 fibers) in area.

The objective of this phase of the program is to engage essentially all of the design and construction problems for the fundamental building block of a full–scale SSC calorimeter detector. This module is inadequate to contain enough of a hadronic shower to provide a definitive test of some vital properties of the calorimeter. These include energy resolution function, and extent of compensation. Complete evaluation of the efficiency of the calorimeter design can be achieved in the next step.

Phase III. (1992) Nine FITCAL Modules

Nine FITCAL modules will be constructed and arranged in a 3 x 3 array. The cross–sectional area of the array is 48 cm x 48 cm. This is adequate to contain enough hadronic energy to test all aspects of the operation of the FITCAL design.

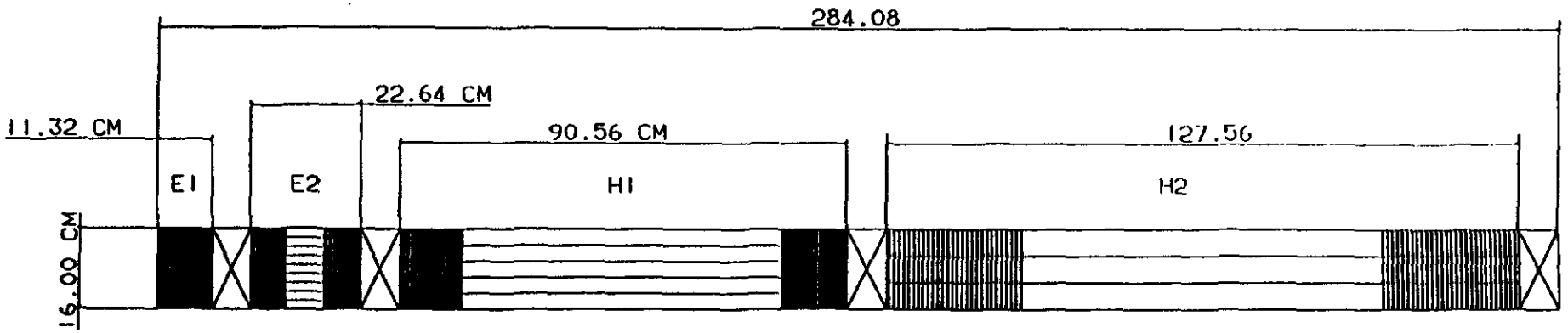

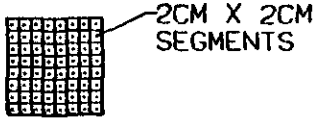

CROSS SECTION
OF E1 & E2 SEGMENTS

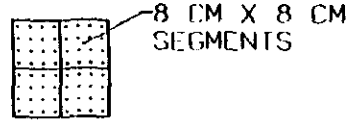

CROSS SECTION
OF H1 & H2 SEGMENTS

FITCAL Prototype Tower Concept
FIGURE III.1

The objective of the engineering development program is to use the construction of the nine tower prototype (Figure III.2) as a vehicle for the analysis of fabrication techniques, assembly methods and materials required to construct a full-scale FITCAL calorimeter.

B. Development Requirements

The requirements of the FITCAL engineering development program were determined through an evaluation of several design approaches to a full-scale SSC calorimeter. That evaluation is summarized in Section IV. The following tabulation of design issues resulted from that analysis. They are divided into four categories: manufacturing, assembly, materials, and structure. The proposed program is designed not only to resolve the issues already forseen, but to expose other issues which will need to be addressed before the design of the SSC detector is undertaken. Each phase is expected to provide a few surprises with the nine tower assembly offering the most potential for practical insights into the actual requirements of the SSC design.

In addition to the construction of the prototype assembly, the development program will include two measures to provide the necessary engineering background to design the SSC calorimeter. First, each aspect of the design will be evaluated in bench-scale tests prior to the inclusion in the prototype assembly. Secondly, design and manufacturing concepts will be subjected to reviews by commercial vendors to confirm the validity of the approach for use in the SSC detector production program.

C. Component Manufacturing

We propose to begin the development of techniques required to fabricate the very large number of pieces necessary to build the SSC calorimeter. The size of this problem is easily realized by consideration of the estimate that a full-scale detector will have approximately 4,000 towers, each of which will require a total of 660 layers of lead and plastic. Further, note that each layer will be slightly different due to the tapering of the towers. Thus, if either a cylindrical or spherical detector configuration is used, the detector will require a total of approximately 1,320,000 pieces of at least 660 different sizes. Similarly, the manufacturing of the 4,000 aluminum tower jackets will also require development with respect to construction, handling, and assembly.

1. Scintillator Plastic: A typical plastic scintillator sheet is shown in Figure III.3a and in Figure III.3b. The scintillator sheets can be manufactured from 1.0mm to 1.5mm (0.04 in. to 0.06 in.), thick polydimethyl-diphenyl siloxane (PDMS) plastic. In addition to being an efficient scintillator, the PDMS has a controllable flexibility. This program has already produced material having a substantially higher Shore number, thereby significantly improving the fabrication and handling characteristics. Development of a coating for the scintillator plastic may also be undertaken to reduce the effects of age on the surfaces of the plastic. Scintillator layers will be divided into segments. The first two longitudinal tower segments (electromagnetic) will have 64 lateral segments while the third and fourth longitudinal segments (hadronic) will also have only 64 lateral segments. Water jet or laser cutters will probably be used to size, segment and drill the scintillator plastic. Both cutting methods

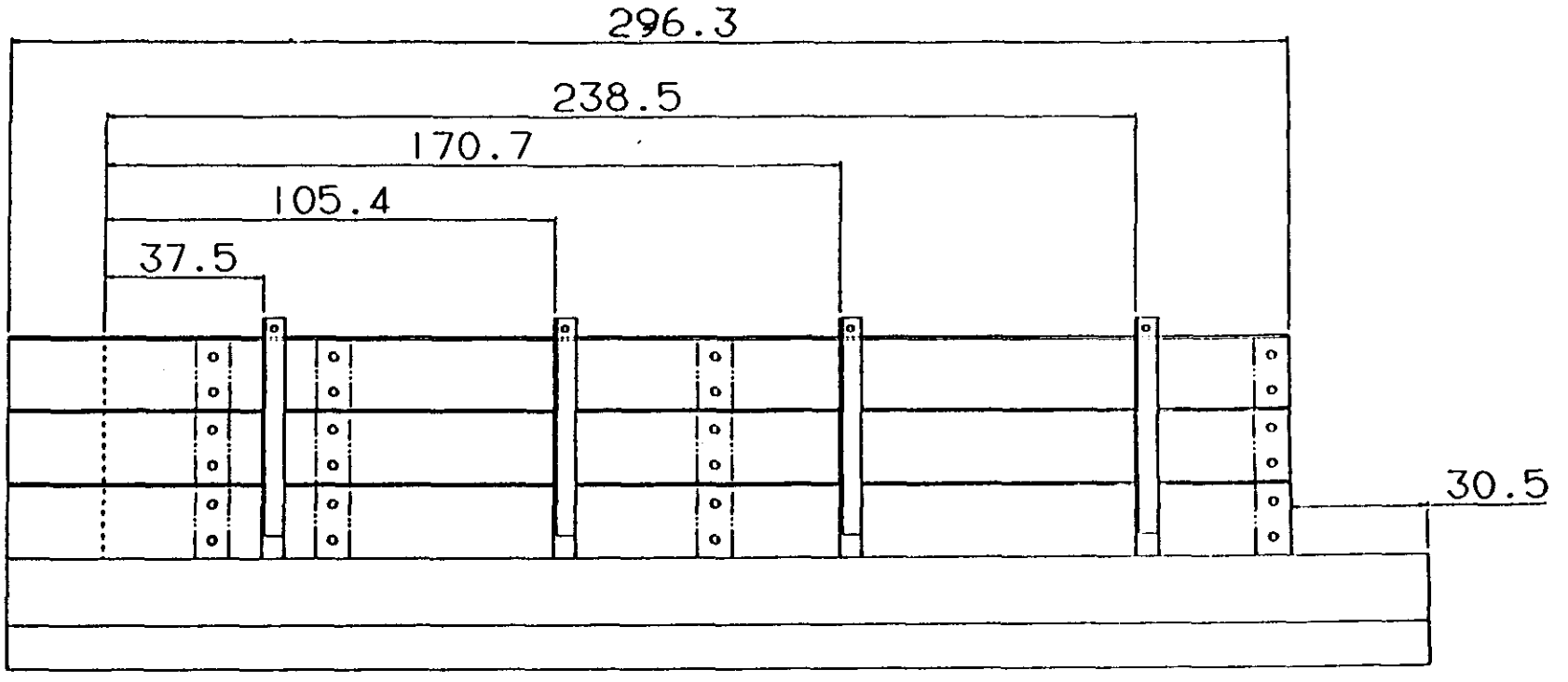

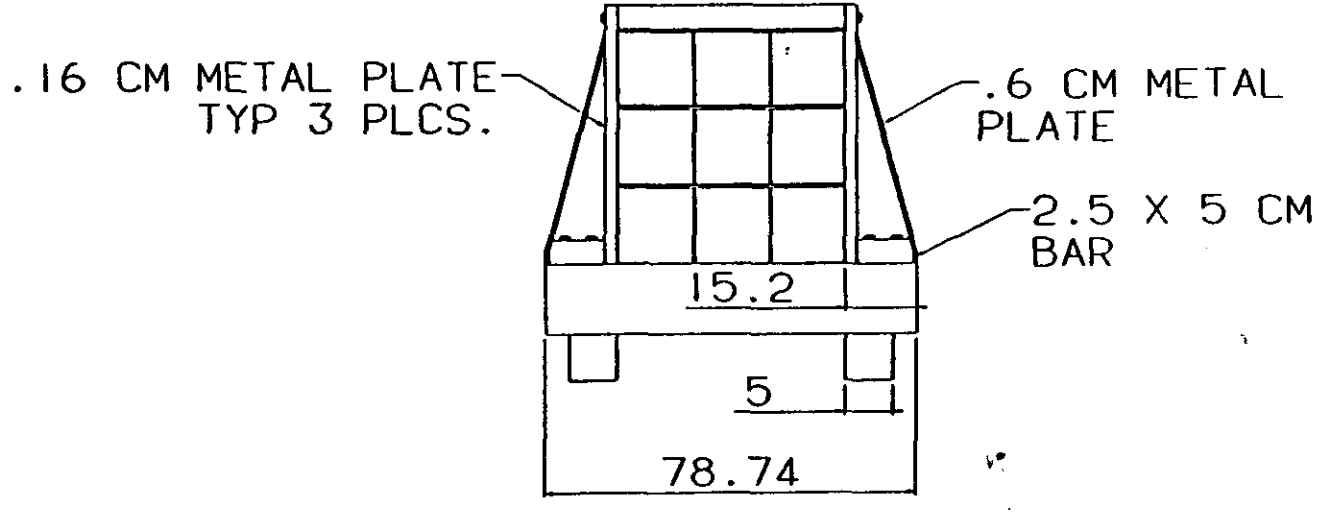

FITCAL Prototype Assembly Concept
FIGURE III.2

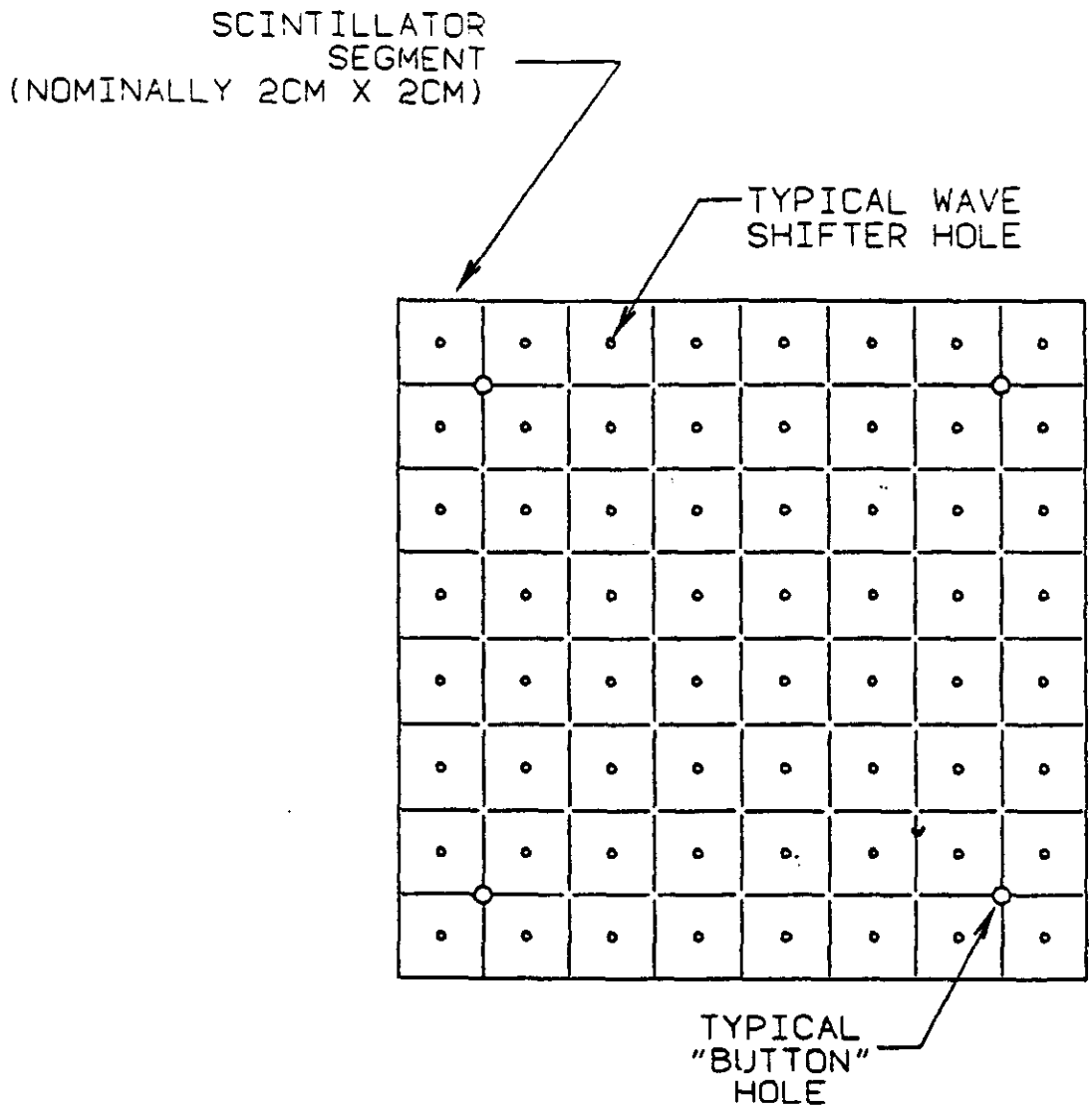

Typical Scintillator Layer
FIGURE III.3a

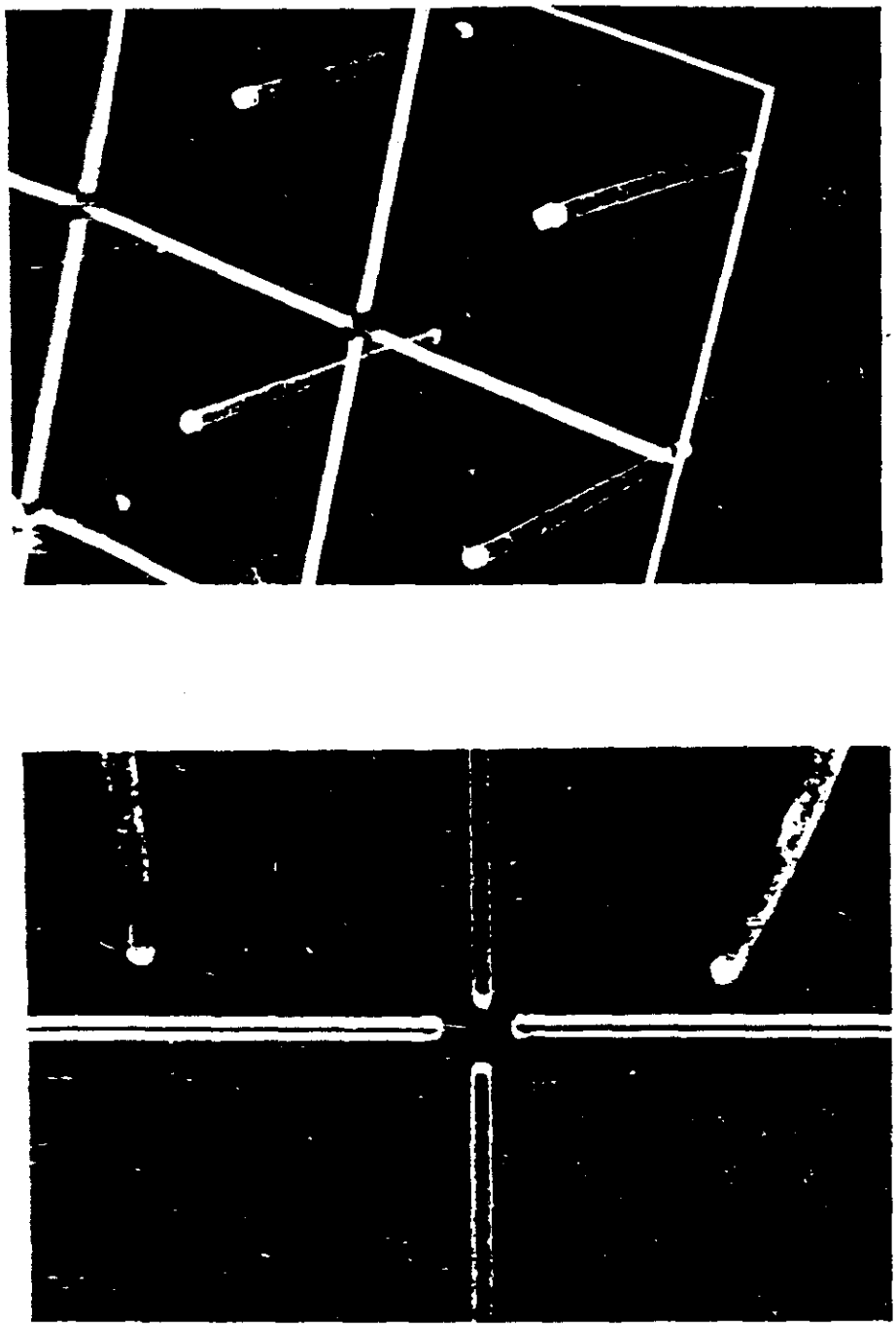

The upper photograph shows a single sheet of plastic scintillator with 0.015 in. width cuts which provide the 2 cm x 2 cm light collection areas required for electromagnetic calorimetry. The lower photograph shows more clearly the boundary of four towers.
FIGURE III.3b

have been used successfully on plastics in the past with excellent precision and surface finish condition. Each layer will be cut in a single set-up to avoid the distortion which may result from handling. Note in Figure III.3b that lateral segments within layers will be joined at the corners to hold the sheet intact for assembly. Bench-scale testing will be used to verify the specific characteristics of the scintillator layers. Extensive bench-scale testing will be carried out. Bench-scale tests will include the determination of the following mechanical characteristics:

- Hole tolerance limits
- Hole surface finish requirements
- Edge surface finish requirements
- Segment slot length
- Optic fiber placement tolerances

It should be noted that Loehr[1] states that the surface of the scintillator holes is not critical. Specifications for the scintillator will be developed and competitive bidding procedures will be followed. ORNL will have responsibility for all aspects of scintillator specifications and bidding procedures. It is expected that companies in Japan, Europe and the U.S.A. will bid on scintillator procurement.

2. Lead Layers: A typical lead layer is shown in Figure III.4. In the first three longitudinal segments, the layers will be 4mm (0.16 in.) thick. In the fourth segment (second hadronic), the lead layers will be 8mm (0.32 in.) thick. In the prototype and bench-scale tests, other thicknesses will be used to permit testing of different ratios of lead to plastic. The layers of lead in all segments will have identical cross sections, including 64 optic fiber holes.

   Methods of mass producing the lead sheets will be developed. Several techniques have been successfully used in the fabrication of existing detectors including drilling, shearing, water jet and laser cutting. Numerically controlled, automated manufacturing promises to be a low cost and precision method which can be applied to all these processes. Special tooling may also be justified by the relatively large numbers of pieces.

   Methods of handling the lead sheet during fabrication and assembly to maintain the flatness of the layers will be developed. A likely solution to this problem is to laminate the lead with thin sheets of aluminum. The addition of a 0.025mm (0.01 in.) thick sheet of aluminum to both sides of a 4mm (0.157 in.) sheet of lead will increase the stiffness by over 300%. Aluminum cladding will also provide clean hole and edge finishes.

3. Aluminum Tubes: Manufacturing methods for forming aluminum tower jackets will be developed. If a spherical detector is built, requirements for tapered thicknesses and triangular cross-sections (Figure III.5) define the

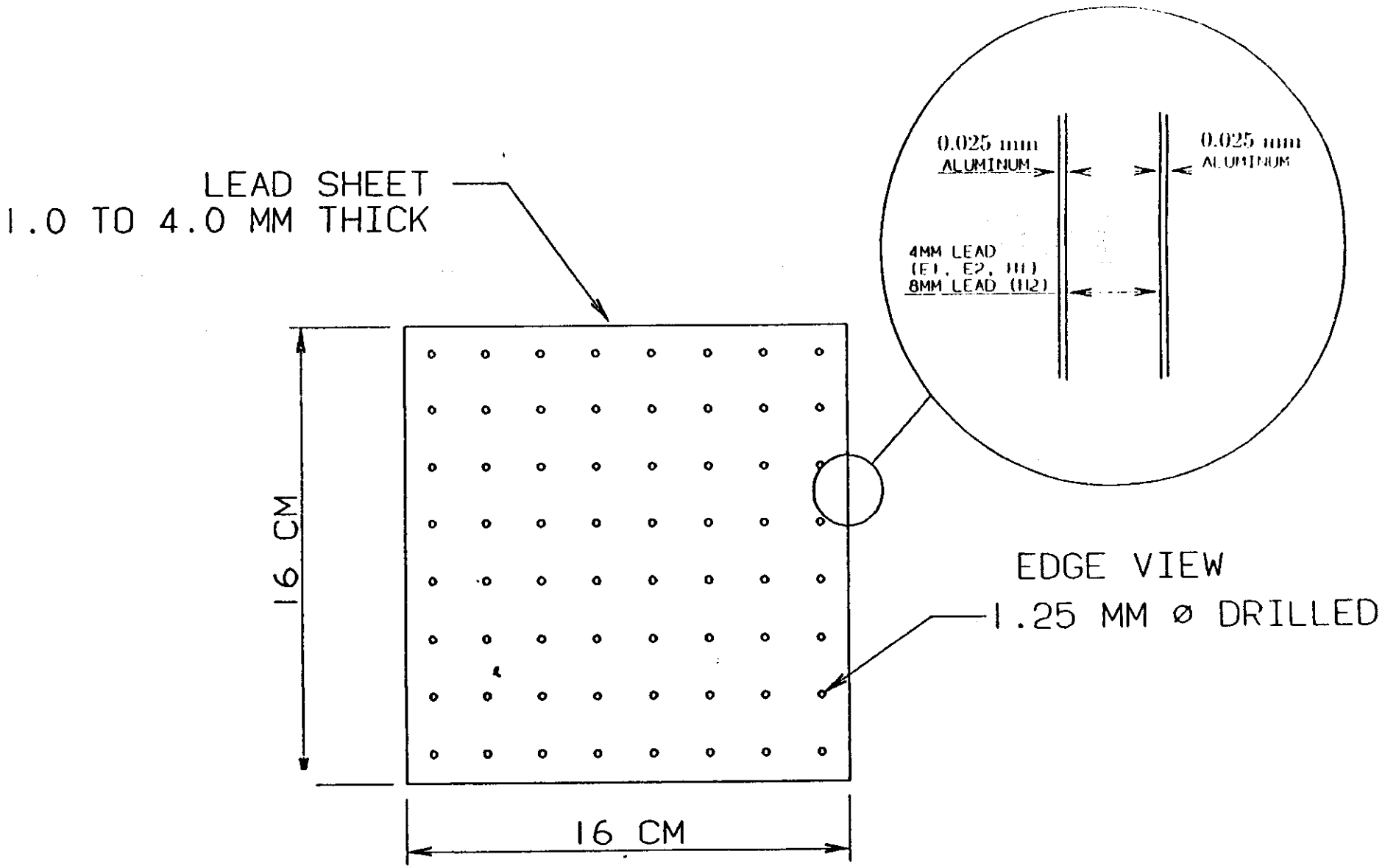

Typical Lead Layer
FIGURE III.4

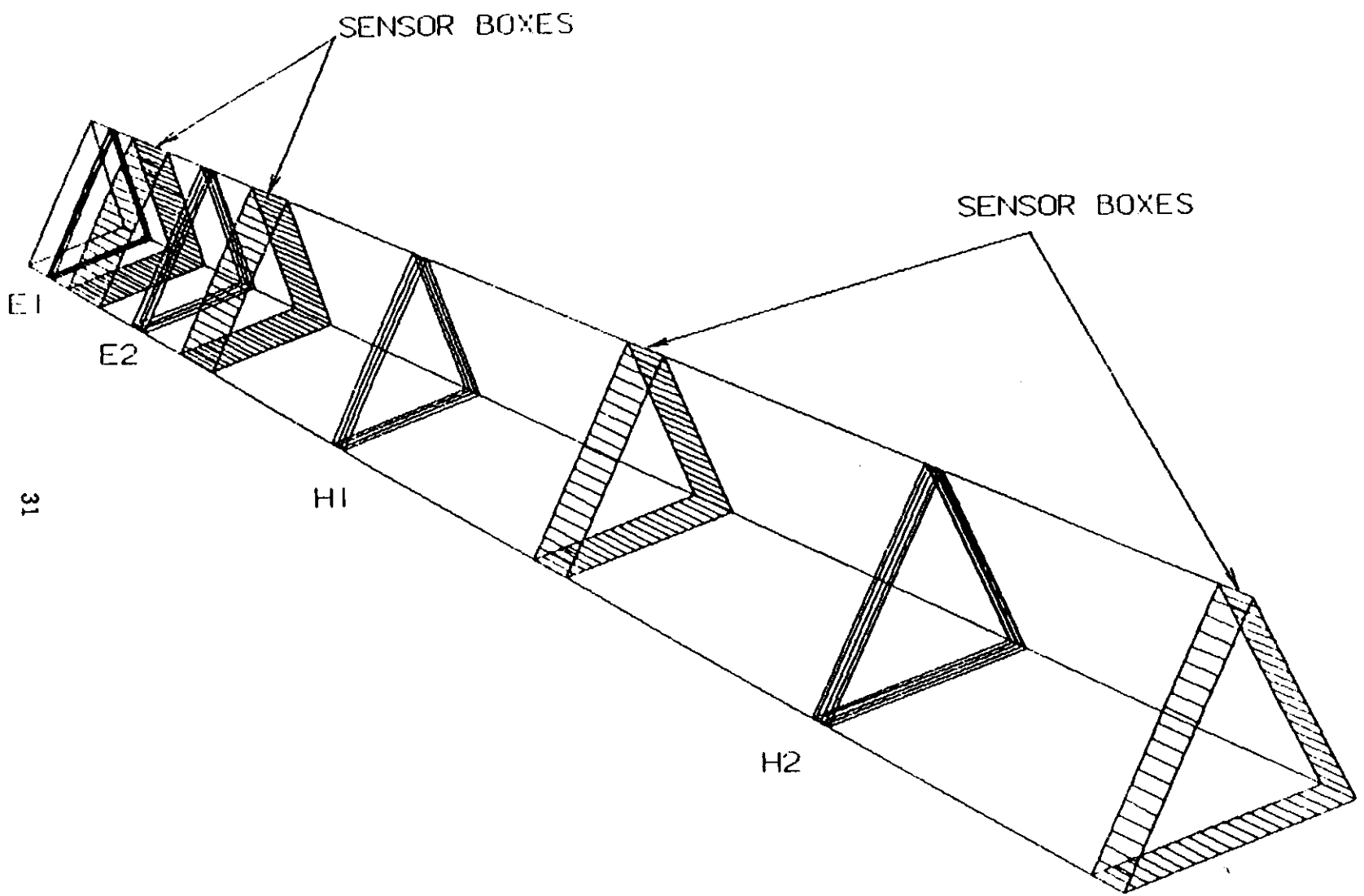

Individual Polygon Tower
FIGURE III.5a

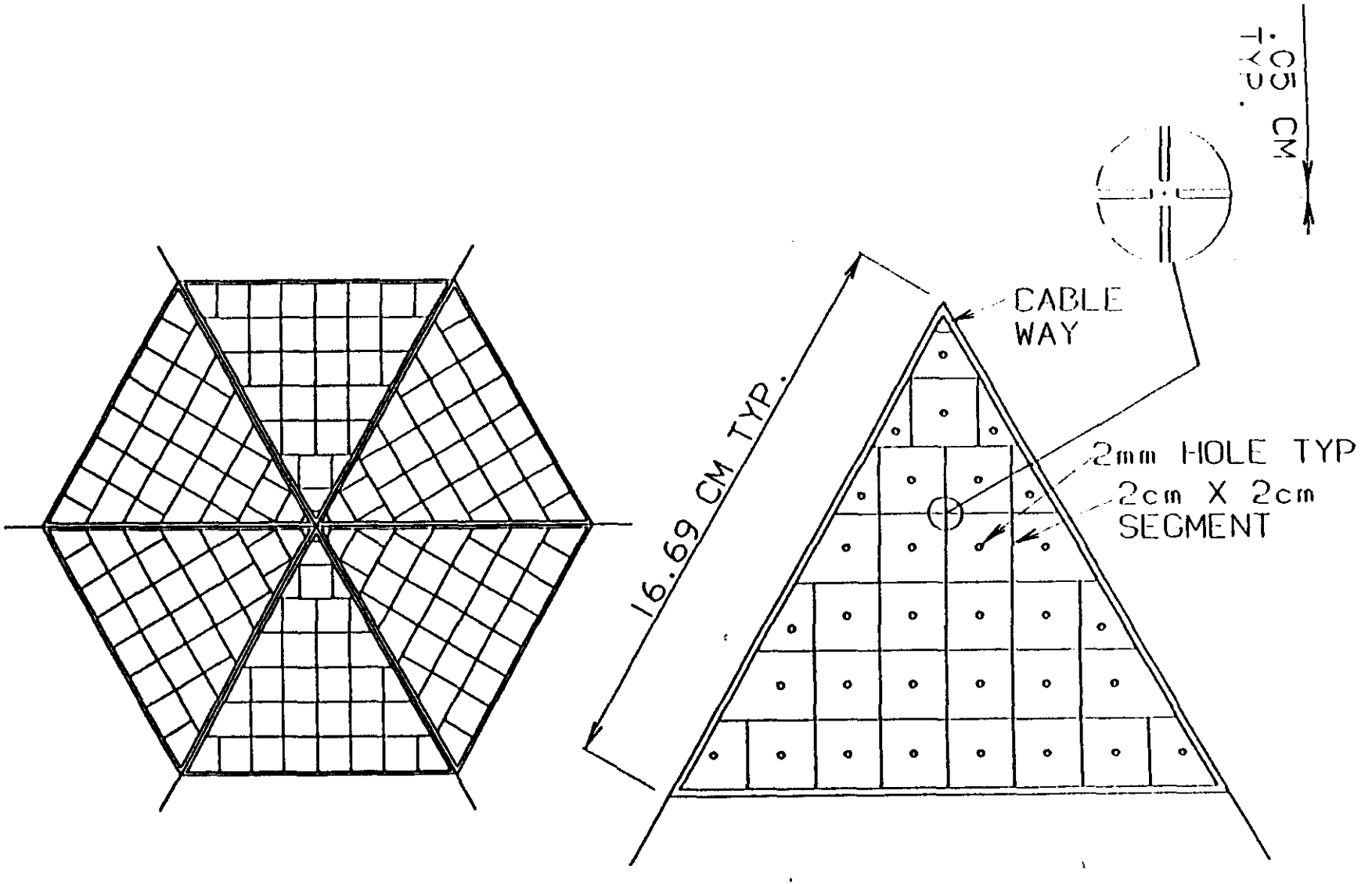

Subdivided Polygon with Frame and Segments
FIGURE III.5b

manufacturing problem. Tapering can be achieved using deep- draw forming while the triangular shape may be realized from a round, tapered tube using a die forming machine. Other methods are available and will also be considered. Industrial participation will be particularly important in this part of the development program.

D. Assembly

Assembly of the SSC FITCAL will require development of special procedures due to the large number of pieces, weight of the subassemblies, inconvenience of the assembly location, and the minimum structural framing available. As an example of the scope of the problem, it should be noted that each tower in the comparatively small prototype assembly will weigh approximately 635kg (1,400 lbs.), and the entire assembly will weigh approximately 6,800kg (15,000 lbs.), including the frame and all nine towers.

Areas of particular concern with respect to handling and assembly which have been identified are discussed below.

1. Installation of Wavelength Shifting Fibers: Methods will be developed to install the small 1 mm (0.04 in.) diameter wavelength shifting fibers in the tower layers. The 64 fibers in each prototype longitudinal segment will be routed through a tunnel of holes in the lead and plastic layers. The holes are to be machined as small as possible to reduce potential losses in the efficiency of the detector while still maintaining an air gap or minimum contact with the plastic and lead. The assembly of each longitudinal segment of a tower will be started by stacking the lead and plastic sheets with metal rods in place of the fibers. After the stacking of each longitudinal segment has been completed, the fibers will be pulled into the holes with the rods. The fibers will then probably be cut and connected to the multinode sensors located in the sensor boxes at the end of each longitudinal segment. Alternatively, the wavelength shifting fibers will be connected to light transmission fibers which will be routed through the cableways to photosensitive devices located outside the detector. If the alternate method of termination is used, the hadronic wavelength shifters will be combined in the sensor boxes and only 4 light transmission fibers will be routed to the end of the tower.

2. Installation of Power and Instrumentation Cabling: Cabling will be routed axially along the length of each tower from the sensor box to the outside of the detector. Methods of minimizing the amount of space required to contain the wires must be developed since the routing path will tend to reduce the hermiticity of the detector. If the wavelength shifting fibers are coupled to light transmission fibers in order to route the light to photosensitive devices outside the detector an approximately 100 mm^2 (0.16 $in.^2$.) in cableway will be needed in the second hadronic segment.

3. Installation of Lead and Plastic Layers Inside Aluminum Tubes: Methods will be developed to install components inside the long tower tubes. Note, for example, the problem of installing the wavelength shifting fibers in a flaring stack-up. Since the hole spacing will change from layer

to layer, a method of moving the wires used in assembly out as the stacking process progresses will have to be developed. Examples of other installation requirements which will be explored in the development program include handling procedures for the plates, control of contaminates, and the establishment of in-process inspection procedures.

4. Handling and Transporting Assembled Towers: A completed tower assembly will represent a significant investment. It will be important to develop methods and standards to both test the completed towers to determine if the units are ready to be installed in the assembly and to protect the units against damage prior to installation. Subassembly testing will be particularly important since the in-place investment increases substantially after the towers are inserted into the full detector. Handling of towers between assembly and installation at the detector assembly site will require special fixtures and methods since the aluminum tubes in which the towers are stacked will not support the tower assembly in a free-standing configuration.

5. Assembly of the Detector: Installation of towers into the assembly will require additional fixturing and detailed procedures to insure uniform frame loading and maintenance of assembly clearances. Additional information will be obtained on the access and support requirements needed to assemble the detector.

6. Detector Maintenance: Methods of replacing individual towers must be developed. This will be particularly difficult since the towers may tend to interlock in the completed assembly. As with the original assembly of the detector, access and support of the maintenance functions will be of particular importance.

E. Materials

While a majority of the materials to be used in the detector are determined by experimental properties, the specific types and alloys remain to be established. For example, a coating for the scintillator sheets is unspecified as is the aluminum or similar material to be used in the framing. Other areas of interest are the radiation resistance of the wiring and the scintillator plastic. We will evaluate the radiation resistance of these component materials in neutron and gamma radiation tests prior the completion of the development program.

F. Structural

The amount of structure is a principle factor in determining the hermiticity of the detector. Consequently, we will devleop a detailed conceptual design for the full–scale calorimeter frame. This effort will be concentrated in three areas.

1. Layer Structure: The towers will be positioned with longitudinal axis oriented through a full 360 degrees. Consequently, the internal structure of each tower must be able to support the lead and plastic layers in a manner which will not load either the plastic or the wavelength shifting fibers in any

orientation. This requirement stipulates that the tower jackets be constructed precisely so that the layers can lay on the inside wall and align with the fibers correctly. To address the local structural loading, particularly on the plastic layers, which will result in both the top and bottom orientations, 'buttons' (Figure III.6) will be installed in the stack to transfer the load to the sensor boxes which in turn will be fastened to the aluminum tower jackets. The 'buttons' will also serve to position the layers with respect to each other since the holes for both the buttons and the optic fibers will be machined in the same set up.

2. Tower Structure: Development of aluminum tower jackets with adequate structural integrity to withstand not only assembly and installation, but removal for repair or replacement will be particularly challenging. It is assumed that the jackets will not be used free-standing, but rather will have strong-back fixturingduring all operations outside the detector assembly. Attachment and containment of the sensor boxes to the jackets will also be resolved and tested in the prototype assembly.

3. Assembly Structure: The design of the exoskeletal frame to support the SSC detector will be analyzed using a finite element code. The symetry of the problem tends to offset the fact that the frame must be able to support the estimated total weight of 3,400,000kg (7,500,000 lbs.), and yet, permit the removal or installation of individual towers. The full-scale frame will be conceptualized to determine the feasibility of the basic assembly technique. This design will provide a basis for the accurate determination of cost, complexity, and hermiticity.

IV. Preliminary Engineering Studies of Several of SSC FITCAL Calorimeter Shapes

In order to prepare an effective engineering development program for an SSC calorimeter, we made a preliminary analysis of possible detector designs. Five basic methods of constructing an SSC FITCAL were identified in that study. The five assembly proposals are described below starting with the spherical concept. While the spherical concept offers many advantages with respect to calorimetry, it is premature to state that it is the preferred concept since other SSC requirements such as the design of the central tracking detector may dictate that another shape be used.

The description of each option applies only to the center section of the detector. The beam openings in this portion of the detector will require outboard plugs which will be smaller, but will use the same basic FITCAL concept of stacked lead and plastic. The plugs are discussed separately at the end of this section.

A. Polygon Based Sphere: The polygon based sphere concept (Figure IV.1) achieves both the optimum geometry and efficiency. This arrangement provides the easiest configuration for accurately recording and analyzing data due to the uniform positioning of the individual towers around the beam interaction point.

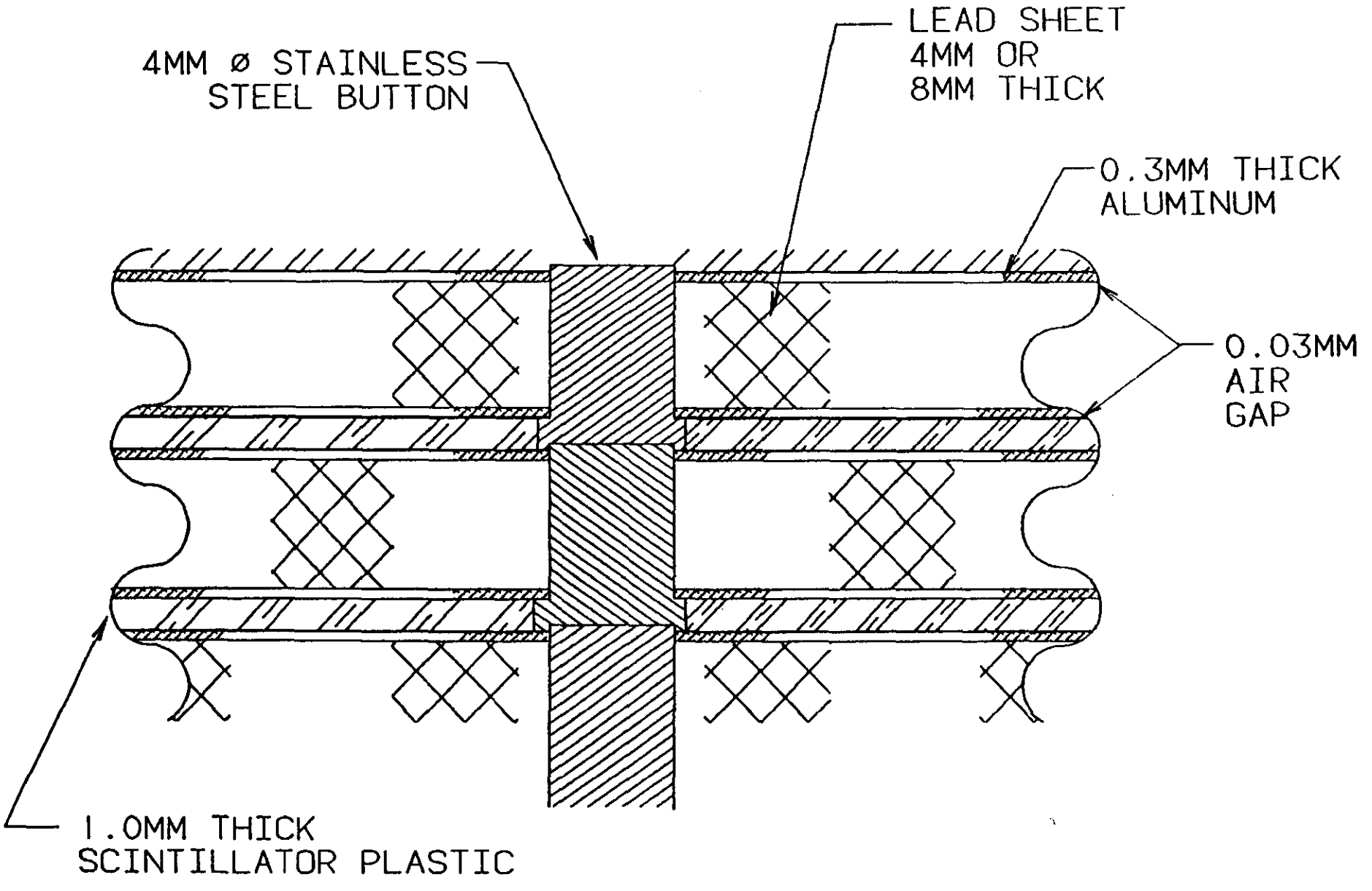

Top and Bottom Orientations: 'Buttons'
FIGURE III.6

Two common types of basic polygons can be used to form the sphere; the dodecahedron and the isocahedron. In either configuration, the polygons would be subdivided into assemblies of triangles. The triangles would be sized to limit the total weight of each tower to a maximum of approximately three thousand. five hundred (3.500 lbs.) pounds for purposes of handling. Beam ports would be provided on either side of the sphere by removing one or more polygon segments.

The polygon based sphere will require the fabrication of many different sizes of components. It should be noted that neither the dodecahedron or isocahedron form a sphere using identical triangles, therefore, several different shapes will be required (a minimum of 19). In addition, the triangles will flare towards the outer diameter, therefore, each layer within the triangle will be slightly different. It is estimated that a minimum of 12,500 different lead and plastic layer sizes will be required to build a sphere with triangles.

B. Rectangular: The rectangular FITCAL concept is based on using identical, rectangular towers stacked as if building a chimney on its side. The obvious advantage of this approach is that it uses the most easily fabricated components (all the layers have the same cross-section) in a simple arrangement. The overriding disadvantage of this concept is the poor detector geometry which would make data analysis difficult and inefficient.

C. Cylindrical: A cylindrical calorimeter has the advantage of having better geometrical and structural characteristics than the rectangular design while not being as complex as a sphere. Only two types of towers would be required to build a cylindrical FITCAL; one for the cylindrical section (a flaring rectangle) and another for the ends (possibly rectilinear boxes). The flaring rectangles represent a significant increase in complexity over rectilinear boxes since the lead and plastic sheets must increase in size slightly with each succeeding layer.

D. Focused: The goal of the 'focused' assembly (Figure IV.2) concept is to provide the maximum volume inside the calorimeter for targeting assemblies while pointing most of the towers at the beam interaction point. A focused FITCAL would represent a major increase in cost and complexity over the cylindrical concept, because it would require both a large number of different lead and plastic sheet sizes due to the flaring on the towers, and a large number of different tower sizes due to the constant change in axial angle. Further, the structure for a focused asembly would be very complex.

E. Igloo: The igloo concept is basically the same as the focused concept except that it attempts to approximate a sphere rather than a cylinder. This technique is used to build ice houses because it allows the fabricator to start from a flat surface and build rows toward the top center. Each row has the same type of flaring, trapezoidal faced tower. Complexity is, however, introduced by the requirement that each succeeding row must be made from either a different number of the same type of bricks (thus, complicating the structure by overlapping the joints), or with bricks having smaller face dimensions. A reasonable design for a FITCAL based on the igloo concept could not be envisioned.

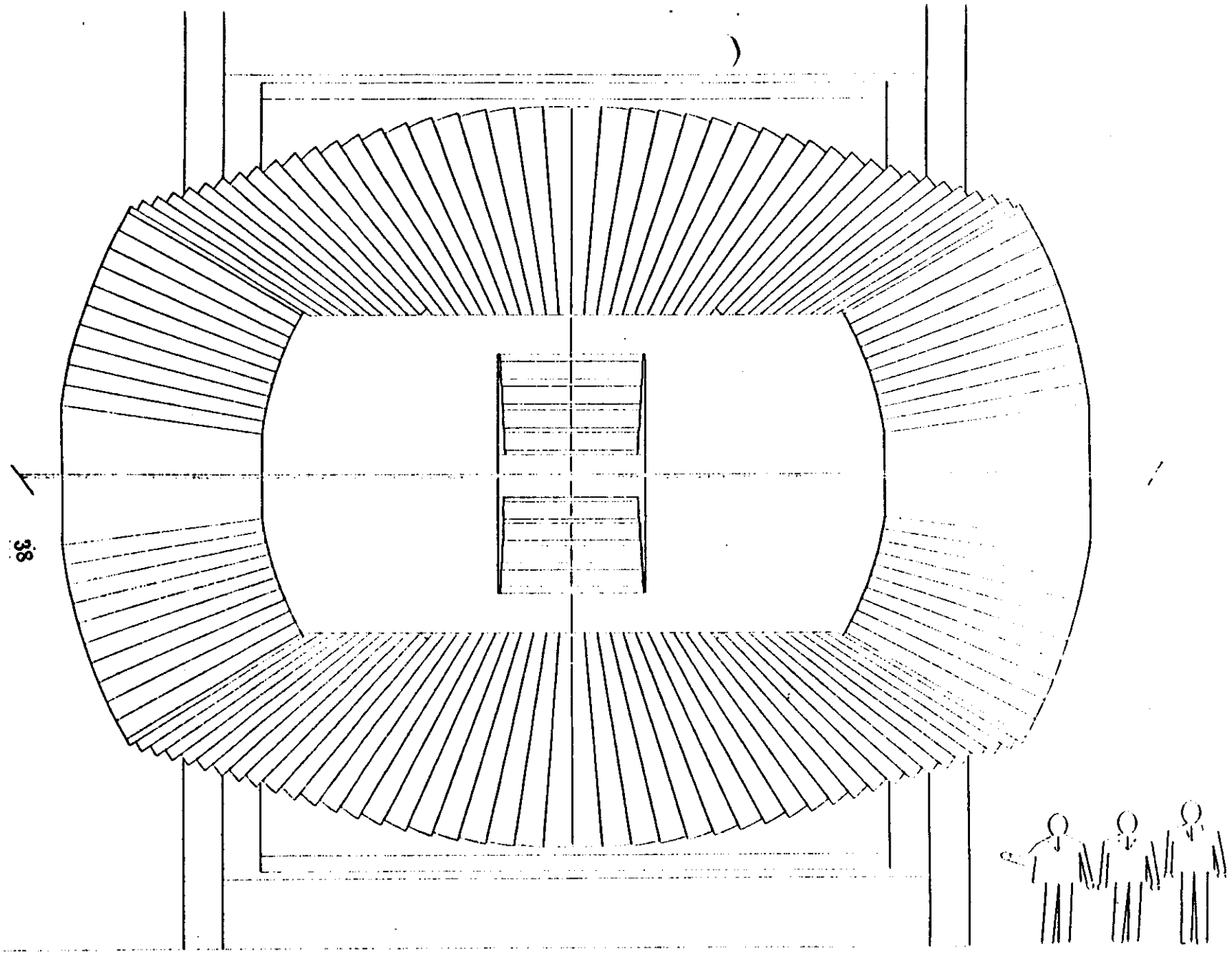

Focused Detector
FIGURE IV.2

F. Detector End Plugs: The FITCAL detector concept includes removable end plugs at both beam openings (Figure IV.1). The end plugs will have the same basic lead and plastic layering configuration as the center portion of the detector. The plugs will receive much more radiation damage than the central portion of the detector. therefore. the end plug mounting frames will facilitate easy removal and repair of individual towers.

G. Engineering Design Procedure

The design of the FITCAL detector for use in the SSC will require a design process similar to that used for airplanes. Specifically, it will require a totally integrated engineering effort in which all factors are considered simultaneously. The program defined in this proposal initiates this process by beginning work on the first two phases of the design. The first step will be the development of fabrication methods for the detector components, including materials selection and performance testing. This will be undertaken in the early bench-scale and prototype testing program. Examples include the determination of the optic fiber hole size tolerance in the scintillator layers. Analysis of scintillator coatings and evaluations of different thickness ratios of lead and scintillator. Secondly, commercial vendors with expertise in applicable fabrication processes will be consulted concerning the best approaches for each of the processes proposed for the FITCAL. The development program presented in this proposal begins making contact with vendors at the inception of testing. The basic objective is to test materials and designs which realistically can be used in the full-scale SSC calorimeter. Finally, the engineering design team will use existing computer based modeling programs to analyze the structural, mechanical, and physics of a full-scale detector from the same data base. Using the computer modeling information, a basic conceptual design for an SSC detector will be completed. Due to cost, this phase of design will not be started until after selection of the FITCAL concept for use in the SSC.

V. Data Acquisition and Calibration for the FITCAL Detector Prototype

A. Introduction

Data acquisition for the FITCAL calorimeter will involve the process of detecting, with an appropriate photomultiplier device, the light that has been coupled into the wavelength-shifting fibers from the scintillator sheet and processing the resulting electrical signal. The two electromagnetic (EM) sections will have 64 data channels each and the two hadronic (HA) sections will have four data channels each. Two pieces of information will be extracted from the data out of each channel. The first is a measure of the total energy deposited in the scintillating sheet in the neighborhood of each wavelength-shifting fiber. The second is the elapsed time from each bunch crossing to some subsequent interaction that takes place in a particular channel. The energy resolution must be at least 1% over three decades of amplitude and the timing resolution must be a least 1-2 nsec. The calorimeter towers must be calibrated periodically, primarily because of the degradation of the scintillator material, wavelength-shifting fibers, and data transmission fibers with accumulated radiation dose.

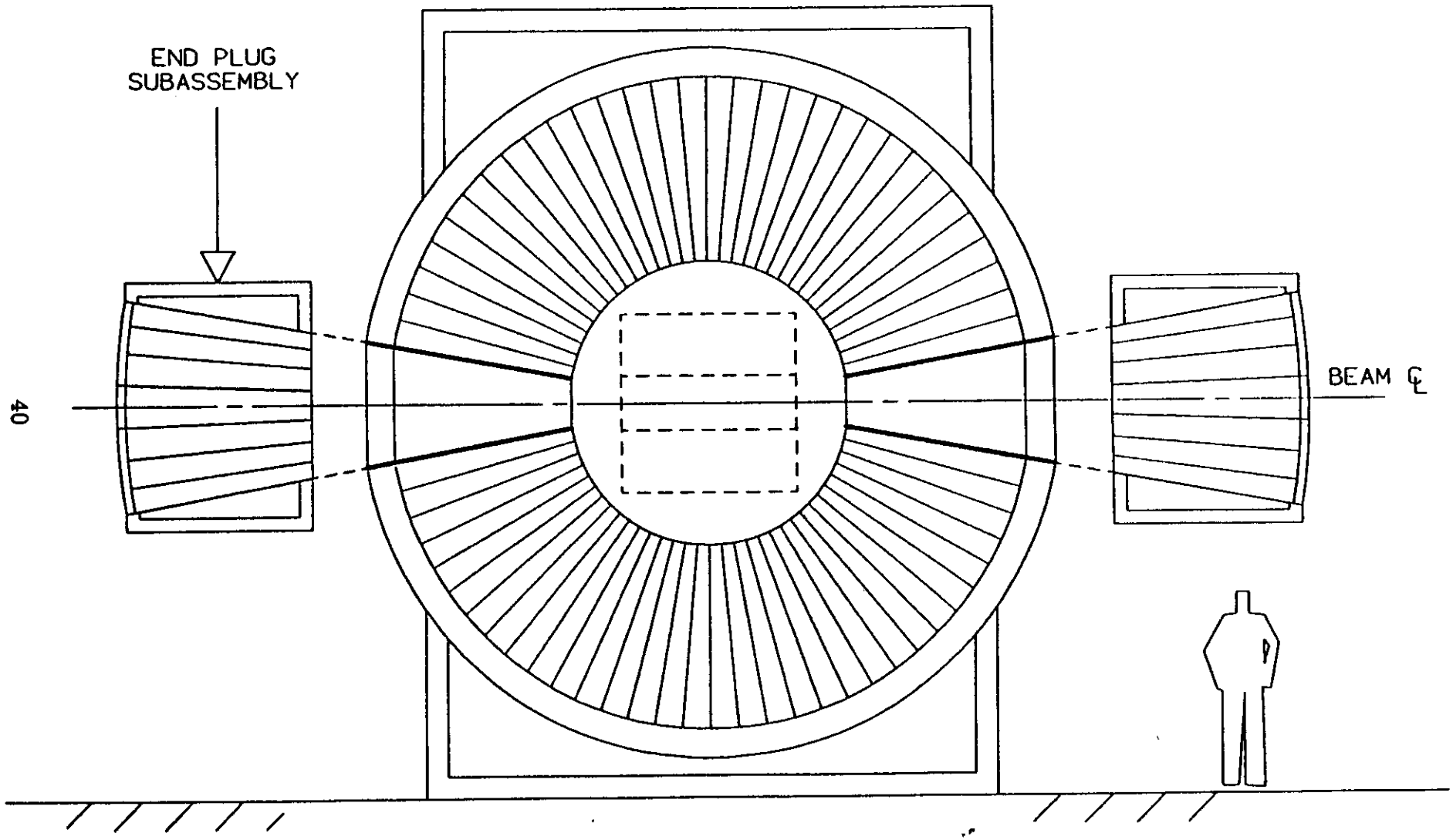

Polygon Based Sphere Concept
FIGURE IV.1

Techniques for calibration as well as determination of the frequency of calibration will be investigated. Testing of components and subassemblies will be performed at appropriate intervals throughout the duration of the project. The development time will be three years from the receipt of funding. A phased approach will be taken in the development of the data acquisition and calibration system. The individual phases will be described in detail below.

B. Data Acquisition for the Prototype

1. General Approach

For the SSC, the ideal characteristic for any detector system would be to acquire and process data at a rate greater than the machine interaction rate ($\sim$ every 16 nsec). To accomplish or even approach this type of performance, data must be handled and processed in a parallel fashion as much as possible. As part of this project we plan to investigate a scheme to send a linear analog representation of the data over optical fibers thus allowing the analog–to–digital processing hardware to be located at the rear of the individual towers. There will be 64 channels of information in each of the two EM sections and four channels of data in each of the two HA sections. Processing in each of the individual channels will be identical as shown in (Figure V.1). Light from the scintillator will be piped into a multi–anode PM device by the wavelength–shifting fibers. The resulting pulses will be fed into an appropriate preamp. At this point, it may be decided to apply some minimal amount of pulse shaping in the prefilter section. The signal will then be input into the optical linearizer which will transform the electrical analog signal to a representative light signal to be transmitted over the optical fiber to the rear of the tower. At the rear of the tower, an optical receiver, matched closely with the operating characteristics of the devices in the optical linearizer, will convert the light signal to an electrical signal for further processing. This approach will involve minimal hardware in an already space–limited arrangement since optical fibers will occupy approximately one–tenth (1/10th) the space of copper cables. All fibers and cables will be run to the rear of the tower in a self contained cable channel allowing the towers to be stacked together without hermeticity problems at the towers' physical interfaces due to cables.

2. Phase I (Year 1)

a. **Light Collection Studies of the Scintillator and Wavelength –Shifting Fibers:** Much testing needs to be done to experimentally determine the light collection efficiency of several different geometric configurations of the scintillating sheet, wavelength–shifting fibers, and PM device. This will include tests to (a) determine the optimum scintillator/fiber interface, (b) explore the use of multiple fibers for individual channels, (c) determine the optimum fiber/PM device interface, and (d) evaluate the trade–offs involved in using a 1mm thick versus a 1.5mm thick scintillator sheet.

b. **Develop the Data Acquisition Architecture:** The primary purpose of this proposal is to determine the feasibility of the FITCAL concept. Accordingly, the thrust of the electronics research and development

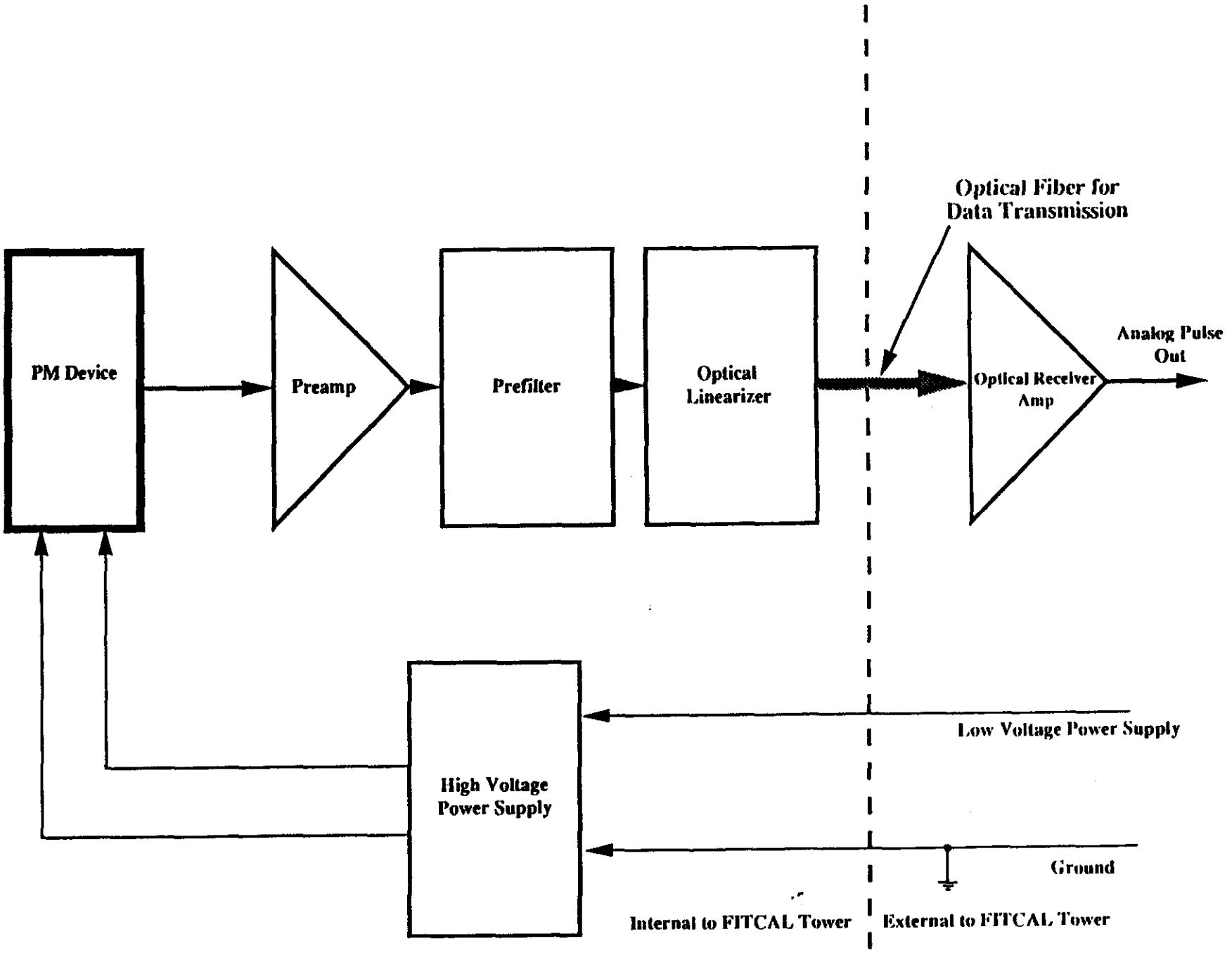

Proposed Front End Electronics for the FITCAL Calorimeter
FIGURE V.I

will be toward those issues that directly impact the performance and construction of FITCAL. We do not propose at this time to develop a new complete architecture for calorimetry data storage. Instead, we intend to address only those issues that pertain uniquely to FITCAL. Specifically, we will research the optical analog data transmission concept with respect to linearity, power dissipation, noise, radiation hardness, and manufacturability. After evaluation of the FITCAL measurements, we will research the optimum pulse shaping and storage for enhancing both count rate and signal-to-noise performance. A preamplifier, prefiliter, optical linearizer, and optical receiver amplifier will need to be researched and developed to exhibit the highest possible speed and linearity. These will probably be a mixture of custom CMOS and bipolar technologies. An area of interest to several types of detectors needing to store analog signals prior to qualification by the level one trigger is analog memory. We are planning to develop a fast, linear, arrayable analog memory cell that will allow high-fidelity storage of analog signals prior to analog/digital conversion. The basic concept is illustrated in (Figure V.2).

High voltage necessary for the PM device will be generated at the tube rather than distributing high voltage from outside the tower. We are presently generating high-voltage for another project using a custom CMOS analog controller developed at Oak Ridge National Laboratory. This controller uses very low power and can generate from 500V to 2000V with some external components. Therefore, only a low voltage power supply level will have to be distributed throughout the tower. Some further development of this controller throughout the tower be undertaken to adapt it to the specific needs of FITCAL.

c. Evaluate Photomultiplier Devices: An evaluation of multi-anode PM tubes will be made to determine the must appropriate choice in terms of anode crosstalk for the scintillator/fiber combination we will be using. Tubes from three vendors will be purchased and evaluated: 64 channel device from Amperex (Model No. XP4702), a 16 or 64 anode tube made by Hamamatsu (Series No. R1712), and a 100 channel device from ITT. In addition, we will explore the possibility of using the new emerging technology of solid state photomultiplier devices currently being developed by Rockwell, Inc., Burle Industries, and RCA.

d. Fabricate, Assemble and Test Data Acquisition Electronics for EM1 Section: Data acquisition electronics for the first EM section will be fabricated, assembled and installed. This assembly will then be tested in an actual beam at a location to be determined.

3. Phase II (Year 2)

a. Fabricate, Assemble and Test Electronics for EM2, HA1, and HA2: Work in the second year will build upon work already done. In addition, we will plan to instrument the second EM section

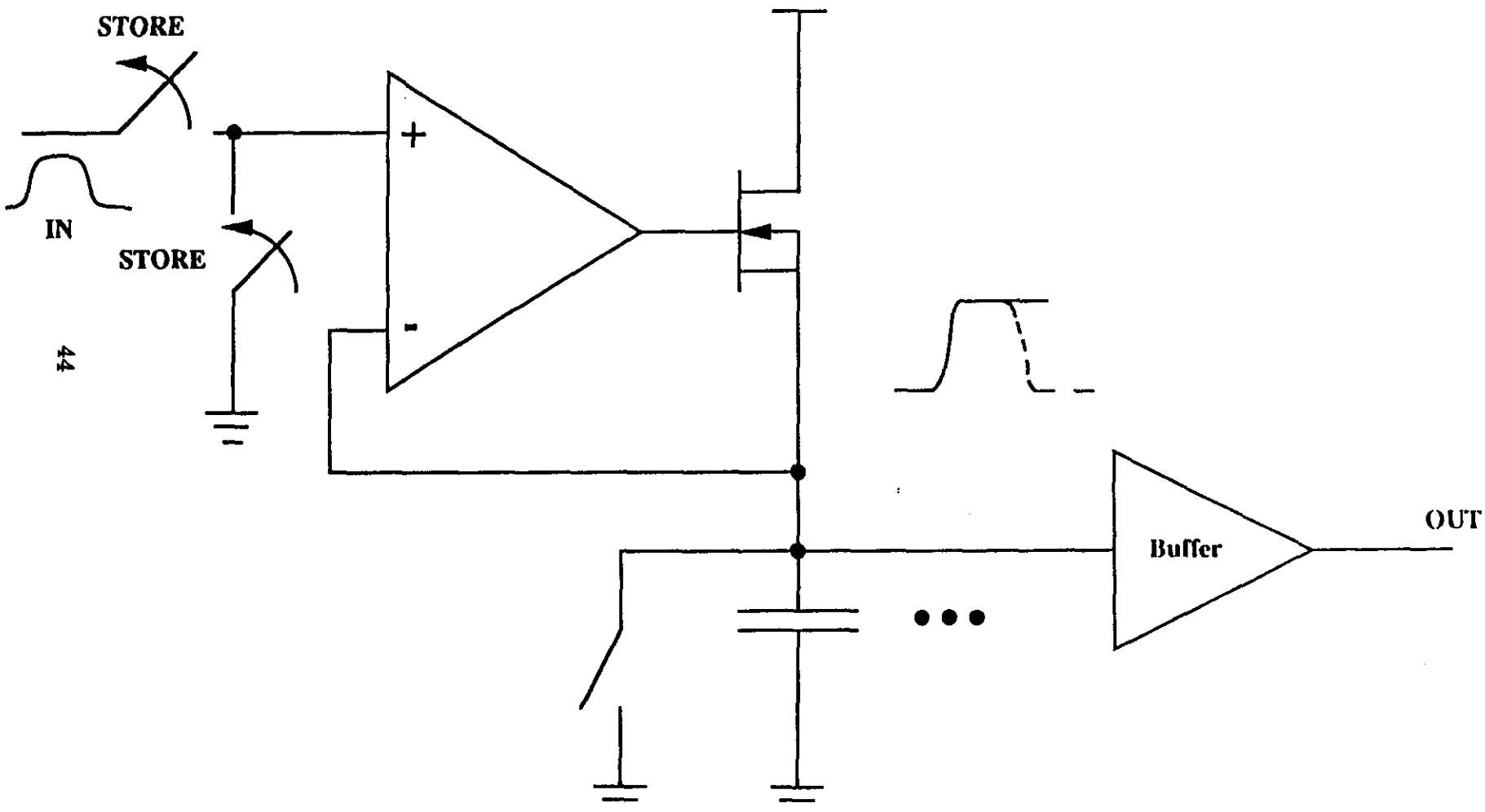

Analog Storage Cell
FIGURE V.2

as well as the two HA sections. Rather than have separate architectures for the EM and HA sections, we plan to use the same general architecture for both to reduce the overall development effort. After all sections have been fabricated, we plan to assemble and instrument a complete tower for testing in a beam. The instrumentation used for this tower will be refined and subsequently duplicated for other towers planned for the third year. Preliminary investigations will be conducted into alternative architectures for digitizing the analog signal and processing the resulting digital information at the rear of the towers.

4. Phase III (Year 3)

   a. Fabricate, Assemble and Test Electronics for an Array of Towers: Work in the third year will involve the instrumenting of either nine or 16 towers that can be arranged in an array similar to the way they would be used in an SSC experiment. This array will then be tested in a beam. A manufacturing plan will be developed for the data acquisition system.

C. Calibration for Prototype Calorimeter Diagnostics

The readout electronics and the detector media in each segment must have the capability to be calibrated. The response of each detector segment, which includes each fiber as well as each scintillating sheet, must be calibrated with no disassembly of the calorimeter. An innovative light-pipe scheme is being proposed. Since this development is not yet proven, a more conservative alternative is also presented which uses an insertable radioactive source. Calibration of the scintillator sheet and the wavelength shifting fibers will be accomplished by illumination with an external source. Calibration of the fibers will be accomplished by illuminating, via fiber optic light pipes, a face plate that sits in the front of each segment (Figure V.3). The scintillator sheets will be tested by illuminating the edges via fiber optics (Figure V.4). It will be impossible to calibrate every single sheet of scintillator material due to being unable to get a source of illumination to every sheet. The approach taken will be to illuminate only sheets along the perimeter of the calorimeter. Calibration information gained in this way will be used for correcting the data as it is processed.

The wavelength-shifter fiber absorbs light in the 450 nm range and re-emits it in the 525 nm range. The calibration of the fiber paths will be by illumination of a face plate where all the fibers are terminated using light pulses at about 450 nm. This will test fiber fitness and conversion efficiency, fiber to PMT connection, and all the electronics. The light will be pulsed in the 5 nsec range to be comparable to the scintillator decay time. all fibers and channels will be illuminated. A nitrogen-pumped dye laser will have suitable optical and timing properties. The illumination will require fibers to be run from the rear of the tower to the face of each section. Large diameter (> 400 u) pure silica fibers should be used. It will probably take at least four fibers, lighting the corners of a frosted face plate, but may take more to achieve a semblance of uniformity. All the fibers will terminate in face plate made of a frosted plastic sheet. Fibers can be loose coupled, like

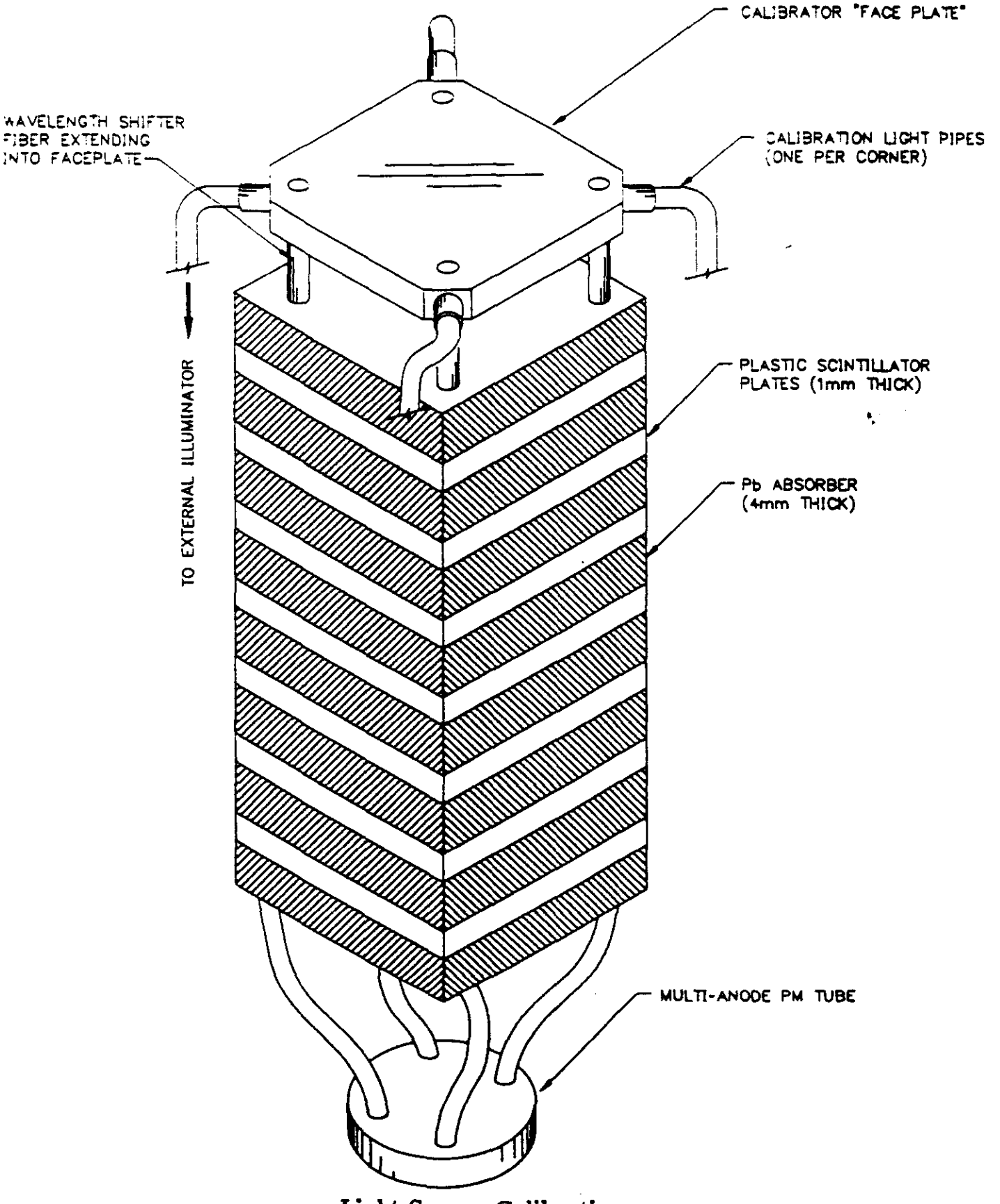

Light Source Calibration
FIGURE V.3

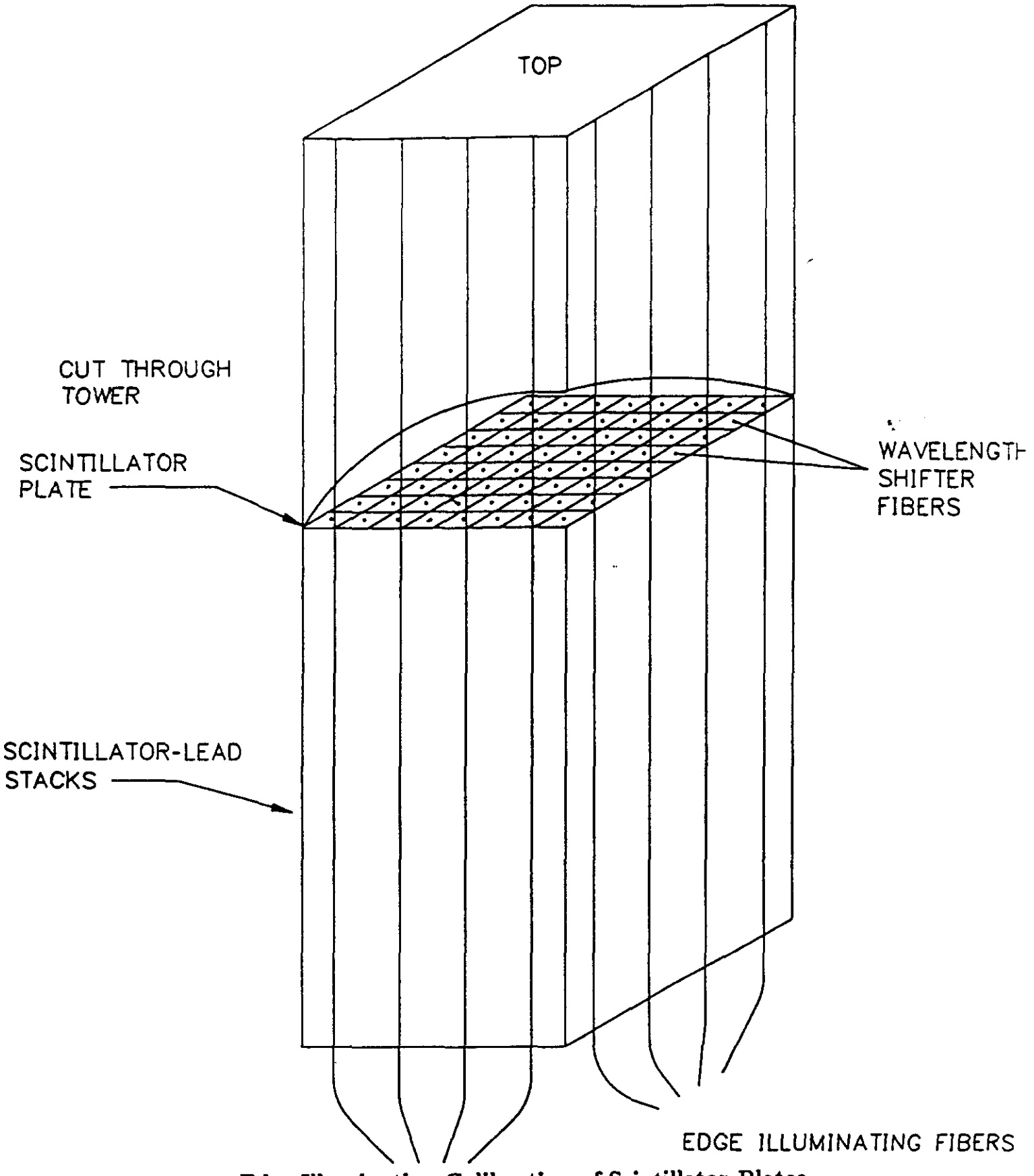

Edge Illumination Calibration of Scintillator Plates
FIGURE V.4

the scintillator stacks. The response of the wavelength-shifting fibers will be measured using the data acquisition electronics.

The scintillator-fiber will be tested by edge illumination of peripheral stacks of scintillator squares using 450 nm light piped to the scintillator plates. Use of 450 nm light will model the scintillations. It may also be feasible to test the scintillation properties of the plates if they can be illuminated with 360 nm light. This is possible, but may not be practical because the 360 nm light will be much harder to pipe and distribute. Large diameter silica fiber will suffice if the 360 nm illumination is not implemented. For the 360 nm pulsing, larger core (> 600 nm) UV-transmitting silica fiber will be required. It is proposed to only test the edge stacks using the technique, thus 28 fibers are required for the 8 x 8 EM sections. Evanescent (EM field in the cladding) coupling will be used to couple the light from the fiber to the scintillators. A coupling gel between the fiber and plate will probably suffice, but protective coatings must be stripped from the fiber first. Nitrogen-pumped dye lasers will be suitable for generating this light.

The use of high purity silica fibers will give an intrinsic radiation hardness to the light calibration system. Fibers with harnesses of greater than 10^7 rads are commercially available. The calibration process should allow for correction to radiation degradation effects of the scintillators and wavelength shifting fibers, as well as other aging processes. An alternative to the light-piped calibration is the use of a small gamma source, driven down guide tubes between towers. The source would illuminate whole sheets of scintillator and fibers from their edges (Figure V.5). Through the use of a small, moving source, each layer of scintillator could be checked, giving information on relative efficiencies from the front-to-back of a tower section. Because the scintillators would be edge illuminated, fairly high efficiencies could be attained. A source of 1 mCi of Cs-137, shot down the middle of the side of a tower would create 100 photons/second in a 2-cm.-square scintillator on the other side of a 16-cm.-square tower. A source this size would fit in a 3-mm-ID tube.

VI. Simulation of the Electromagnetic and Hadronic Cascades Including Light Collection in the High Resolution Fiber Tower Calorimeter

A. Background

In order to have a strong experimental calorimeter development program, a substantial effort must be involved in calculational analysis of the detector system. This calculational capability must be fundamentally sound and based on previous interchange between theoretical calculations and experimental test programs. The CALORS9 code system for analyzing calorimeters offers a solid approach for investigating all facets of detector systems and will be used in this work.

Due to financial constraints, only a few prototype detectors can be built and tested. However, once the calculated results have been shown to agree with the test program data, a much wider variation of the design can be calculationally investigated. This will be the approach followed in this proposal so as to maximize effort and minimize cost.

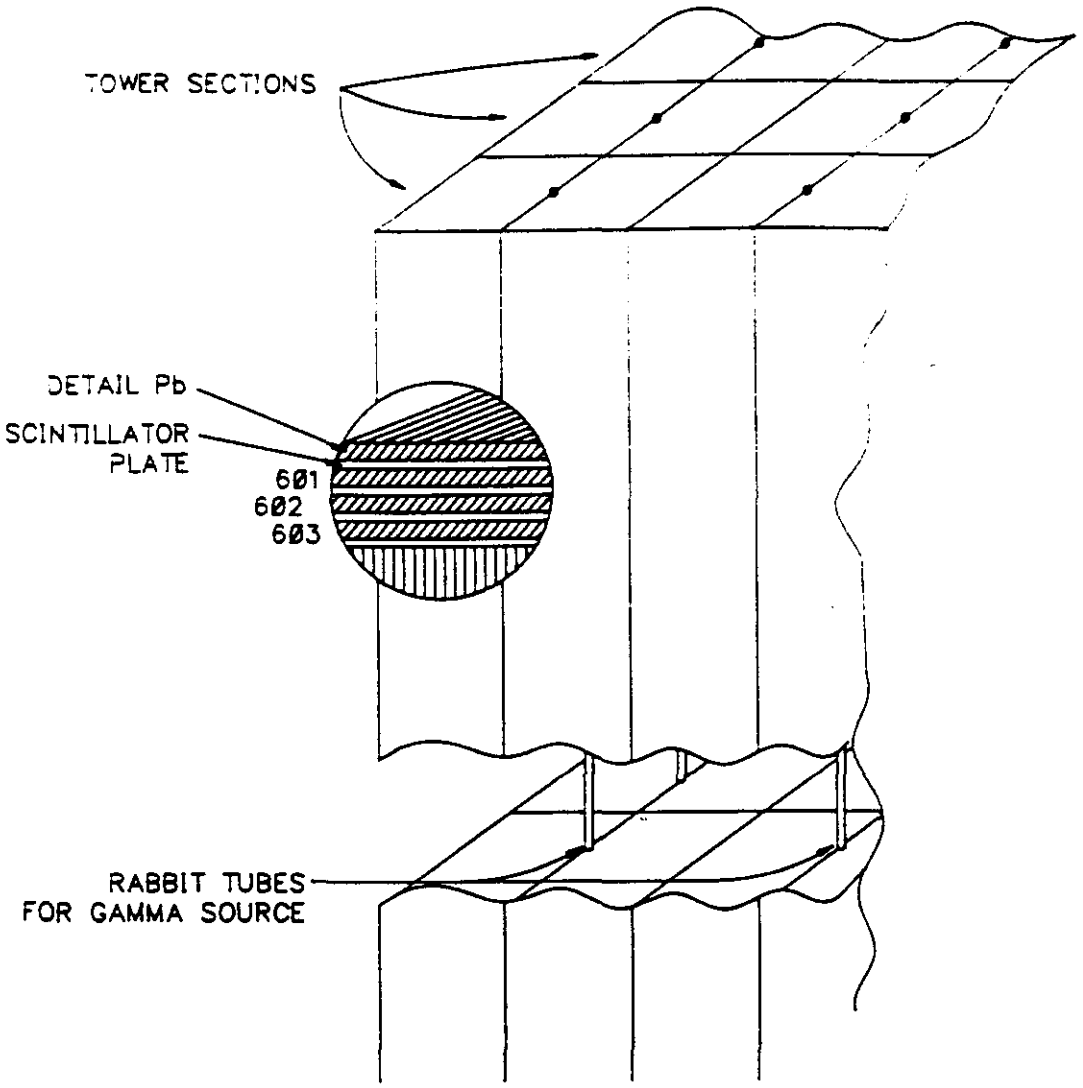

Gamma Source Calibration
FIGURE V.5a

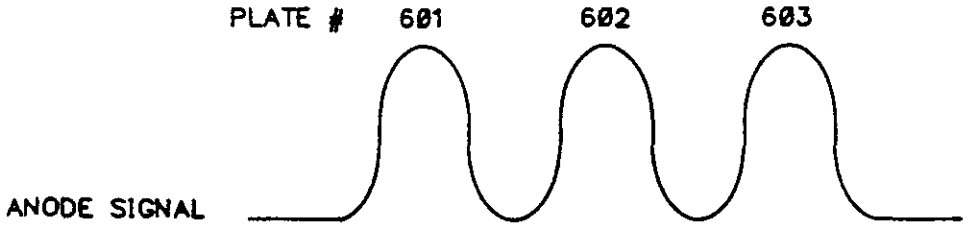

Signal from Individual Plates as the Source Traverses
FIGURE V.5b

B. Methods of Calculations

The calculations to be carried out in this proposal will be performed with the new CALORS9 computer system following approximately the procedures used in previous calculations.[1,2,3,4,5] The major changes in CALOR are in an improved high energy collision model following FLUKAS7 and a better low energy neutron transport by the code MICAP. A flow diagram of the codes in CALOR is given in Figure VI.1. The three-dimensional, multimedia, high-energy nucleon-meson transport code HETCSS[6,7,8] was used, with modifications, to obtain a detailed description of the nucleon-meson cascade produced in the absorbers considered in this paper. This Monte Carlo code takes into account the slowing down of charged particles via the continuous slowing-down approximation, the decay of charged pions and muons, inelastic nucleon-nucleus and charged-pion-nucleus (excluding hydrogen) collisions through the use of an intermediate-energy intranuclear-cascade evaporation (MECC) model (E < 3 GeV), a scaling model (3GeV < E < 5 GeV), and a multi-chain fragmentation model (E > 3 GeV), and inelastic nucleon-hydrogen and charged-pion-hydrogen collisions via the isobar model (E < 3 GeV), and a fragmentation model (E > 3 GeV). Also accounted for are elastic neutron-nucleus (E < 100 MeV) collisions, and elastic nucleon and charged-pion collisions with hydrogen.

The intranucelar-cascade-evaporation model as implemented by Bertini is the low energy (20-3000 MeV) heart of the HETC code.[9] This model has been usedd for a variety of calculations and has been known to agree quite well with many experimental results. The underlying assumption of this model is that particle-nucleus interactions can be treated as a series of two-body collisions within the nucleus and that the location of the collision and resulting particles from the collision are governed by experimental and/or theoretical particle-particle total and differential cross-section data. The types of particle collisions included in the calculations are elastic, nonelastic and charge exchange. This model included in the calculations are elastic, nonelastic and charge exchange. This model incorporates the diffuseness of the nuclear edge, the Fermi motion of the bound nucleons, the exclusion-principle, and a local potential for nucleons and pions. The density of the nuetrons and protons within the nucleus (which is used with the total cross sections to determine the interaction locations) are determined from the experimental data of Hofstadter.[9] Nuclear potentials are determined from these density profiles by using a zero-temperature Fermi distribution. The total well depth is then defined as the Fermi energy plus 7 MeV. Following the cascade part of the interaction, excitation energy remains in the nucleus. This energy is treated by using an evaporation model which allows for the emissions of protons, meutrons, d, ^3He, α, *and* t. Fission, induced by high-energy particles, is accounted for during this phase of the calculation by allowing it to compete with evaporation. Whether or not a detailed fission model is included has very little effect on the total number of secondary neutrons produced.

In recent years, a large amount of experimental and theoretical work has been done, and more reliable models are now available for the description of high energy (>5-10 GeV) hadron-proton and hadron-nucleus collisions. In particular, a multi-chain fragmentation code by J. Ranft, et al.,[10] following the work of A. Capella and J. Tran Thanh Van.[11] The version of the model that is used in the work reported here, with some modifications, is that provided by the transport code FLUKAS7. The modifications that have been

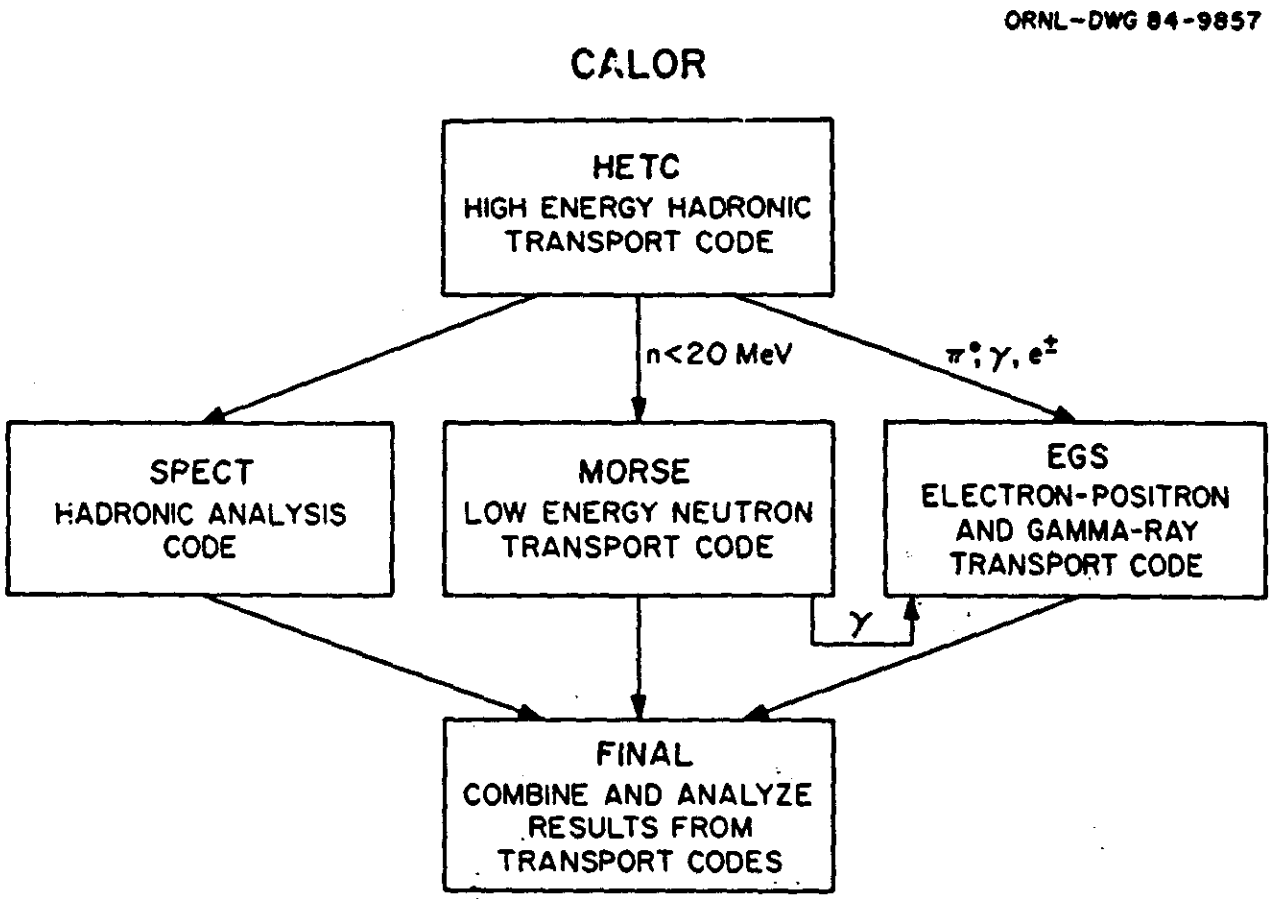

Flow Diagram of the CALOR System
FIGURE VI.1

made are mostly those necessary to predict such things as residual nuclei and excitation energies.[12] This information is needed in HETC for evaporation calculations which yield the production of low-energy neutrons, protons, deuterons, alpha particles, etc.

At high energies, a complete intranuclear cascade does not develop when a nucleon is hit by a hadronic projectile inside the nucleus. The time-scale governing typical hadronic interactions is very long, and therefore, the most energetic secondaries are actually produced as the jet decays beyond the target nucleus, and therefore, have no change of re-scattering.

EVENTQ is the hadron-nucleus collision code taken from FLUKA. In this code, a simplified Monte Carlo model is used in which no tracking or cascading of particles occurs. Fragmentation of the produced jets is carried out with possible formation of 180 stable particles or resonances.[13] The resonances decay with either two-body isotropic decay or three-body decay. Experimental decay products and branching ratios are input[14] to the code so that all quantum numbers are conserved. In this way, exclusive events are generated, and correlation studies can be carried out. All particles produced in the fragmentation of the jets are assumed not to interact with the nucleus.[15,16] Cascade style nucleons are sampled from data tables.

The source distribution for the electromagnetic cascade calculation is provided by HETC; it consists of direct photon production from hadron-nuclear collisions, photons from neutral pion decay, electrons and positrons from muon decay (although this is usually not of interest in calorimeter calculations because of the long muon lifetime), de-excitation gamma rays from nonelastic nuclear collisions and fission gamma rays. Since the discrete decay energies of the de-excitation gammas are not provided by HETC and only the total available energy until it is completely depleted. The transport of the electrons, positrons, and gammas from the above sources is carried out using EGS system.[17]

Neutrons which are produced with energies below 20 MeV are transported using the MORSE[18,19] or MICAP[20] Monte Carlo transport codes. The neutron cross sections used by MORSE or MICAP are obtained from ENDFB/V. Gamma rays (including those from capture, fission, etc.) produced during this phase of the calculations are stored for transport by the EGS code. The MORSE code was developed for reactor application. The MICAP code was developed specifically for detector analysis. Both codes can treat fissioning systems in detail. This ability is very important since a majority of the fissions results from meutrons with energies less than 20 MeV. Time dependence is included in MORSE and MICAP, but since neither HETC nor EGS has a timing scheme incorporated, it is generally assumed that no time passes for this phase of the particle cascade. Therefore, all neutrons below 20 MeV are produced at $t + 0$. General time cuts used in the MORSE or MICAP codes are 50ns for scintillator and 100ns for TMS or Argon.

The nonlinearity of the light pulse, L, in scintillator due to saturation effects is taken into account by the use of Birk's law[21]

$$\frac{dL}{dx} \propto \frac{dE/dx}{1 + k_B de/dx} \ ,$$

where k_B is the saturation constant. For plastic scintillator k_B is generally between 0.01– and 0.02–g cm^2 MeV^{-1}. A similar law is assumed to apply to the charge collected in ionization detectors. This takes into account the loss of signal resulting from recombination effects int he ionization column.[22] For electrons at all energies, it is assumed that $k_B = 0$.

Efficient collection of scintillation light produced by the energy deposition of a charged particle (or of wavelength shifted light) is important in the overall performance of a scintillator detector system. The detection efficiency is determined by many factors including the geometry of the modular section, the index of refraction of the scintillatory material and external material (usually air) which determines the internal reflection efficiency of the phototubes, and the size of the phototubes. The MORSE[18] Monte Carlo code has been modified to include all of the above factors so that accurate scintillation light transport can be carried out. This code will be referred to as MORLIGHT.

A simplified flow of the calculations is as follows:

1. Determine the wavelength group of the scintillation photon.
2. Determine the direction of the photon from an isotropic distribution.
3. Determine the flight path distance from ϵ^{λ}, where λ is the inverse absorption length for the group.
4. If the total path distance is completed before the next boundary is encountered, kill the photon (no downscatter or wavelength change allowed in current calculation, but can be included).
5. If the next boundary encountered is not the phototube boundary, determine angle of incidence and compare to critical angle.
6. If the angle of incidence is less than the critical angle, kill the photon (leakage).
7. If the angle of the incidence is greater than the critical angle, then continue transport after reflection until the path length is completed or the photon reaches the phototube. (Kill the photon as in statement 4.)
8. If the photon reaches the phototube, determine the probability that the photon will produce a photoelectron. If an electron is produced, score and kill the photon, otherwise, just kill the photon.
9. Start at statement 1. again.

Several modifications to the above procedure currently implemented in MORSE will have to be carried out in order to study the light gathering characteristics of the plastic towers connected to a single light shifter fiber. For example, changes will have to be made to include the conversion probability of the light shifter when the scintillator light enters the fiber.

C. Design Calculations

Part of the geometry of a FITCAL module is given in Figure VI.2. This represents two segments of a much larger system. The scintillation light from each of the scintillators is read out by a 1 mm diameter fiber wavelength shifter passing through holes in the lead and plastic plates. The depth and width of the calorimeter will be chosen so as to contain a typical high energy hadronic shower.

The design calculations will be used to confirm or adjust the 4 to 1 ratio of Pb to plastic thickness for compensation with the Pb/plastic calorimeter. In addition, the effect of streaming will be investigated. The energy resolution and compensation of the calorimeter as a function of energy will also be calculated. In general, the CALOR code system will be used to determine the optimum design of the Fiber Tower Calorimeter (FITCAL) with respect to energy resolution and compensation. The initial FITCAL design will be analyzed in detail and appropriate changes made. As experimental data become available, changes in the code system will be made to remove any discrepancies.

As part of this analysis, the light collection efficiency must be included in the calculation. The MORLIGHT code will be modified and data added so that scintillation light transport can be carried out in the plastic towers. The data that are necessary for such calculations include frequency distribution of the emitted scintillation light, the number of scintillation photons emitted per 100 eV of energy deposition, the light absorption characteristics and index of refraction of the scintillator, the conversion probability of light in the wavelength shifter fibers, the light absorpotion characteristics of the light guides (fibers), phototube conversion efficiency, etc. Much of these data are available and cannot be easily obtained, realistic data based on past experience will be substituted. Since there are variations in the types of data needed, some sensitivity studies will be carried out. The final results of the MORLIGHT calculations will be a spatial and energy deposition dependent light collection efficiency including fluctuations. By varying the light absorption characteristics of the plastics scintillator and the light guides, levels of radiation damage can be simulated so that performance degradation can be studied. These data will be used in the electromagnetic and hadronic cascade calculations.

VII. Test Beam Program

The proposed test beam program is in two parts:

A. Phase I

Prototype electromagnetic calorimeters will be constructed and tested for resolution, uniformity, and linearity. To study the constant term in the energy resolution, an electron beam energy of at least 100 GeV is required. The beam energy resolution must be $\leq 1\%$ for this purpose and the intensity should be in the range of 10^2 to 10^6 particles per second. Beam energy should be 1 to 6 GeV. The initial tests for the electromagnetic calorimeter can be performed at Brookhaven National Laboratory (BNL). We expect to use a total of three weeks of BNL beam time in three periods of a week each.

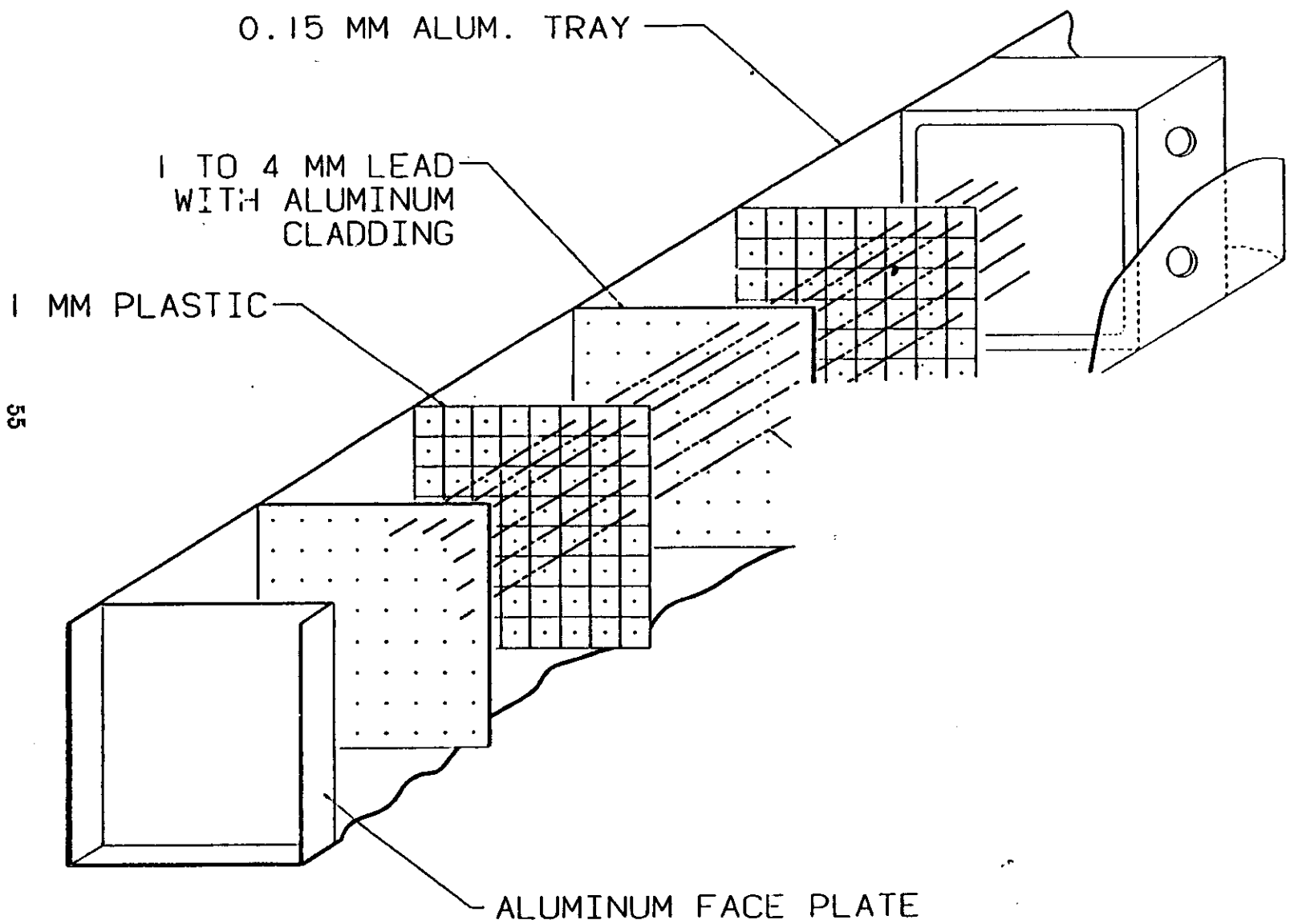

Unit Cells in a FITCAL Calorimeter

B. Phase II

High energy tests of the electromagnetic calorimeter will be performed at FERMILAB. Beam energy from 5 to 250 GeV will be required and the beam must be fully instrumented. The full electromagnetic plus hadronic calorimeter will be tested. Electron pion separation techniques will be investigated. Hadronic resolution and linearity will be studied. The ratio of lead to scintillator will be varied to explore the compensation mechanism and also its time dependent structure. We expect to use four weeks of FERMI beam time in four periods of a week each.

VIII. MILESTONES AND SCHEDULES

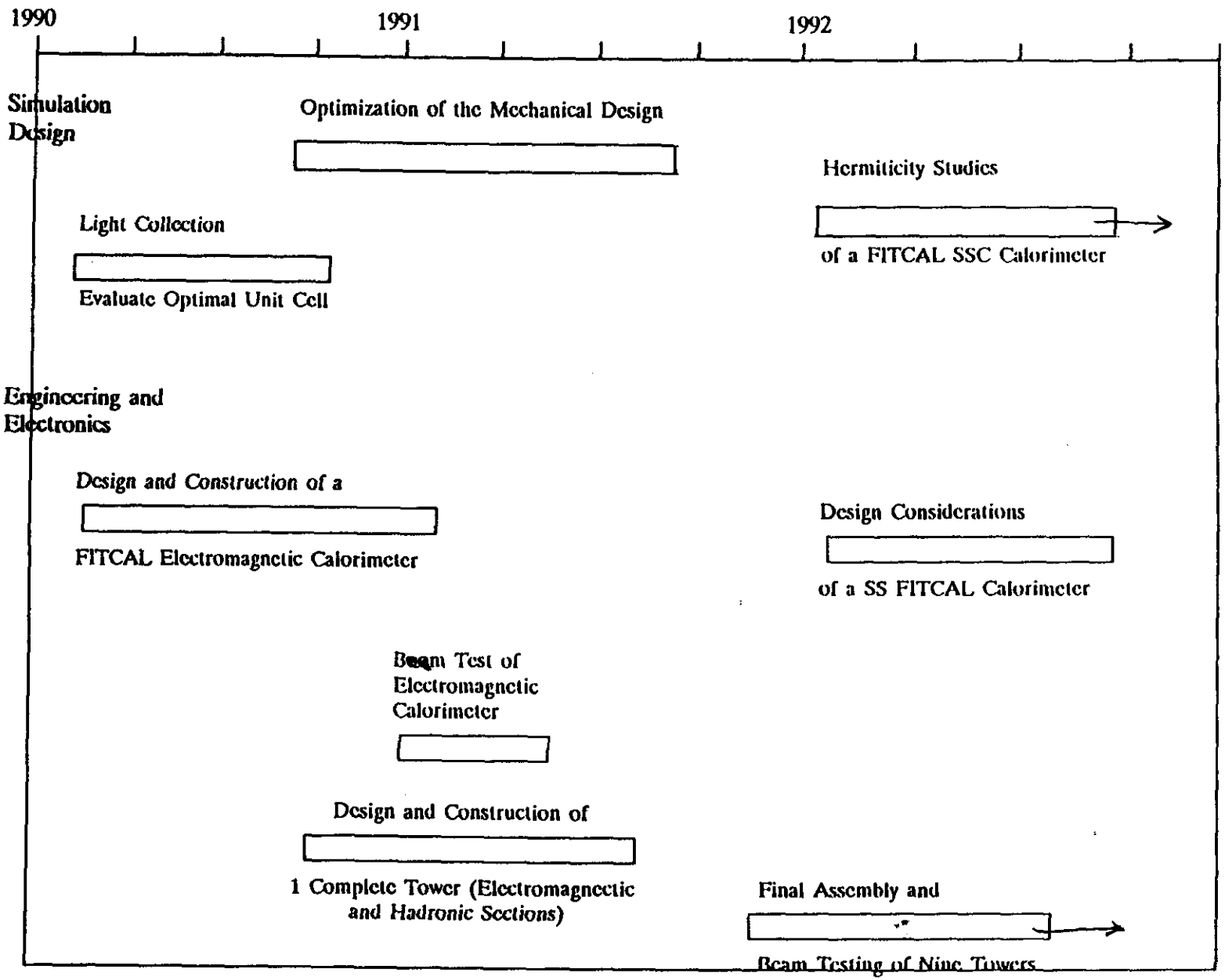

IX. Budget Discussion

The proposed budget is summarized by year and by institution in the following Table. Detailed budgets are given for each collaborating institutions in Tables 2 through 16.

TABLE 1
Budget Summary

	1990	1991	1992
University of Florida	$ 321,673	$ 337,757	$ 353,840
University of Sherbrooke	$ 86,720	$ 91,056	$ 95,392
Oak Ridge National Laboratory	$1,370,200	$1,261,500	$1,540,500
TOTAL:	$1,778,593	$1,690,363	$1,989,732

TABLE 2
Detailed First Year Budget (1990)

University of Florida - (1990)

1. Salaries		
a. Research Scientist (Assistant)	$ 40,000	
b. Two Post Doctoral Associates @ $28,000 ea.)	$ 56,000	
c. Technician	$ 22,000	
d. Two Graduate Students	$ 21,000	
		$ 139,000
Overhead (at 24% of a., plus c.; 2.1% of b.)		$ 16,050
2. Material		
a. Photosensitive Device Evaluation	$ 20,000	
b. Plastic Scintillator for Tests	$ 5,000	$ 25,000
3. Equipment		
a. Fast Electronics for Light Output	$ 20,000	
		$ 20,000
4. Travel		
a. Two per month to ORNL at $350 ea.	$ 8,400	
b. One per month to collaboration meeting at $500 ea.	$ 6,000	
c. One per two months for SSC meetings at $600 ea.	$ 3,600	
d. Beam Tests at $10,000	$ 10,000	
		$ 28,000
Total Direct Costs:		$ 228,050
Modified Total Direct Costs:	$ 208,000	
Overhead at 45% of MTDC:	$ 93,623	$ 93,623
TOTAL:		**$ 321,673**

TABLE 3
Detailed First Year Budget (1990)

University of Sherbrooke - (1990)

1. Salaries		
a. C. Carrier, Res. Assist.	$ 20,000	
b. One Engineer	$ 28,000	
c. Graduate Student	$ 10,000	
		$ 58,000
Overhead (at 24% of a. and b.)	$ 9,120	
		$ 9,120
2. Material		
a. Scintillator samples, sources and miscellaneous	$ 5,000	
		$ 5,000
3. Equipment		
a. Components for amp. construction and testing	$ 5,000	
		$ 5,000
4. Travel		
a. One per month to collaboration meeting at $500 ea.	$ 6,000	
b. One per two months for SSC meeting at $600 ea.	$ 3,600	
		$ 9,600
TOTAL:		$ 86,720

TABLE 4
Detailed First Year Budget (1990)

Oak Ridge National Laboratory - (1990)
Engineering and Design

1. Fabrication

   a. The first fabrication will be composed of the E1 and E2 longitudinal segments only. It will require many of the developments of fabrication methods for lead and plastic layers. Component handling and assembly procedures will be worked out in this model.

Short Stack Aluminum Container:	100 MH	$ 5,000	
Lead Layers (60 ea.):	500 MH	$ 25,000	
Plastic Layers (30 ea.):	500 MH	$ 25,000	
Assembly:	500 MH	$ 25,000	
			$ 80,000

   b. The full tower will expand on the engineering and experimental lessions learned in the short stack.

Full Tower Aluminum Container:	150 MH	$ 7,500	
Lead Layers (300 ea.):	750 MH	$ 33,000	
Plastic Layers (150 ea.):	500 MH	$ 25,000	
Assembly:	1000 MH	$ 80,000	
Subtotal:			$ 425,500
Contingency (25%):			$ 106,000
Programmer (Includes Computing and Overhead:			$ 120,000
Subtotal:			$ 651,500

TABLE 5
Detailed First Year Budget (1990))

Oak Ridge National Laboratory - (1990)
Instrumentation and Controls

Labor (2 man-years)

1. Material

a. 1 Amperex PM Tube ($7,500 ea.)	$ 7,500	
b. 1 Hamamatsu PM Tube ($6,000 ea.)	$ 6,000	
c. ITT PM Tube	$ 12,000	
d. ASIC Fabrication	$ 50,000	
e. Components	$ 10,000	
f. PC Board Layout and Fabrication	$ 15,000	
g. Miscellaneous	$ 10,000	
Subtotal:		$ 275,500
Indirect (40%):		$ 110,200
Subtotal:		**$ 385,700**
Scintillator Acquisition:		$ 333,000
TOTAL ORNL:		**$1,370,200**

TABLE 6
Detailed Second Year Budget (1991)

University of Florida - (1990)

1.	Salaries		
	a. Research Scientist (Assistant)	$ 42,000	
	b. Two Post Doctoral Associates @ $28,000 ea.)	$ 58,800	
	c. Technician	$ 23,100	
	d. Two Graduate Students	$ 22,050	
			$ 145,950
	Overhead (at 24% of a., plus c.; 2.1% of b.)		$ 16,853
2.	Material and Equipment	$ 47,250	$ 47,250
3.	Travel and Tests	$ 29,400	$ 29,400
	Total Direct Costs:		$ 239,453
	Modified Total Direct Costs:	$ 218,453	
	Overhead at 45% of MTDC:	$ 98,304	$ 98,304
	TOTAL:		**$ 337,757**

TABLE 7
Detailed Second Year Budget (1991)

University of Sherbrooke - (1991)

1. Salaries		
a. C. Carrier, Res. Assist.	$ 21,000	
b. One Engineer	$ 29,400	
c. Graduate Student	$ 10,500	
		$ 60,900
Overhead (at 24% of a. and b.)	$ 9,567	$ 9,567
2. Materials and Equipment	$ 10,500	$ 10,500
3. Travel	$ 10,500	$ 10,500
TOTAL:		$ 91,056

TABLE 8
Detailed Second Year Budget (1991)

Oak Ridge National Laboratory - (1991)
Engineering and Design

1. Engineering

   a. The primary engineering goal of the second year will be the fabrication of the complete nine tower prototype.

a. Engineering: 1 man year			
b. Drafting: .25 man years		$ 150,000	$ 150,000
TOTAL:			**$ 576,000**

2. Fabrication

   a. Fabrication and assembly of a nine tower assembly. This assembly will be based on the technology developed for the single tower.

Aluminum Containers:	600 MH	$ 30,000	
Structural Frame:	600 MH	$ 30,000	
Lead Layers (3000 ea.):	3000 MH	$ 100,000	
Plastic Layers (30 ea.):	3000 MH	$ 100,000	
Assembly:	1500 MH	$ 75,000	
Total for Nine Tower Fab.:			$ 335,000
Contingency (25):			$ 121,000
Programmer (Includes Computing and Overhead):			$ 120,000
Subtotal:			**$ 726,000**

TABLE 9
Detailed Second Year Budget (1991)

Oak Ridge National Laboratory - (1991)
Instrumentation and Controls

Labor (2 man-years)

1. Material

a. ASIC Fabrication	$ 35,000	
b. Components	$ 20,000	
c. PC Board Fabrication	$ 15,000	
d. PM Tubes (2 additional)	$ 15,000	
Subtotal:		$ 258,250
Indirect (40%):		$ 103,300
Subtotal:		**$ 361,550**
Scintillator Acquisition:		$ 174,000
TOTAL:		**$1,261,500**

TABLE 10
Detailed Third Year Budget (1992)

University of Florida - (1992)

1. Salaries			
a. Research Scientist (Assistant)		$ 44,000	
b. Two Post Doctoral Associates @ $28,000 ea.)		$ 61,600	
c. Technician		$ 24,200	
d. Two Graduate Students		$ 23,100	
			$ 152,900
Overhead (at 24% of a., plus c.; 2.1% of b.)			$ 17,655
2. Material and Equipment		$ 49,500	$ 49,500
3. Travel and Tests		$ 30,800	$ 30,800
Total Direct Costs:			$ 250,855
Modified Total Direct Costs:		$ 228,855	
Overhead at 45% of MTDC:		$ 103,985	$ 103,985
TOTAL:			$ 353,840

TABLE 11
Detailed Third Year Budget (1992)

University of Sherbrooke - (1992)

1. Salaries		
a. C. Carrier, Res. Assist.	$ 22,000	
b. One Engineer	$ 30,800	
c. Graduate Student	$ 11,000	
		$ 63,800
Overhead (at 24% of a. and b.)	$ 10,032	$ 10,032
2. Materials and Equipment	$ 11,000	$ 11,000
3. Travel	$ 10,560	$ 10,560
TOTAL:		$ 95,392

TABLE 12
Detailed Third Year Budget (1992)

Oak Ridge National Laboratory - (1992)
Engineering and Design

1. Engineering

   a. In the final year of the proposal, we will evaluate the nine tower assembly, begin preliminary design for the full-scale SSC detector, and make modifications to the test prototype.

a. Engineering: 2 man years	$ 270,000	
b. Drafting: 1 man years	$ 120,000	
TOTAL:		$ 390,000

2. Fabrication

a. Miscellanous	$ 150,000	
Subtotal for Year Three:		$ 540,000
Contingency (25):		$ 135,000
Subtotal:		$ 120,000
Subtotal:		**$ 795,000**

TABLE 13
Detailed Third Year Budget (1992)

Oak Ridge National Laboratory - (1992)
Instrumentation and Controls

Labor (2 man-years)

1. *Material*

a. ASIC Fabrication	$ 35,000	
b. Components	$ 30,000	
c. PM Tubes for Eight Towers	$ 240,000	
Subtotal:		$ 496,500
Indirect (40%):		$ 199.000
Subtotal:		**$ 695,500**
Scintillator Acquisition:		50.000
TOTAL ORNL:		$1,540,500

X. References

REFERENCES FOR SECTIONS I. AND II.

1. T. A. Gabriel, 'Detectors for the Superconducting Super Collider Design Concepts and Simulation', to be published in the proceedings for the Workshop on Calorimetry for the Superconducting Super Collider, University of Alabama, (March 13-17, 1989). J. E. Brau and T. A. Gabriel, 'Theoretical Studies of Hadronic Calorimetry for High Luminosity, High Energy Colliders,' Nucl. Ins. and Methods in Physics Research, A279 (1989) 40-56, North Holland Amsterdam.
2. R. Wigmans CERN/EF 86-18.
3. E. Bernardi, et al., DESY 87-041.
4. B. Musgrave, Internal Note, Argonne National Laboratory, July, 1989.
5. M. Dennek, Internal Note, Argonne National Laboratory, July, 1989.
6. Calorimetry Group Report, Physics for the SSC, Snowmass, p. 355, 1986 and references given therein.
7. J. K. Walker, Report presented at BNL, Workshop on SSC Detectors, July, 1989.
8. H. Gordon and P. Grannis, Snowmass, p. 541, 1984.
9. M. D. Petroff, M. G. Stapelbrock, W. A. Kleinhaus, Appl. Phys. Lett., Vol 51, No. 6 (Aug. 1987), 406.
10. M. D. Petroff and M. Atac, to be published in Proc. of 1988, Nucl. Sci. Symposium.
11. M. Atac, private communication to Jimmy K. Walker.
12. F. Capano, J. Allam, et al., IEEE Trans. Electron Devices, ED-30, 381 (1983).
13. Recent Results in Scintillation Detection with Silicon Avalanche Photodiodes, R. Lecomte, C. Markel and C. Carrier, NIM 278 (1989), p. 585. These results were with APD type RCA, C30994. Our new results are with developmental RCA APD's.

REFERENCES FOR SECTION III. AND IV.

1. B. Loehr, et al., 'An Electromagnetic Calorimeter with Wavelength Shifting Fiber Readout,' Hamburg, DESY 86-072.

REFERENCES FOR SECTION V., VI. AND VII.

1. T. A. Gabriel, et al., 'Compensation Effects in Hadron Calorimeters,' IEEE Trans. Mucl. Sci. NS-32, 1 (1985).
2. J. E. Brau and T. A. Gabriel, SLD – New Detector Note No. 119, May 22, 1984.
3. J. E. Brau, 'A Monte Carlo Investigation of Compensation in Uranium Calorimeters,' Proceedings of the September 1984 Seattle Meeting of the SLD Collaboration.

4. T. A. Gabriel, 'Codes, Models, and Cross Sections for Use in Analyzing Compensated Calorimeters,' Proceeduings of Workshop on Compensated Calorimetry, Pasadena (1985) CALT-68-1305.

5. J. Brau and T. A. Gabriel, 'Monte Carlo Studies of Uranium Calorimetry,' Nucl. Instrum. & Methods Vol. A238, p. 487, 1985.

6. T. A. Gabriel, 'The High Energy Transport Code HETC,' Oak Ridge National Laboratory, ORNL/TM-9727, 1985.

7. T. A. Gabriel, et al., 'CALOR87: HETC87, MICAP, EGS4, and SPECT, A Code System for Anaylzing Detectors for Use in High Energy Physics Experiments,' Proceedings of the Workshop on Detector Simulation for the SSC, Argonne National Laboratory, August 24-28, 1987.

8. The latest HETC code will be referred to as HETC88.

9. H. W. Bertini, Phys. Rev. Vol. 188, p. 1711, 1969.

10. P. A. Aarnio, et al., CERN TIS Divisional Report, TIS-RP/106-ReV, 1984.

11. A. Capella and J. Tran Thanh Van, Phys. Letts. Vol. 93B, p. 2, June, 1980.

12. F. S. Alsmiller, et al., 'Low-Energy Particle Production and Residual Nuclei Production from High-Energy Hadron-Nucleus Collisions,' Proceedings of Conference on Theory and Practices in Radiation Protection and Shielding, Knoxville, Tennessee, April 22-24, 1987.

13. S. Ritter and J. Ranft, Acta Physica Polonica Vol. B11, 1980.

14. K. Hanbgen and S. Ritter, Karl-Marx Universitat, Leipzig, DDR, KMU-HEP 8301.

15. R. G. Alsmiller, Jr., et al., 'Modifications of the High-Energy Transport Code (HETC) and Comparisons with Experimental Results,' Proceedings of Conference on Theory and Practices in Radiation Protection and Shielding, Knoxville, Tennessee, April 22-24, 1987.

16. R. J. Glauber, Lectures in Theoretical Physics, Ed. W. E. Brittin and L.G. Dunham, Vol 1, (Interscience, NY), 1959.

17. R. L. Ford and W. R. Nelson, SLAC-0210, 1978.

18. M. B. Emmett, Oak Ridge National Laboratory, ORNL-4972, 1975.

19. N. M. Greene, et al., Oak Ridge National Laboratory, ORNL/TM-3706, 1973.

20. J. O. Johnson and T. A. Gabriel, Oak Ridge National Laboratory, ORNL/TM-10196, 1987.

21. J. B. Birks, Proc. Phys. Soc. Vol. A64, p. 874, 1951.

22. A. Babaev, et al., Nucl. Instrum. & Methods Vol. 160, p. 427, 1979.

XI. PERSONNEL LIST

Paul Avery has been a member of the CLEO collaboration since 1980. and has been a faculty member at the University of Florida since 1985. He has had extensive experience performing detector simulations and is currently studying the performance of silicon vector detectors.

Martin Bauer is a member of the Instrumentations and Controls Division at Oak Ridge National Laboratory (ORNL). Presently, he is a group leader of the Sensor System Development Group doing work in the area of radiation detection and environmental monitoring instrumentation. He has expertise in electron beam, optical sensing, and signal processing technologies, extensive experience in analog and digital design, and process measurement systems, as well as expertise in the area of fiber optic systems and radiation effects on materials.

Barbara Bishop is a member of the Computing and Telecommunications Division assigned to the Engineering Physics and Mathematics Division at ORNL. A major part of her current effort is in calculations involved with radiation transport. She also has experience in radiation damage calculations. A large part of her professional career recently has been involved with using the CALOR code system at ORNL.

Hugh Brashear has been head of the Research Instruments Section (RIS) for the past eight years at ORNL. This Section has a staff of approximately seventy professionals engaged in applied research, development, design, and fabrication of nuclear instrumentation for the experimental community, applied health physics and related scientific fields.

Christian Carrier has studied the light collection from high refractive index scintillators with avalanche photodiodes (APD) through theoretical modelisation and Monte Carlo simulation. He is currently investigating the performance of APDs with miscellaneous scintillators for potential applications in nuclear medical imaging, nuclear physics and high energy physics.

Tony Gabriel is currently a Senior Research Staff member in the Engineering Physics and Mathematics Division at ORNL. He has been involved with the analysis of high energy physics detector systems for the last twenty years. The CALOR89 code system, HETC88, SPECT89, EGS4, MORSE, MICAP, and LIGHT which was developed as part of this reserach is one of two major codes recommended for the SSC detector research. Major understandings of the physics of calorimetry has resulted from the utilization of CALOR89.

Julie Harmon, Chief Materials Research Chemist at Nanoptics, Inc. and Associate Research Scientist at the University of Florida. She obtained her Ph.D. at the University of Rochester. She holds patents in the area of dye/polymer interactions and has worked as a Research Scientist in the industry of polymer physics.

Roger Lecomte of the University of Sherbrooke has been involved with the development of scintillation detectors based on avalanche photodiodes (APD) for

applications in medical imaging over the last seven years. His contributions include the design of adequate electronics for APD detectors and the optimization of detectors performance for low energy radiation detection and fast coincidence timing measurements. He is currently investigating the first large–scale implementation of APD detectors in positron emission tomography.

Robert McIntyre is with RCA Victor Research Laboratories in Montreal where he helped establish a solid state physics laboratory. During this period he was involved in building semiconductor characterization equipment, developing transistor equivalent circuits, and long wavelength infrared detector development and characterization (dope silicon and germanium).

He has extensive expertise in the avalanche effects in silicon and the initiation and termination of microplasmas in avalanching diodes. He has worked on the development of new photodetectors, specifically silicon PIN and avalanche photodiodes for use in optical communications, silicon APD arrays, and avalanche photodiodes for use with fiber optics.

Mark Rennich has designed research and development hardware for twelve years with an additional four years of industrial experience in the plastics industry. he has been the lead engineer on a wide range of experimental equipment design projects, including extensive commercial vendor involvement, special materials, and precision machining. Professional experiences with applicability to the SSC detector engineering including the design of calorimeter structures for the WA80 project (CERN) and the calorimeter/absorber No. 4 accelerator, the design of test bed assemblies for the advanced laser isotope separation process for Lawrence Livermore Laboratory, and the design of a refrigeration test loop in conjunction with the National Bureau of Standards.

James Walker has worked on many high energy experiments in Europe and the United States. At present, he is a member of the DO collaboration at Fermilab. He has consulted with the plastic scintillator industry over a twenty–five year period.

Andrew White, a Research Scientist at the University of Florida, serves as co–spokesperson on the DO experiment at Fermilab, with responsibilities in the areas of detector construction and the study of the physics signals for Supersymmetry in the DO detector. He has also been responsible, with Paul Avery, for the establishment of the powerful VAX multiprocessing computer system and its use on the DO experiment. In addition, he has been studying the issues involved in the design of future detectors for the SSC.

John Yelton obtained his Ph.D. from Oxford University in 1981, with his thesis work taking place at the CERN intersecting Storage Rings. He has worked with the MARK II collaboration operating at the PEP electron–positron collider. He returned to Oxford to analyze data from the TASSO detector at DESY, and building apparatus for the DELPHI experiment now running at the LEP electron–positron collider at CERN. He came to Florida in 1987 as an Assistant Professor and has been studying charmed particle production with the CLEO collaboration at the Cornell Electron Storage Rings.

APPENDICES

DESY 86-072
FTUAM-EP-86-04
July 1986

ISSN 0418-9833

AN ELECTROMAGNETIC CALORIMETER WITH WAVELENGTH SHIFTING FIBER READOUT

B. Loehr

Deutsches Elektronen-Synchrotron DESY, Hamburg

S. Weinzierl

Universität Hamburg, II.Institut für Experimentalphysik

F. Barreiro, E. Ros

Universidad Autónoma de Madrid

ABSTRACT

We investigate the response of an electromagnetic calorimeter using wavelength shifting fibers for the readout. The calorimeter is a sandwich of lead and scintillator plates and the fibers are inserted in holes perpendicular to the plates. We study in particular light yields, uniformity of response and energy resolution. We also present a Monte Carlo interpretation of our experimental results.

Typeset by AMS TEX

I) INTRODUCTION

A characteristic of the detectors planned for the electron proton collider HERA [1], presently under construction at DESY, is the use of large calorimeters. They have to be compact, cover a large solid angle, and present a high granularity in the readout. The energy and angular resolution of the calorimeter determines to a great extent the performance of the whole detector.

As part of the design studies for the ZEUS detector [2] at HERA, we have constructed and tested several electromagnetic calorimeter modules with an optical fiber readout system, in order to investigate the energy resolution, uniformity of the response and photoelectron yield. Other experimental results on the same subject can be found in reference [3].

II) DESCRIPTION OF THE MODULES AND EXPERIMENTAL SETUP

Each calorimeter module is a sandwich of 70 lead plates and 70 scintillator plates (see a schematic drawing in fig.1). The thickness of the lead plates is 2 mm and the thickness of the scintillator plates is 5 mm. The total size of a module is $19 \times 19 \times 49$ cm^3, the total length in 25.8 radiation lengths and the Moliere radius about 6 cm.

The light produced in the scintillator is collected by 16 optical fibers connected via a piece of lucite lightguide to a photomultiplier placed at the rear of the calorimeter. These fibers are inserted in 16 holes of 2 mm diameter drilled perpendicularly to the plates. We used optical fibers [4] of 1.5 mm diameter containing a wavelength shifting agent. They consist of a polystyrene core (refractive index: 1.59) doped with 400 mg/l of K 27 [5] and a cladding of Polymethylmetacrylat (PMMA, refractive index: 1.46). The average fiber length was 120 cm. We used two scintillator materials, *KSTI-390* [6] and *SCSN-38* [7]. The edges of the plates were polished and the plates themselves wrapped in reflective aluminum foil. The surfaces of the holes in the scintillator were not polished after drilling. The module equipped with the *KSTI-390* scintillator will be referred to in the following as module A, and the one equipped with SCSN-38 as module B. Module A had a photomultiplier Valvo 56DVP and module B an XP2011. Table I summarizes the description of both calorimeters.

These modules were tested in a DESY test beam which provided electrons from 1 to 5 GeV. The momentum spread of this beam was found to be at most 3% from a measurement with a BGO crystal. The modules were installed on a remotely controlled moveable support allowing the impact point of the incident beam on the calorimeter to be varied. The trigger was defined with the help of two pairs of crossed scintillation counters defining a beam size of 5×5 mm^2 at the front face of the calorimeter. A veto counter with a central hole of 2 cm diameter was used to reject beam halo particles. The experimental setup in the beamline is shown in fig.2. The photomultiplier signal was integrated by a LeCroy ADC 2249A with a gate time of 140 ns. The ADC output was read into a NORD computer and transferred to the DESY IBM for offline analysis.

III) LINEARITY AND RESOLUTION AT THE CENTER OF THE MODULE

We measured the response of the 2 calorimeter modules to incident electrons of 1 to 5 '. The main results are summarized in table I. The calorimeter response and resolution function of the energy for an incident beam at the center of the module are displayed in res IIIa and IIIb. Both modules show a linear response with deviations less than 1% for gies in the range between 1 and 5 GeV.

The measured resolutions suggest an energy dependence of the type :

$$\frac{\sigma}{E} = \frac{a}{\sqrt{E}} \oplus b \qquad (\oplus \text{ means the square root of a quadratic sum})$$

fitted values for both calorimeters are (for E in GeV):

$a = (13.1 \pm 0.8)\%$ and $b = (2.2 \pm 1.4)\%$ for module A,

$a = (\ 8.6 \pm 0.3)\%$ and $b = (1.9 \pm 0.5)\%$ for module B.

constant term b is compatible with the beam resolution. The parameter a includes nly the resolution of the calorimeter due to sampling fluctuations and also the fluctuation to photoelectron statistics.

The contribution to the resolution due to fluctuations in the number of photoelectrons ased at the cathode of the photomultiplier (σ_{ph} in table I) has been determined by two rent methods. In the first one a grey filter is inserted between the light guide and photocathode and the pulseheight is consequently reduced by a factor f; then σ_{ph} is rmined according to the formula :

$$\sigma_{ph} = \sqrt{\frac{\sigma_2^2 - \sigma_1^2}{f - 1}}$$

re σ_2 and σ_1 are the resolutions with and without grey filter respectively. In the second thod, the pulseheight of a light emitting diode (L.E.D.), mounted in front of the tube, is ed to the same value as the calorimeter signal. Under the assumption that the L.E.D. ivers a stable light output during the measurement time, the width of the pulseheight dis- ution gives directly σ_{ph}. Both methods were checked against each other, giving compatible ults.

The measured resolutions are :

$\sigma_{ph} = (9.0 \pm 1.0)\%\sqrt{E}$ for module A,

$\sigma_{ph} = (5.6 \pm 0.3)\%\sqrt{E}$ for module B.

The contribution from sampling fluctuations to the resolution can be estimated using the ower Monte Carlo simulation program EGS [8]. In this program, the secondary electrons d photons are followed until they reach some minimal energies, normally 1.5 MeV and 0.1 eV respectively, and then all their energy is deposited. It turns out that the resolution and rage energy deposited in the scintillator depends on these cuts (see fig.10a). We have used

for these quantities the values which follow from extrapolating the cutoff energies to zero : $\sigma = 5.6\%\sqrt{E}$ and 18.9% of the incident electron energy deposited in the scintillator. They also correspond to a semi-infinite medium, but the Monte Carlo also predicts for our finite size calorimeter an energy leakage of 3.2%, mainly transverse and independent of the incident electron energy, and a fluctuation for this leakage of $1.3\%\sqrt{E}$ (see fig 10b). The resolution of the calorimeter is therefore the quadratic sum of the sampling and the leakage fluctuation :

$$\sigma_{EGS} = 5.8\%\sqrt{E} \qquad (E \text{ in GeV})$$

If we subtract quadratically the contribution of photoelectron statistics from the $\sqrt{E}$ dependent part of the measured resolution, we obtain a resolution (σ_{stoch} in table I) of $(9.5 \pm 1.5)\%\sqrt{E}$ for module A and $(6.5 \pm 0.5)\%\sqrt{E}$ for module B. The value for module B is compatible with the resolution predicted by EGS; for module A, however, an additional contribution is not excluded.

The number of photoelectrons per MeV of deposited energy in the scintillator can be calculated from the formula $\sigma_{ph}/E = 1/\sqrt{N_{ph}}$ and from the result given by EGS that the fraction of deposited energy in the scintillator is 18.3% once leakage is included. We obtain in this way 0.7 ± 0.2 photoelectrons for module A and 1.7 ± 0.2 for module B. We note that the thickness of the scintillator plates is such that a minimum ionizing particle deposits 0.9 MeV per plate at normal incidence and therefore produces 1.5 photoelectrons.

IV) UNIFORMITY OF THE CALORIMETER RESPONSE

Module B was scanned with an electron beam of 3 GeV along 3 horizontal lines between rows of fibers. The results are shown in figure 4. The calorimeter is found to be uniform in response within $\pm 1\%$, except in the proximity of a border where energy leakage becomes an important effect. In particular scans along the two symmetric lines shown in fig 4 give the same result within statistical errors.

We have also measured the calorimeter response when scanning across two neighbouring fibers in the center of the module. The results are shown in fig 5a and 5b. One can see that the response at the fiber positions is bigger than at the center of the calorimeter. The enhancement is of the order of 50% for the module equipped with the BSTI-390 scintillator and 20% for the one equipped with SCSN 38. All the pulseheight distributions have been normalised to 1 at the center of the module. Differences at the level of 10% between fibers are also observed.

To investigate the origin of the nonuniform calorimeter response near the fibers we performed scans across fiber positions under various conditions using the module B. Fig 6a shows the measured response for the following setups :

(1) module equipped with all 16 fibers (same as fig 5b)
(2) one fiber is pulled out
(3) all fibers but one are pulled out
(4) the scintillator plates are removed
and only one fiber stays in the calorimeter

By comparing the results of (1) to (3) one finds that the response at the fiber position
s the same shape independent of the number of fibers in the calorimeter. It is very well
scribed by a $1/r$ dependence, plus a constant term, r being the distance between the impact
int and the fiber position. In fig. 6b, which displays the data of setup (3), it is shown
at this dependence persists to large distances. At small distances, less than 1 cm, the
ower spread and the beam size produce a smearing of this $1/r$ behaviour. In setup (4) the
stribution of shower particles creating scintillation and Cerenkov light in the polystyrene
er is determined. This contribution to the total signal is found to be small. We note also
at a small signal enhancement persists at a fiber position even when the fiber has been
lled out. A possible explanation for this effect is that the collected light, coming from late
owering inside the hole, suffers less attenuation than in the case of normal showers.

V) EFFECT OF THE NON-UNIFORMITIES IN THE RESOLUTION

The energy resolution of the calorimeter depends on the impact position of the beam. We
ve analysed this dependence for module B. At the center of the calorimeter the resolution
s a $\sqrt{E}$ dependence plus a small constant term possibly due to a beam effect. At the fiber
osition, not only the average pulseheight is bigger than at the center but also the distribution
broader and exhibits a tail to higher values. This is shown in figures 9a and 9b. If we try
ain the fit (see fig.7):

$$\frac{\sigma}{E} = \frac{a}{\sqrt{E}} \oplus b \qquad \text{, we find a=10.3\% and b=5.3\%.}$$

he constant term is now significantly bigger than a possible momentum spread from the
am.

A larger calorimeter built in the same way as our test module can be regarded as being
mposed of successive reflections of one quadrant of the square formed by the innermost 4
bers as shown in fig. 8a. This is certainly an idealisation since different fiber qualities, cracks
etween modules and other effects also contribute to the nonuniformities in a real calorimeter.
order to determine the average resolution of such a calorimeter we have performed a scan
cross the regions 1,2,3 and 4 indicated in figure 8a with the 3 GeV electron beam. Any of
ese regions is representative of the response of the whole calorimeter and differences can
nly be attributed to the quality of the fibers themselves. This scan proceeded in steps of
mm as indicated in figure 8b. The result for the scanned regions and the corresponding
bers are summarized in figure 8c. We see in the case of fiber 1 for example, that there is a
5% increase in the signal at the fiber position with respect to the center of the calorimeter,
hereas this increase is only 3% averaged over the corresponding scanned region. Fig. 9c
hows the pulseheight distribution averaged over the indicated area in fig. 8a. In fig. 8d
e show the resolution at an energy of 3 GeV after subtracting the resolution at the center
hich is 5.4% at this energy. If we assume again an energy dependence for the resolution of
he type $\sigma/E=a/\sqrt{E}\oplus b$, as suggested by the measurements described previously, and take
or a the same value as in the center, this subtraction procedure gives directly the constant
. We find for example in region 1 a constant term of b=4% in addition to the beam effect
hich is also present at the center.

We note that a bad quality fiber can create around it a more uniform region than the average and then produces a smaller constant b, this is the case for fiber 4 and the reason why the constant b for the average of all 4 regions is only 2.6%.

We can conclude from these measurements that the resolution of the module B if the impact position is not known can be parametrized by :

$$\frac{\sigma}{E} = \frac{a}{\sqrt{E}} \oplus b$$

where a≈10% and b≈4% in the case where all fibers give a 25% increase with respect to the center of the calorimeter. It should be noted that the energy distribution is not a gaussian but shows a tail due to the nonuniformities. In case of non-gaussian distributions we have systematically taken the r.m.s. as resolution

VI) MONTE CARLO SIMULATION

In order to explain our experimental results we have performed a Monte Carlo simulation. This simulation uses the EGS code for shower development and a simulation for the light collection by the fibers (see ref.[9] for more details). The result of this Monte Carlo simulation is a probability for light collected by a single fiber of the type :

$$p(r) = a + \frac{b}{r} e^{-r/\lambda_0} \qquad (r > r_0)$$

where r is the distance between the fiber and the point where light is produced, r_0 is the hole radius and λ_0 is an effective attenuation length of light inside the scintillator (λ_0 ≈ 80 cm for SCSN-38). The parameter a can be interpreted as the contribution of light reaching the fiber after one or more reflections at a lateral surface of the plate, whereas the b term is the contribution of light reaching the fiber directly. The parameter b depends only on geometrical quantities like the hole radius r_0; for r_0= 1 mm we obtain b = 1.17% (r is in cm). However, a depends both on the reflectivity R at the surface of the plate and on λ_0; this dependence is shown in fig.11. The $1/r$ behaviour of light collection by a single fiber is in agreement with our data (see fig.6a and 6b). The Monte Carlo simulation can in fact reproduce the data of fig.6a with a=0.6% and assuming a uniform beam spot of 4×4 mm (see fig.12a). It includes also the contribution from particles hitting the fibers. This contribution was tuned in order to reproduce the data of setup 4 in fig.6a

When we go to the 16 fibers case, the parametrisation for the light probability is:

$$p = p_0 f(p_0) \qquad \text{with} \qquad p_0 = \sum_{i=1}^{16} w_i \left(a + \frac{b}{r_i} e^{-r_i/\lambda_0}\right)$$

f is a function which can be found in ref.[9] and accounts for the screening between fibers. a and b are the same as in the one fiber case, and r_i is the distance to hole i. Each fiber has a weight w_i; for practical purposes we will take w_i = 1 for all fibers. As a consequence each fiber

t a different a parameter. The module B data (see fig.5b) can be reproduced with the parameters as for the 1 fiber case by simply tuning the a parameter (see fig. 12b). The er response is reproduced with a =0.30% and the right fiber with a=0.57%. These suggest big differences in the response of individual fibers.

can calculate as a function of a the response at a fiber position P_f, at the center of lorimeter P_c, and for the average P_a, with the associated resolutions σ_f, σ_c and σ_a. quantities are plotted in fig.13. The resolutions are the constant terms obtained after the same way as for the data. The Monte Carlo prediction for a=0.5% is P_f/P_c=1.22, =1.02, σ_f/P_f=3.5% and σ_a/P_a=2.5%. All these values are in agreement with our We can also observe that the constant term in the resolution for the average signal, , falls below 1% only for very high values of a. We also note that smaller values of λ_s also smaller values of a and therefore higher values of P_f/P_c; this explains why module as uniform than module B since λ_s is smaller for KSTI-390 than for SCSN-38.

is also possible to include in the Monte Carlo the attenuation length λ_f along the We introduce in this way a new constant term in the resolution and deviations from ty. These deviations, after a linear fit in the range between 1 and 5 GeV, are smaller % even for values of λ_f as small as 40 cm (see fig.14a). In fig.14b the dependence of nstant term as a function of λ_f is shown. Our data for module B are compatible with e of λ_f greater than 60 cm; if λ_f is greater than 1 m, the constant term falls below 1%.

II) CONCLUSIONS

e have tested an electromagnetic calorimeter of the lead scintillator sandwich type with readout. We have considered two scintillator options : KSTI-390 and SCSN-38. We for both options 16 polystyrene fibers doped with K27 in a concentration of 400 mg/l.

he best resolution is achieved with the calorimeter equipped with SCSN-38 scintillator. resolution is σ=8.6%$\sqrt{E}$ at the center of the calorimeter, corresponding to 5.8%$\sqrt{E}$ sampling fluctuations and 5.6%$\sqrt{E}$ from photostatistics. This combination satisfies equirement of providing enough light (about 1.5 photoelectrons per minimum ionising le and plate).

owever the presence of fibers leads to nonuniformities in the response of the calorime- om a geometrical origin (the response varies like $1/r$ plus a constant, where r is the nce to the fiber). If the impact position at the calorimeter surface is not known, these niformities translate into a constant term in the expression of σ/E which is of the order for the test module considered. This constant term will dominate the resolution for ons above 6 GeV. Additional contributions to this constant term due to boundaries or uniform fiber density are also expected in a calorimeter as proposed in the ZEUS letter ent [2].

Acknowledgement

We gratefully acknowledge K. Westphal for taking care of the mechanical construction of the modules. We are very grateful for fiber material obtained from Saclay, France and Kyowa-Gas, Japan. We would like also to thank E. Hilger, H. Klanner, H. Kowalski, L. Labarga, G. Levman and G. Wolf for helpful discussions. This study was supported by the *Bundesministerium für Forschung und Technologie, Germany* and CAICYT, Spain. One of us (F.B.) would like to thank Prof. Brandt for his hospitality at Siegen University and the Deutsche Forschungsgemeinschaft for financial support

REFERENCES

[1] Experimentation at Hera, DESY HERA 83/20, October 1983
[2] ZEUS letter of intent, DESY, June 1985
[3] H.Fessler et al., NIM A240(1985)284
[4] Produced by J.C.Thevenin et al. at CEN Saclay
[5] Experimental product of Hoechst, Germany
[6] Product of KSH, Belgium
[7] Product of Kyowa Gas, Japan
[8] R.L.Ford, W.R.Nelson, Slac Report 210(1978), the version used is EGS3
[9] L.Labarga, E.Ros, Siegen University preprint SI 86 07

FIGURE CAPTIONS

Table I: Description of the modules and summary of the results

Fig. 1 : A schematic view of a calorimeter module

Fig. 2 : A schematic view of of the experimental setup

Fig. 3a: Linearity and resolution at the center of module A

Fig. 3b: Linearity and resolution at the center of module B

Fig. 4 : Result of a scan between rows of fibers for module B. The normalisation is taken he center of the module.

Fig. 5a: Result of a scan across two neighbouring fibers for module A. The normalisation aken at the center of the module.

Fig. 5b: Result of a scan across two neighbouring fibers for module B. The normalisation aken at the center of the module.

Fig. 6a: Investigation of the origin of nonuniformities. Several setups where one or more rs are missing are considered. The normalisation is taken at the center of the module en all fibers are in place.

Fig. 6b: Verification of the 1/r behaviour of the response close to a fiber. The data respond to the setup 3 of figure 6a.

Fig. 7 : Linearity and resolution at a fiber position for module B

Fig. 8a: Position of the four scanned regions inside the calorimeter. Any of them is presentative of the whole calorimeter response

Fig. 8b: A detail of the scan for region 1. This scan proceeds in 25 steps.

Fig. 8c: Response of the calorimeter in the four scanned regions and in average. The gnal is normalised to the value at the center of the calorimeter.

Fig. 8d: Resolution of the calorimeter in the four scanned regions and in average. The oted values result after subtracting quadratically the resolution at the center of the module means a quadratic subtraction).

Fig. 9a: Pulseheight distribution at the center of module B

Fig. 9b: Pulseheight distribution at the position of fiber 1 in module B. Note the tail to gh values.

Fig. 9c: Pulseheight distribution for the scanned region 1 in module B. Note again the il to high values.

Fig. 9d: Response of the calorimeter in the four scanned regions. This figure gives a etail of the pulseheight for each step of the scan.

Fig.10a: Energy resolution and average energy deposited in the scintillator, given by EGS r 1 GeV electron showers as a function of the cutoff energies of photons and electrons. These utoff energies are in units of the minimum values : 1.5 MeV for electrons and positrons and .1 MeV for photons.

Fig.10b: Average value and fluctuation of the leaked energy given by EGS as a function of the incident electron energy.

Fig.11 : Dependence of the a parameter on the reflectivity at the surface of the plate R and on the attenuation length of light in the scintillator λ_s.

Fig.12a: Comparison between the data and the Monte Carlo prediction for the 1 fiber calorimeter. The data correspond to setup 3 and 4 in fig 6a.

Fig.12b: Comparison between the data and the Monte Carlo prediction for the 16 fiber calorimeter. The data correspond to setup 1 in fig 6a.

Fig.13 : Monte Carlo prediction for the signal at center, at a fiber position and in average (P_c, P_f, P_a) and the corresponding constant terms in the resolution (σ_c, σ_f, σ_a) as a function of the a parameter.

Fig.14a: Monte Carlo prediction for the deviations from linearity due to the attenuation length λ_f along the fibers.

Fig.14b: Monte Carlo prediction for the constant term in the resolution due to the attenuation length λ_f along the fibers.

	Module A	Module B
number of fibers	16	16
diameter of fibers	1.5 mm	1.5 mm
fiber material	Polystyrene	Polystyrene
fiber doping	K27 400 mg/l	K27 400 mg/l
scintillator	KSTI-390	SCSN-38
diameter of holes in scintillator	2.5 mm	2.0 mm
phototube	56 DVP	XP 2011
$\sigma/\sqrt{E}$ (E in GeV)	13.1 ± 0.8 % ⊕ 2.2 ± 1.4 % $\sqrt{E}$	8.6 ± 0.3 % ⊕ 1.9 ± 0.5 % $\sqrt{E}$
method for photostatistics	grey filter	L.E.D.
$\sigma_{ph}/\sqrt{E}$ (E in GeV)	9.0 ± 1.0 %	5.6 ± 0.3 %
$\sigma_{other}/\sqrt{E}$ (E in GeV)	9.5 ± 1.5 %	6.5 ± 0.5 %
photoelectrons per Mev	0.7 ± 0.2	1.7 ± 0.2

Table 1

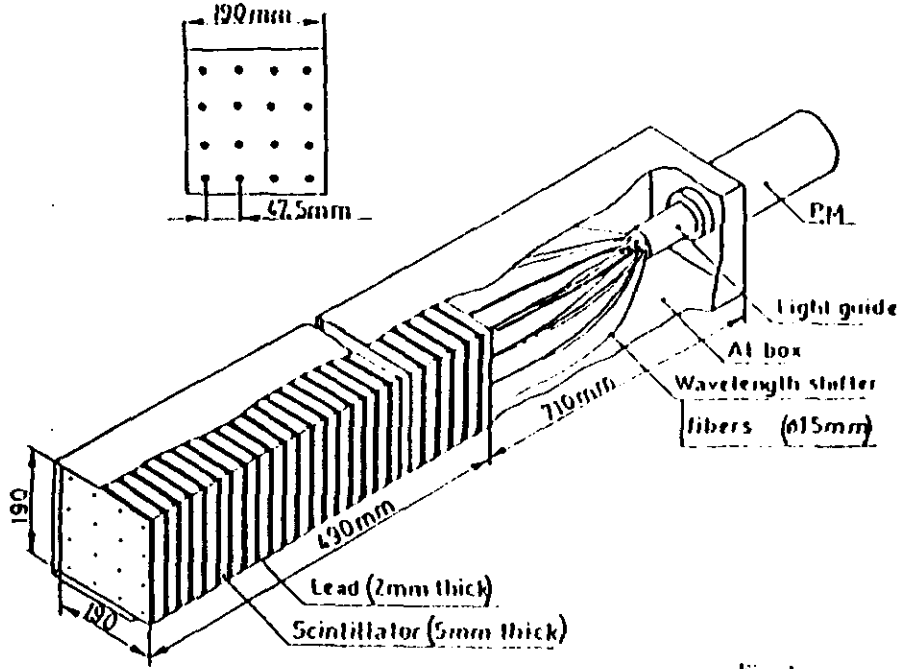

Fig. 1

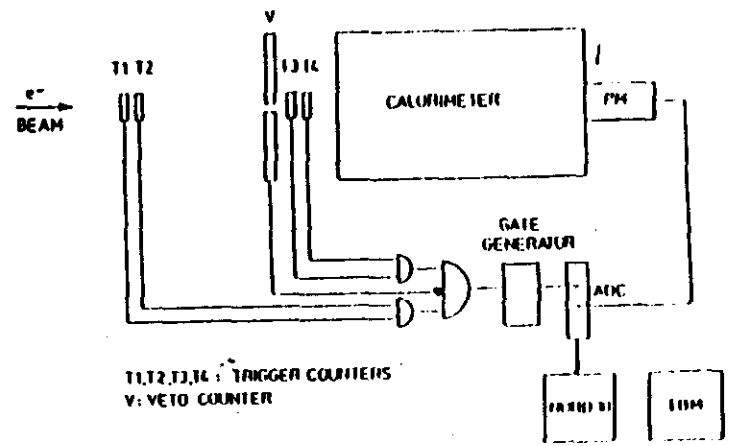

Fig. 2

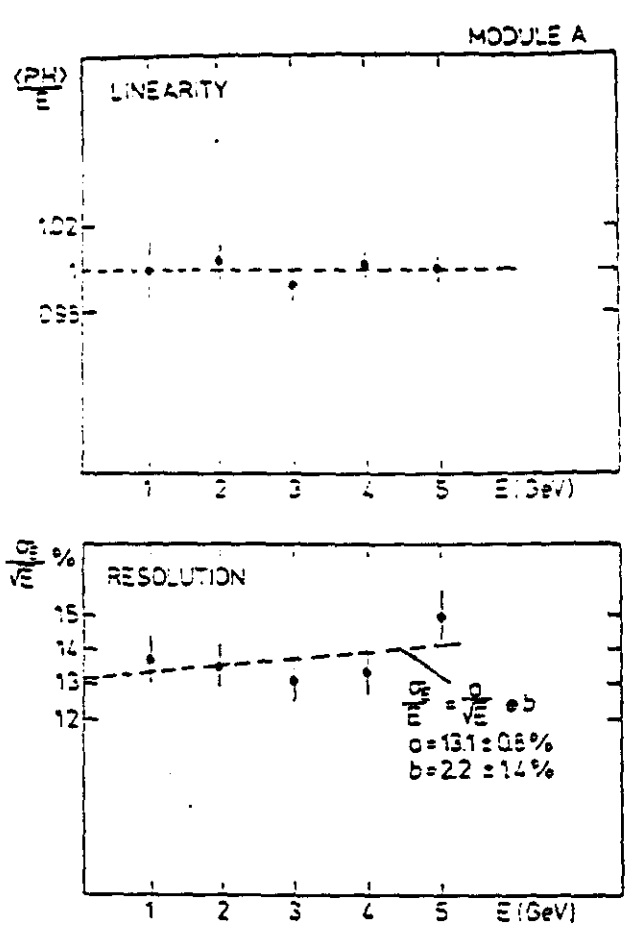

Fig. 3a

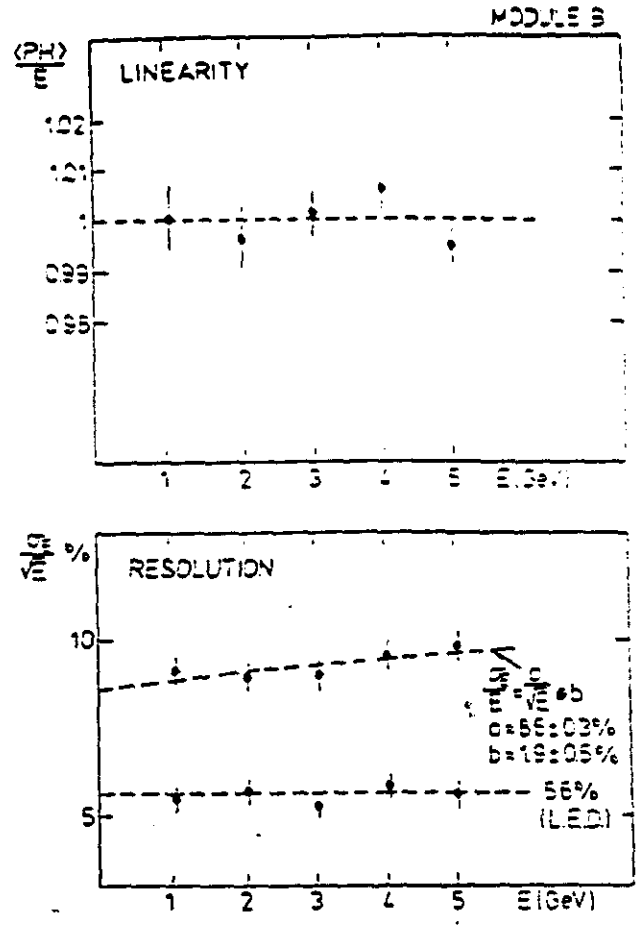

Fig. 3b

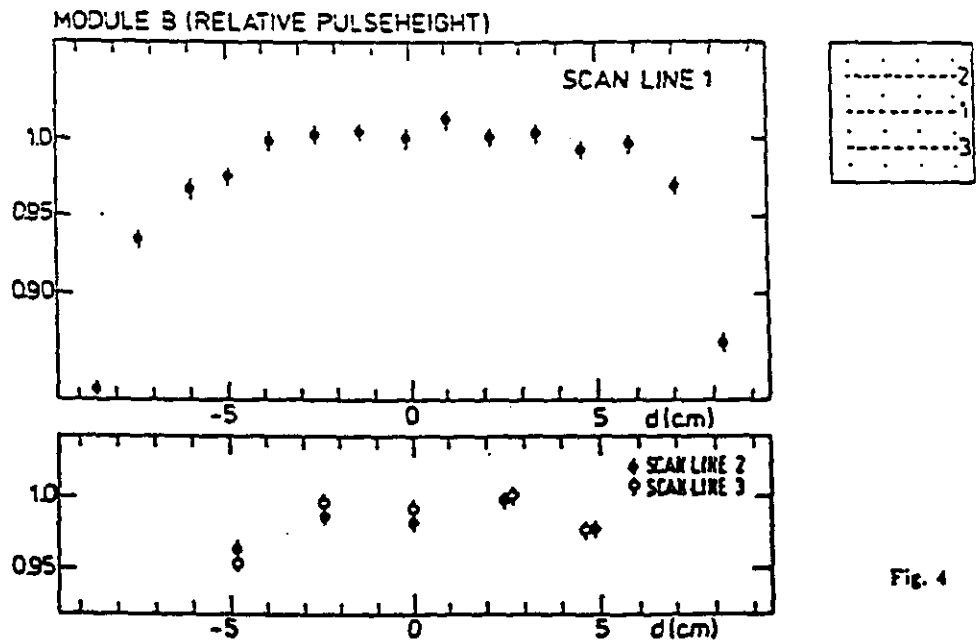

Fig. 4

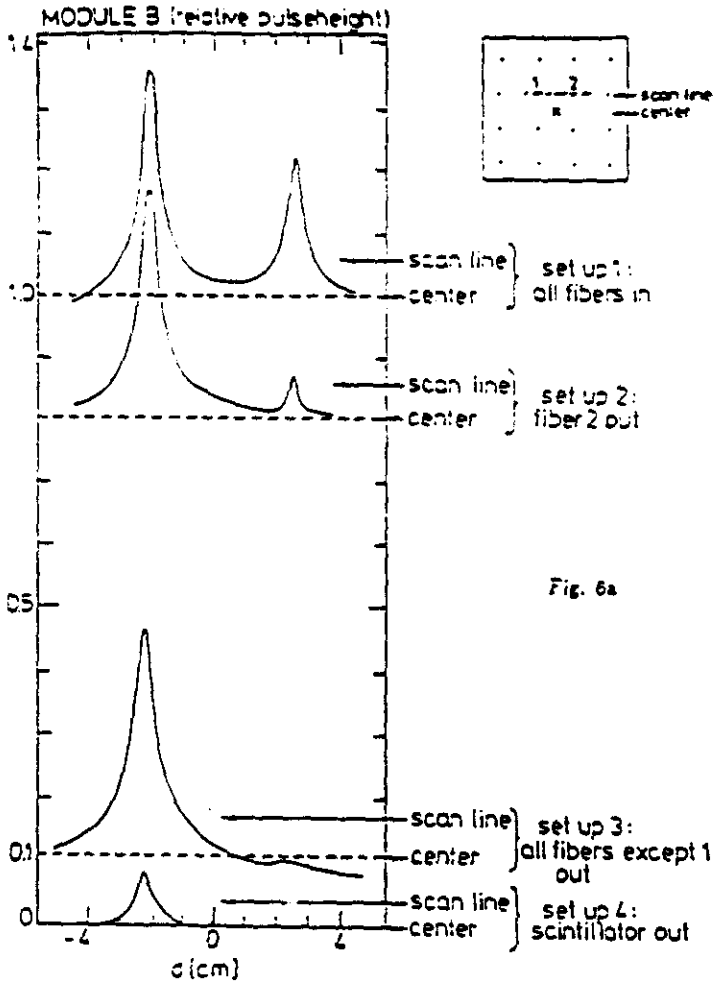

Fig. 6a

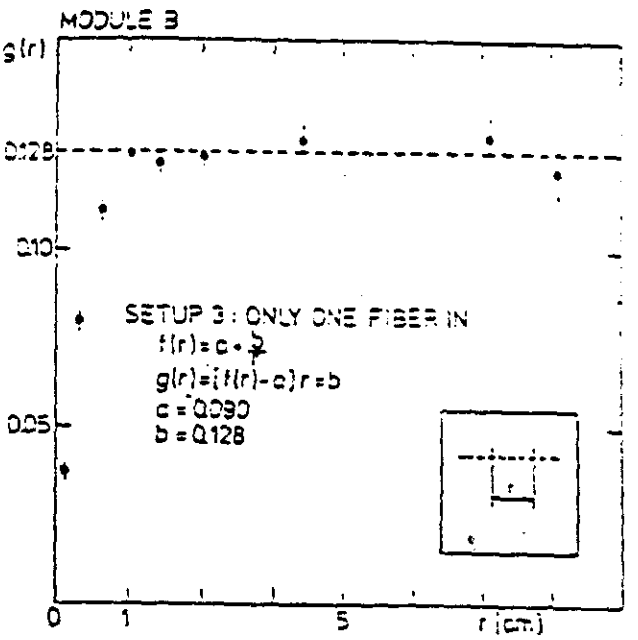

Fig. 6b

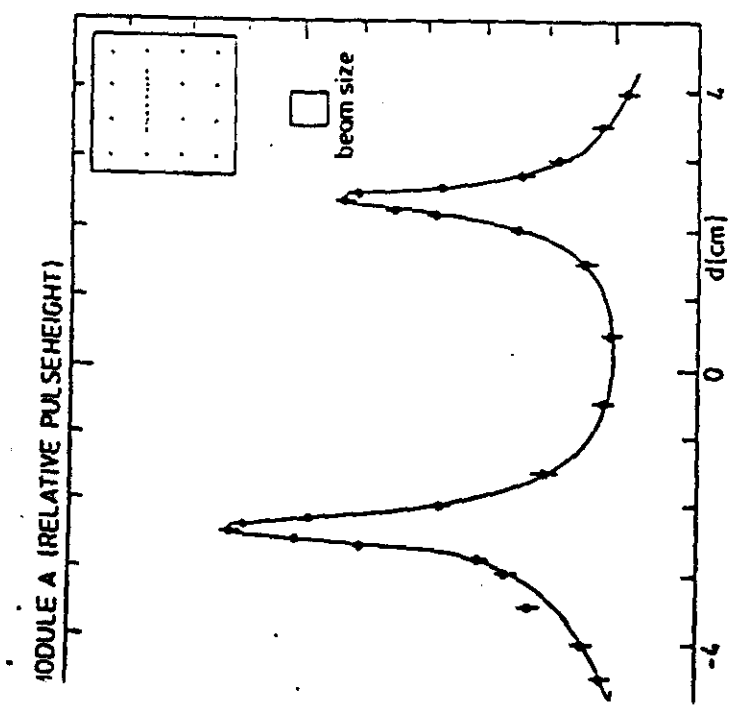

Fig. 5a

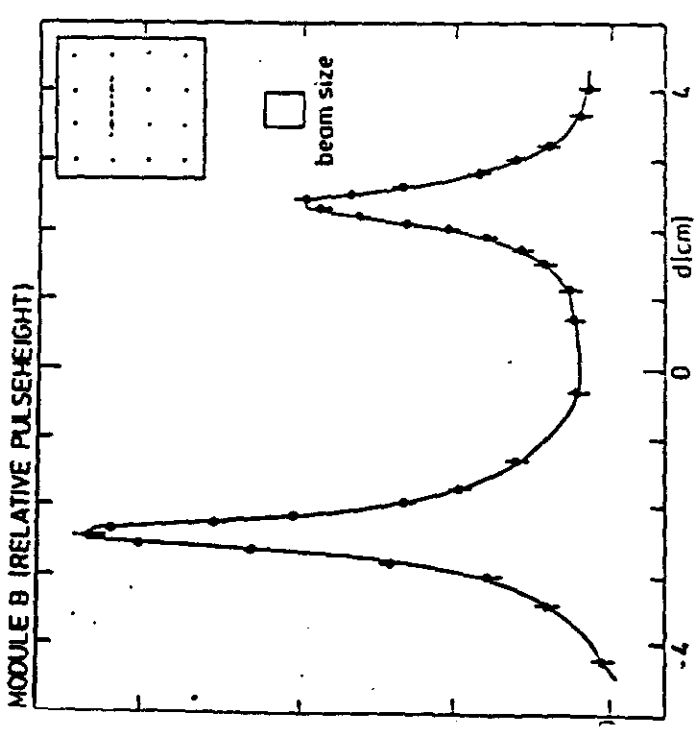

Fig. 5b

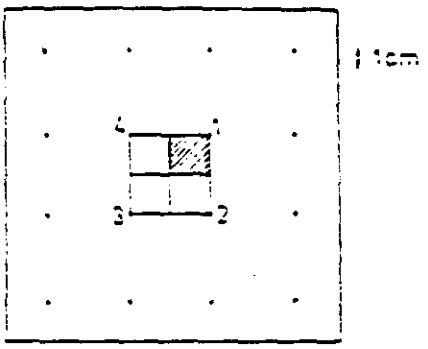

Fig. 8a

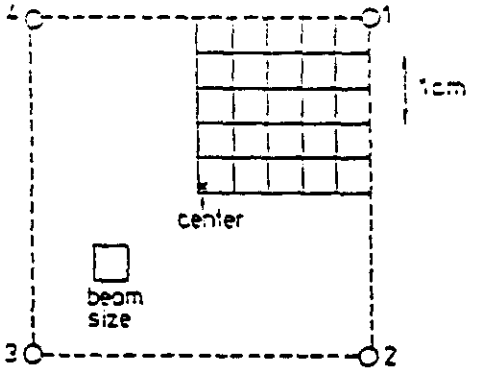

Fig. 8b

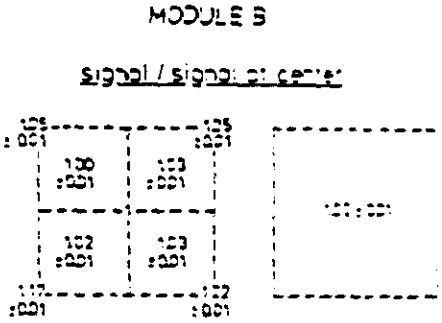

Fig. 8c

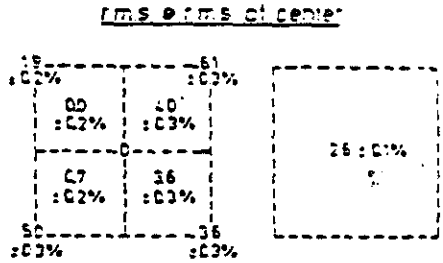

Fig. 8d

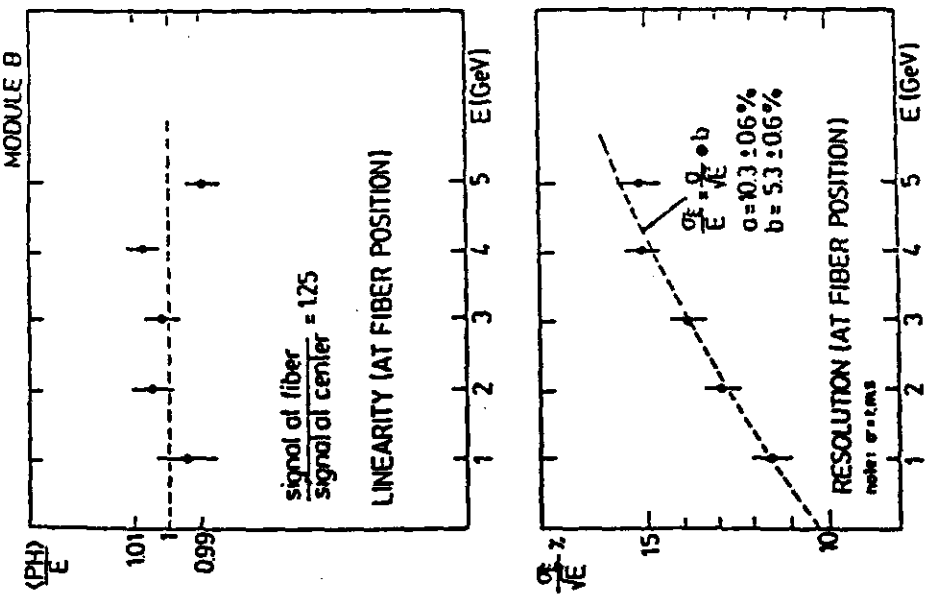

Fig. 7

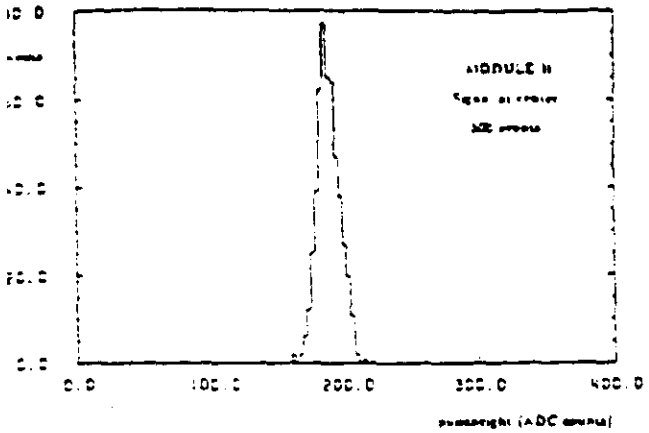

Fig. 9a

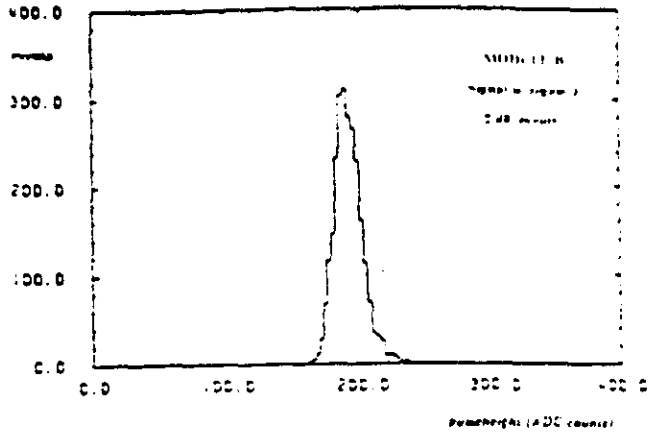

Fig. 9c

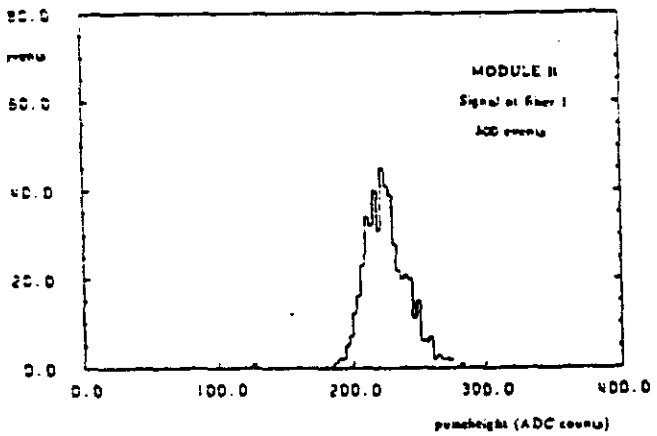

Fig. 9b

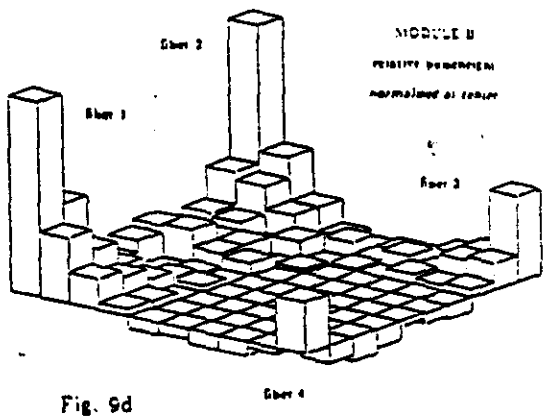

Fig. 9d

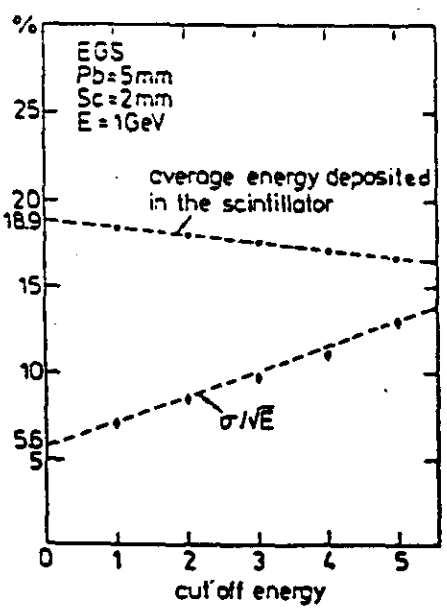

Fig.10a

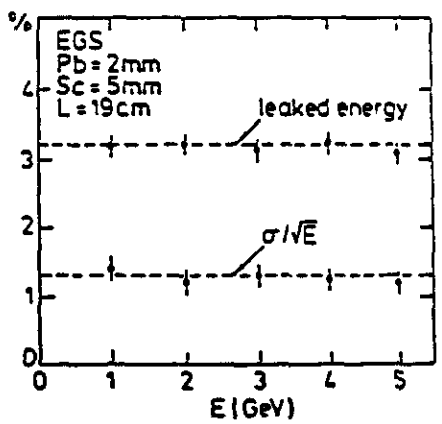

Fig.10b

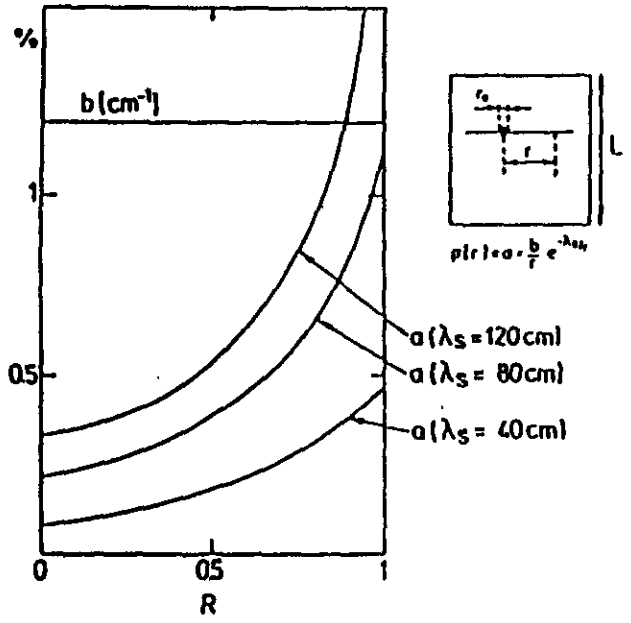

Fig.11

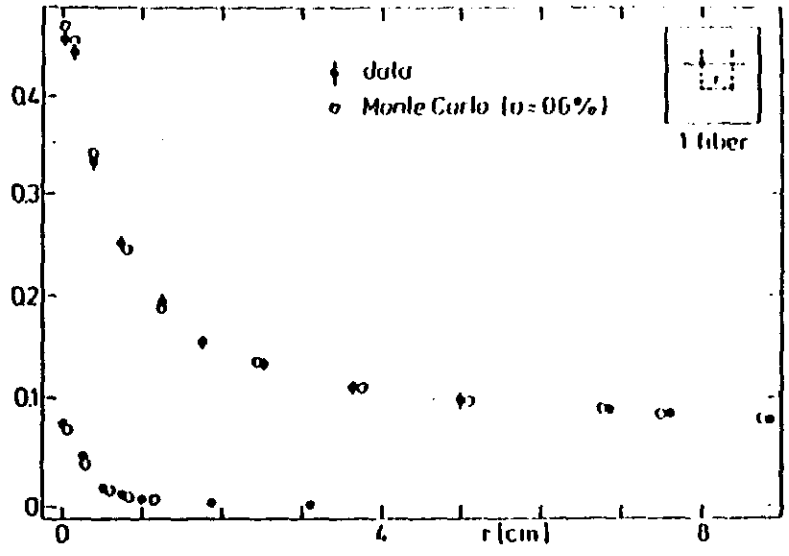

Fig.12a

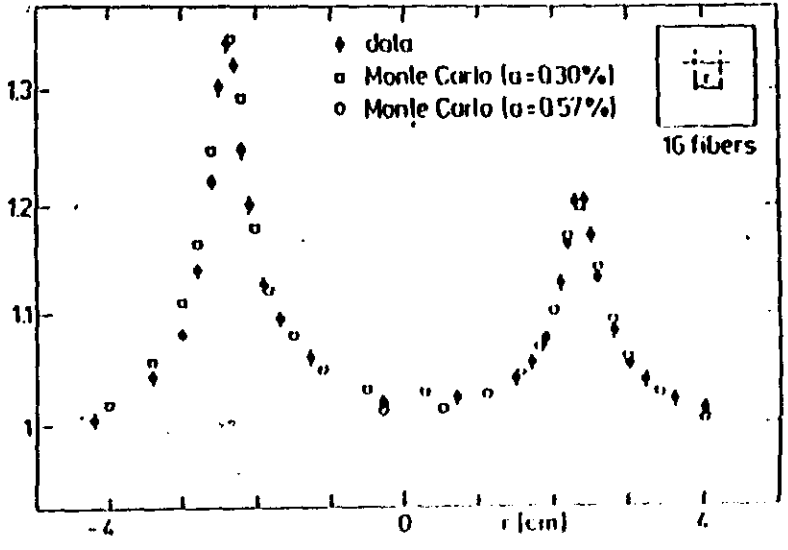

Fig 12b

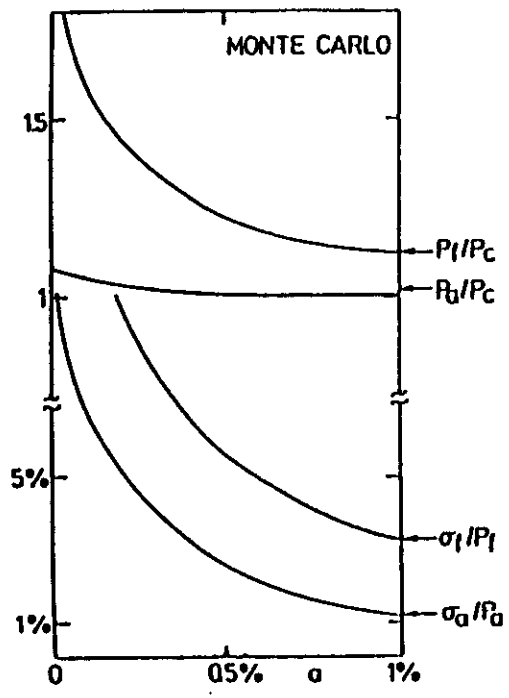

Fig.13

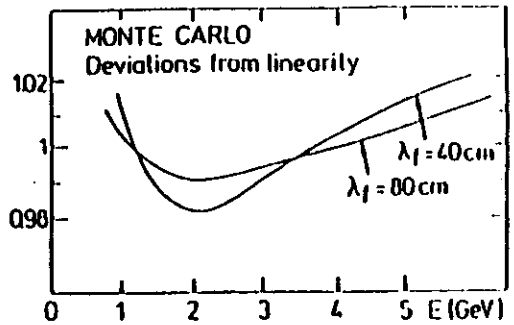

Fig.14a

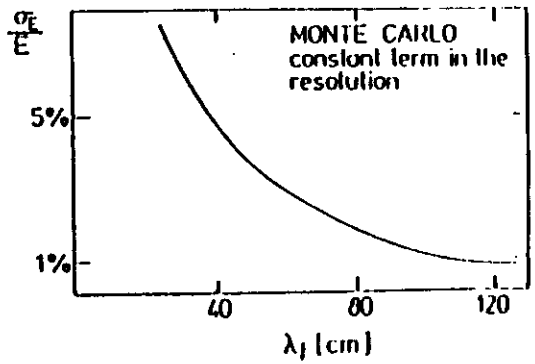

Fig.14b

MAX-PLANCK-INSTITUT FÜR PHYSIK UND ASTROPHYSIK
WERNER-HEISENBERG-INSTITUT FÜR PHYSIK

MPI-PAE/Exp.El. 149
February 1985

MAR 18 1985

A SCINTILLATOR-LEAD PHOTON CALORIMETER USING OPTICAL FIBER READOUT SYSTEMS

H. Fessler, P. Freund, J. Gebauer, K.M. Glas, K.P. Pretzl,
P. Seyboth and J. Seyerlein
Max-Planck-Institut für Physik und Astrophysik, München, Germany

J.C. Thevenin
Département de Physique des Particules, CEN-Saclay
B.P. 2, F-91190 Gif-sur-Yvette, France

ROUTE TO

NAME	LOCATION

RETURN TO

8000 MÜNCHEN 40 - FÖHRINGER RING 6

A SCINTILLATOR-LEAD PHOTON CALORIMETER USING OPTICAL FIBER READOUT SYSTEMS

H. Fessler, P. Freund, J. Gebauer, K.M. Glas, K.P. Pretzl,
P. Seyboth and J. Seyerlein
Max-Planck-Institut für Physik und Astrophysik, München, Germany

J.C. Thevenin
Département de Physique des Particules, CEN-Saclay
B.P. 2, F-91190 Gif-sur-Yvette, France

ABSTRACT

The construction and performance of a tower structured scintillator-lead photon calorimeter using a novel fiber optics readout system is described. An energy resolution of $\sigma/E = 0.10/\sqrt{E}$ was obtained with incident electrons in the range of 0.5 - 5.0 GeV/c. The uniformity of response across the front face of the tower was measured. Results obtained with a silicon photo-diode are compared to those obtained with a photomultiplier.

Submitted to Nuclear Instruments and Methods

1.) Introduction

Optical fibers doped with wavelength shifter (WS) material have been introduced to read out scintillator light from tower structured photon calorimeters [1]. It was shown in Ref.1 that optical fibers can effectively replace complicated and work-intensive light guide systems and still maintain good light collection and light transmission efficiencies. They offer the possibility to build calorimeters with high granularity, in which the cross sections of the individual towers are small and well matched to the shower size.

These small diameter fibers (1-2 mm) allow the transmission of the light from the calorimeter cell over several meters to the photomultipliers with low loss. This technique may find an interesting application for shower detectors which have to operate in a magnetic field.

In Ref.1 we described a scintillator-lead calorimeter using an optical fiber readout system based on the double WS principle. In this paper we report on new results which we obtained with a scintillator-lead photon calorimeter using an optical fiber readout based on the single WS principle.

We describe in section 2 the mechanical construction of the calorimeter and in section 3 the performance of the calorimeter in a test beam. In section 4 we compare the results which we obtained with a silicon photo-diode (Hamamatsu S1790) and a photomultiplier (PM) (Hamamatsu R647-1) respectively attached to the optical readout fibers.

2.) Mechanical construction

The configuration of the photon calorimeter tower is shown in Fig.1. The tower consists of 60 lead plates with the dimensions 54 x 54 x 2 mm^3 sandwiched with 60 scintillator plates (NE110) with the dimensions 54 x 54 x 5 mm^3. The total radiation length of the tower is 22 X_o.

The scintillator plates were glued (hot foil glue, Product of H. Rost and Co., Hamburg, Germany) to the lead plates, providing self-supporting strength to the tower.

The optical readout fibers (with a diameter of 2 mm) were made of polystyrene base material (Product of STIPE, Saclay, France) which was doped with K-27 (200 mg/l) WS material. The polystyrene core and the cladding material of the fiber had refractive indices of n_1=1.59 and n_2=1.46 respectively.

Thus the opening angle Θ of a light cone which is internally reflected through the fiber was $\Theta = \pm 23.3^{\circ}$. The light attenuation length of the fiber was measured to be 11 m for a K-27 doping of 100 mg/l [1]. The attenuation length of the fibers used in this experiment (200 mg/l K-27 doping) was measured to be only 2 m. It is not clear at this moment whether this is a result of the higher concentration of the K-27 material.

The fibers were inserted into 3 mm diameter holes which were drilled through the scintillator and lead converter material. The four fibers were optically coupled to one Hamamatsu R647-1 photomultiplier (with a diameter of 1.3 cm).The scintillator-lead tower together with the readout fibers was inserted into a box made of 0.5 mm thick reflecting aluminum sheet.

3.) Performance of the calorimeter

The calorimeter tower was exposed to incident electrons with energies of 0.5, 1, 2, 3 and 5 GeV. The electrons were selected by threshold Cerenkov counters. The incident beam was defined by beam and veto scintillation counters to a divergence of ±3.3 mrad and a spot size of 5 x 10 mm^2. In order to account for the lateral shower leakage the test calorimeter tower (T_{11} in Fig.1) was surrounded by 8 towers ($T_{1,2,3,4,5,6,7,8}$) of the type described in Ref.1. The towers were placed on a remotely controlled movable support structure. Thus the impact point of the incident electron beam on the calorimeter could be varied.

3.1.) Energy resolution

The energy resolution of the calorimeter was measured with the electron beam hitting the central tower T_{11} of the calorimeter. For each event the responses of the nine PM's of the nine towers were summed, taking the relative calibration factors into account. The obtained energy resolution σ/E as a function of $1/\sqrt{E}$, with E in GeV, is shown in Fig.2. A linear fit through the data points gives an energy resolution of

$$\frac{\sigma}{E} = 0.014 + \frac{0.10}{\sqrt{E/GeV}}$$

The energy resolution $(\sigma/E)_s$ due to sampling fluctuations was determined [2] to be

$$\left(\frac{\sigma}{E}\right)_s = 0.075/\sqrt{E/GeV}$$

The energy resolution $(\sigma/E)_{Ne}$ due to photoelectron statistics, with Ne the number of photoelectrons per GeV deposited energy, can be estimated from the observed energy resolution and the sampling fluctuation using the relation:

$$\left(\frac{\sigma}{E}\right) = \sqrt{\left(\frac{\sigma}{E}\right)_s^2 + \left(\frac{\sigma}{E}\right)_{Ne}^2}$$

One obtains

$$\left(\frac{\sigma}{E}\right)_{Ne} = \frac{0.066}{\sqrt{E/GeV}}$$

From $(\sigma/E)_{Ne} = \frac{1}{\sqrt{Ne \cdot E}}$, we calculate Ne = 229 photoelectrons/GeV. From the approximation $(\sigma/E)_s \simeq \frac{1}{\sqrt{Ns \cdot E}}$, with Ns the number of equivalent minimum ionizing particles crossing a calorimeter layer per GeV deposited energy, the photoelectron yield n_e = Ne/Ns per minimum ionizing particle per layer can be estimated to be 1.3.

As shown in Fig.3 the calorimeter response is linear from 0.5 GeV to 5 GeV.

3.2.) Uniformity of response

The uniformity of response of the calorimeter tower T_{11} was studied with 5 GeV electrons performing a horizontal scan through towers with the numbers T_4, T_{11} and T_3 (see Fig.1). For this uniformity scan the electron axis was parallel to the optical readout fibers.

In Fig.4 the results of a scan through the towers T_4, T_{11} and T_3 as indicated by the dashed line are shown. The black dots represent the peak pulse heights obtained from the sum of all nine PM's, while the crosses, the squares and the triangles indicate the peak pulse heights obtained from the PM's of the individual towers T_4, T_{11} and T_3 respectively.

As shown in Fig.5 a second horizontal scan was performed in which the electron beam was impinging near the optical readout fibers. The black dots and the crosses in this figure represent the peak pulse heights from the sum of all nine PM's and from the PM of the individual tower T_{11} respectively.

As the results show, the uniformity of response of the calorimeter tower T_{11} is ± 2% over a large region. Near the optical readout fibers the uniformity worsens to ± 10%. This is probably due to a geometrical effect. The non-uniformity can also be influenced by Cerenkov light in the fibers and by additional ultra-violet scintillator light (with wavelength shorter than

420 nm, the emission of NE 110) which can reach the readout fibers [3].

Measurements were also made with the calorimeter rotated about a vertical axis through its center by an angle Θ as shown in Fig. 6. The results show that the uniformity increases slowly with increasing Θ.

4.) Results with a silicon photo-diode

The use of silicon photo-diodes in connection with scintillator-lead shower detectors has already been studied [4, 5]. The main advantages of silicon photo-diodes as compared to photomultipliers are their stability, their insensitivity to a magnetic field, their small size and their relatively low price.

We tried to take advantage of the light collection by the small area fibers and replaced the PM at the end of the four fibers by a small area (10 x 10 mm^2) silicon photo-diode (Hamamatsu S1790). The configuration of the electronics in connection with the silicon photo-diode is shown in Fig.7. The signal of the photo-diode was fed into a charge-sensitive preamplifier and a shaping amplifier with a shaping time of 2 µsec. The preamplifier and the shaper were both developed at the Max-Planck-Institut für Physik in Munich. The noise of the amplifier (without load) was measured to be 500 photoelectrons and of the photo-diode 500 photoelectrons. The total noise of the arrangement was 1000 photoelectrons. The system was calibrated by injecting a well defined charge through the test capacitor into the signal line. The signal we obtained with 5 GeV incident electrons on tower T_{11} was Ne = 500 photoelectrons/GeV. Because of the noise level of 1000 photoelectrons a signal only above 2 GeV incident electron energy could be observed.

Compared to the PM signal of Ne = 229 photoelectrons/GeV the silicon photo-diode is about a factor 2 more efficient. This is explained by the expected higher quantum efficiency of the silicon photo-diode at 500 nm (emission peak of K-27) as compared to the PM.

The results show that for the layout and energy range studied in this paper the use of silicon photo-diodes is unfortunately limited by the large noise level and (or) the limited light output from the fiber optics readout system.

5.) Conclusions

The optical fiber readout technique allows to build calorimeters with fine granularity, minimal dead space between individual towers and a good energy resolution.

The uniformity of response was measured to be ± 2% over a large area of the calorimeter. Part of the non-uniformity near the optical fibers can possibly be reduced in the future by using adequate filter material. Perhaps some filter material in the fiber cladding already helps.

The use of silicon photo-diodes seems to be limited at present due to the high noise level and (or) the limited light output from the fiber optics readout system.

The light transmission in the fibers could be increased by a factor of ~ 2 if a cladding material with a low index of refraction (~1.36) could be found.

REFERENCES

1.) H. Fessler et al., NIM 228 (1985) 303.

2.) K.M. Glas, Untersuchung eines segmentierten, mit Fiberoptik ausgestatteten Photonkalorimeters, Diplomarbeit, TU München 1984.

3.) C. De Marzo et al., NIM 217 (1983) 405.

4.) J. Ahme et al., NIM 221 (1984) 543.

5.) G.G. Winter et al., DESY-Report 84-120, submitted to Nucl. Instr. and Meth.

FIGURE CAPTIONS

Fig. 1 Configuration of the scintillator-lead photon calorimeter. The readout system using optical fibers is shown in detail.

Fig. 2 The energy resolution σ/E for incident electrons with 0.5, 1, 2, 3 and 5 GeV is shown. The straight line represents a linear fit through the data points.

Fig. 3 The peak pulse height as a function of the electron energy.

Fig. 4 The peak pulse heights obtained from a horizontal scan (dashed line in insert) over towers T_4, T_{11} and T_3. The black dots represent the peak pulse heights obtained from the sum of all nine PM's. The crosses, the squares and the triangles indicate the peak pulse heights obtained from the PM's of the individual towers T_4, T_{11} and T_3 respectively.

Fig. 5 The peak pulse heights obtained from a horizontal scan (dashed line in insert) over the towers T_4, T_{11} and T_3 crossing the optical readout fibers. The black dots and the crosses represent the peak pulse heights obtained from the sum of all nine PM's and from the PM of the individual tower T_{11} respectively.

Fig. 6 The non-uniformity as a function of the tilt angle Θ about a vertical axis.

Fig. 7 The electronic configuration of the silicon photo-diode readout.

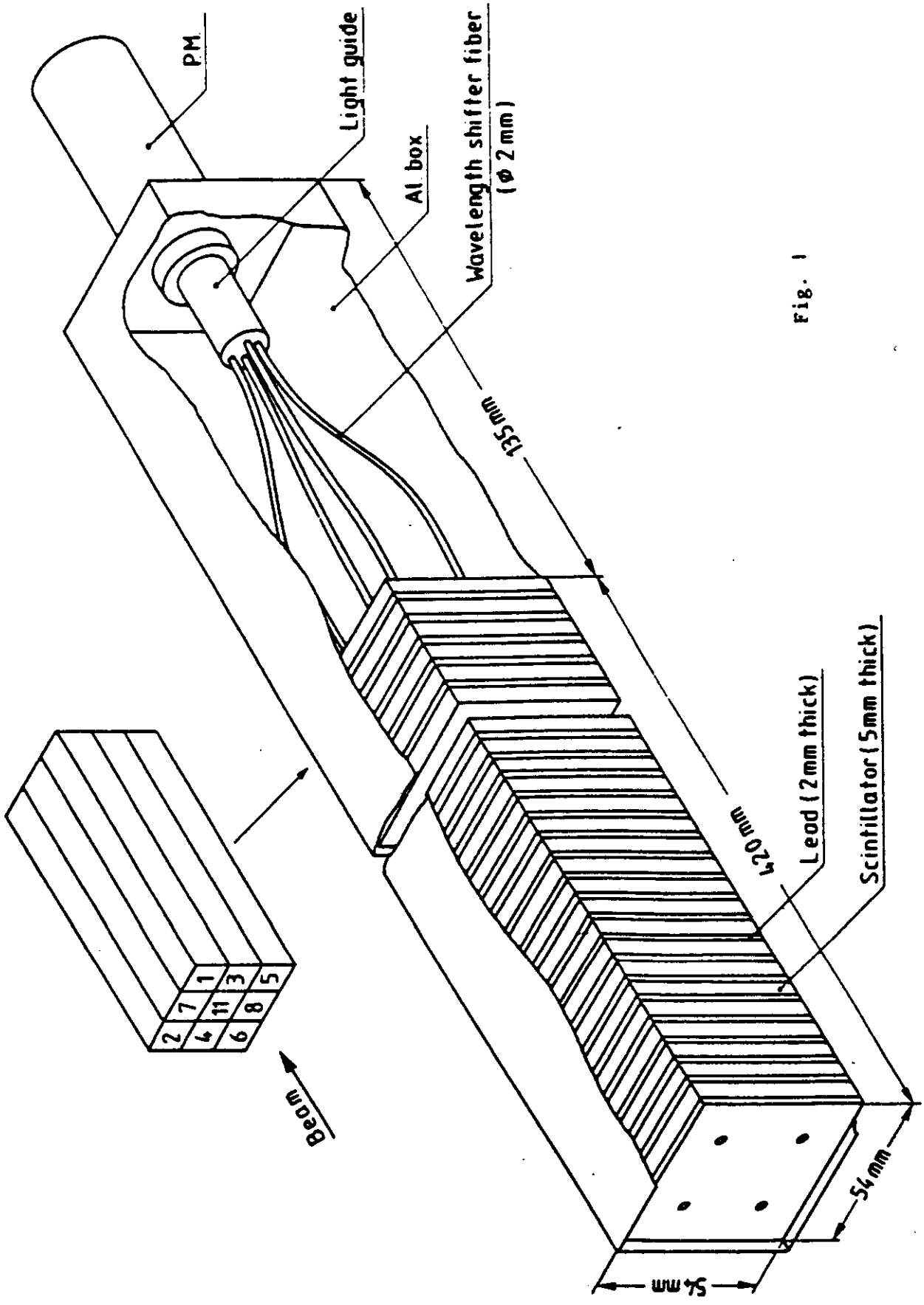
PM
Light guide
Al box
Wavelength shifter fiber
(φ 2mm)
135mm
120mm
Lead (2mm thick)
Scintillator (5mm thick)
54mm
54mm
beam
2
7
1
4
11
3
6
8
5

Fig. 1

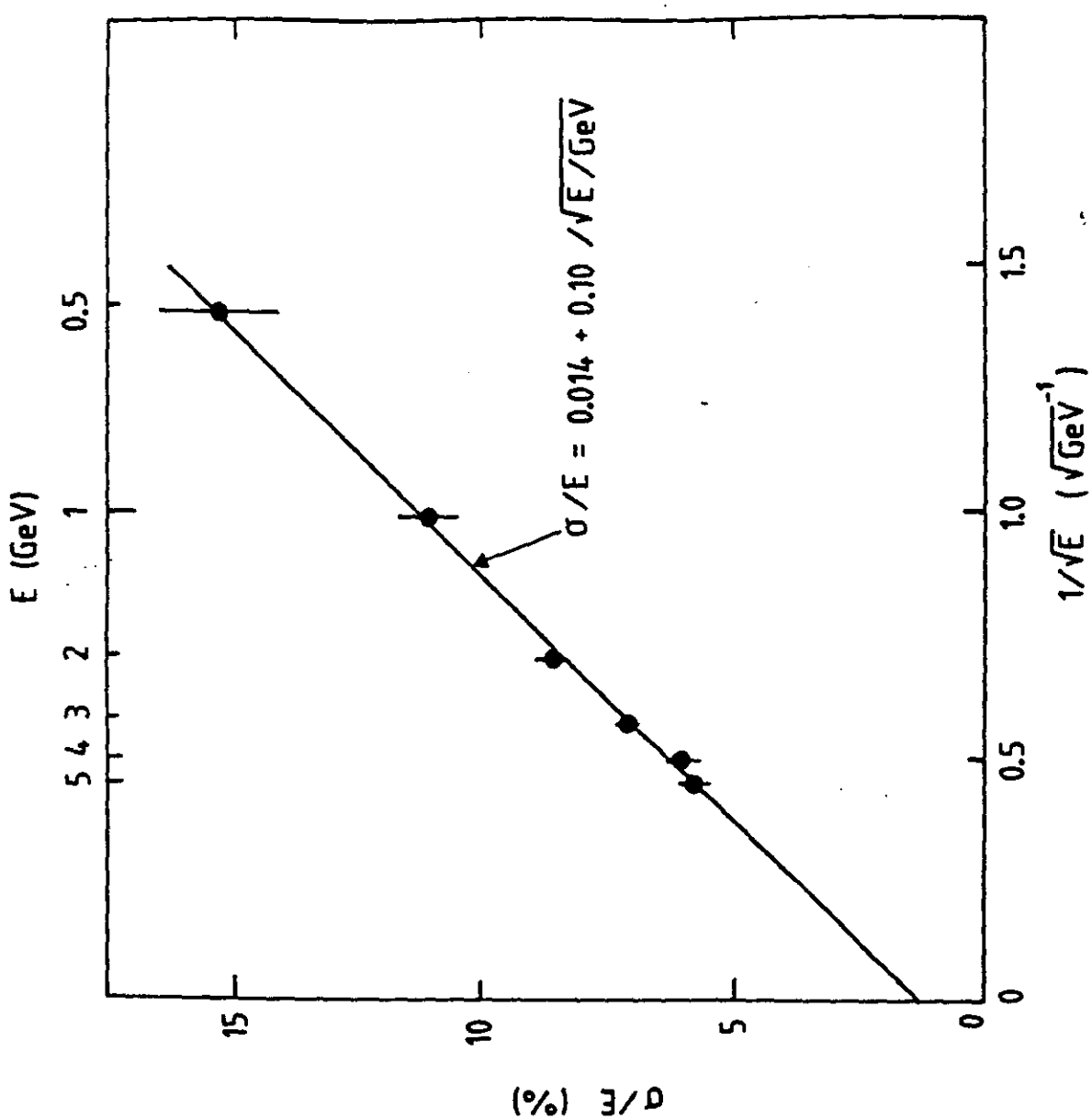

Fig. 2

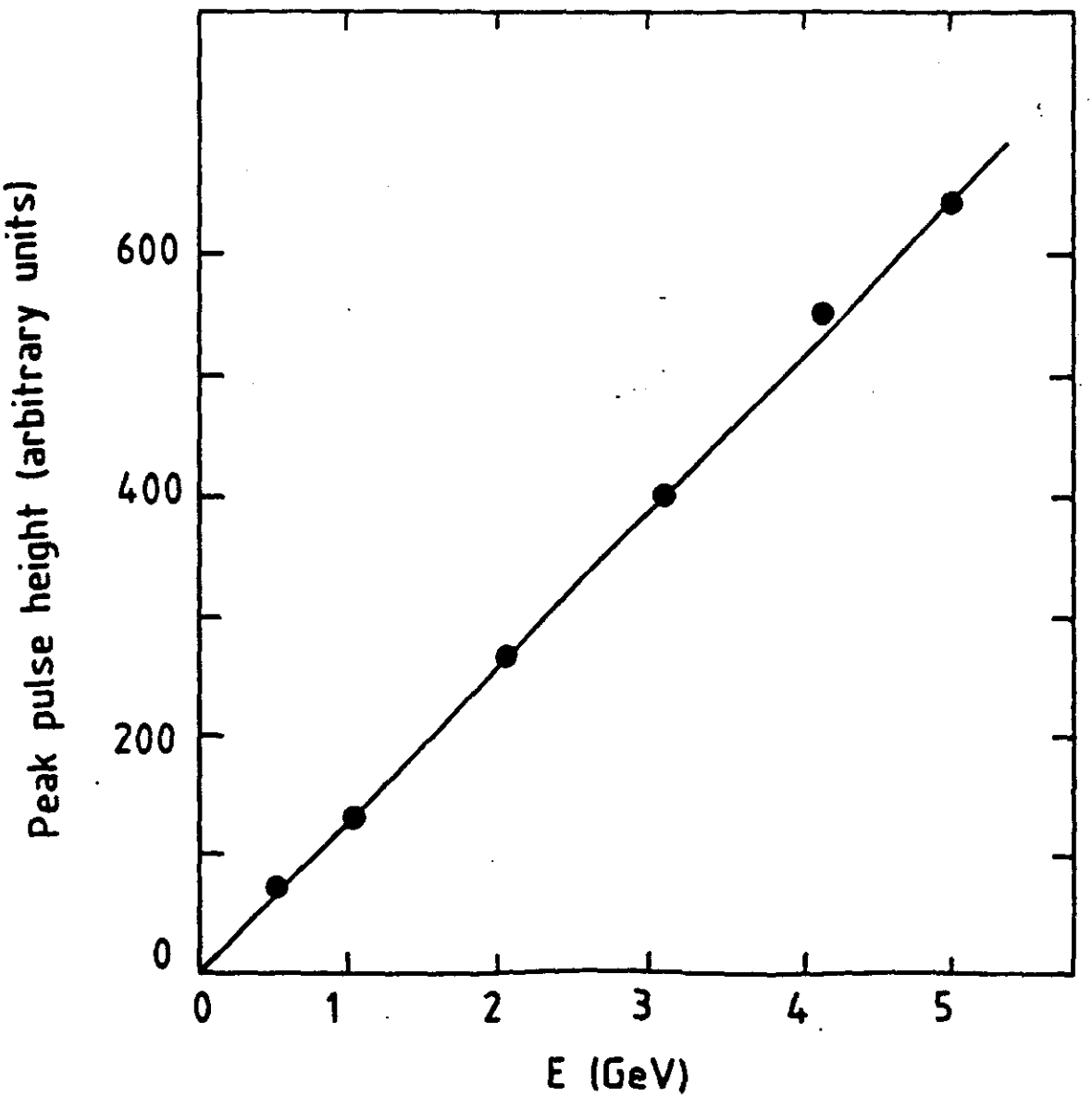

Fig. 3

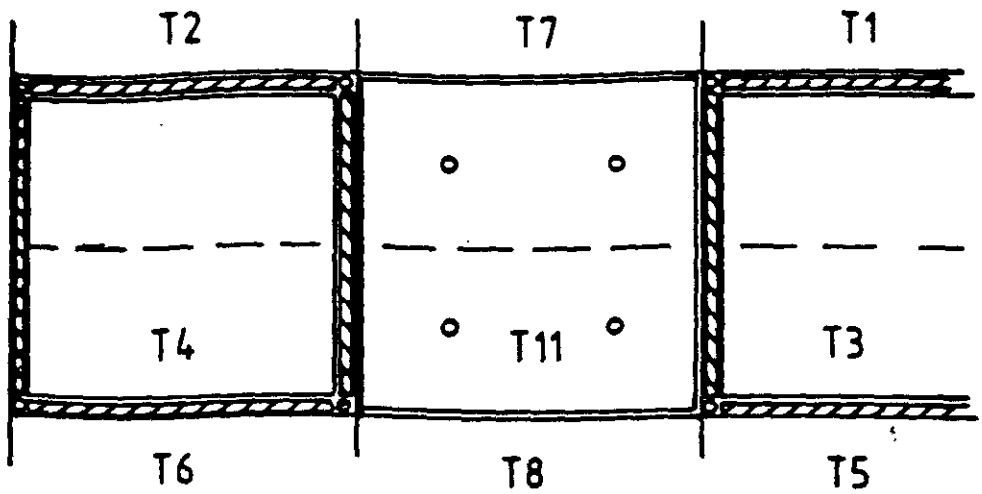
T2
T7
T1
T4
T11
T3
T6
T8
T5

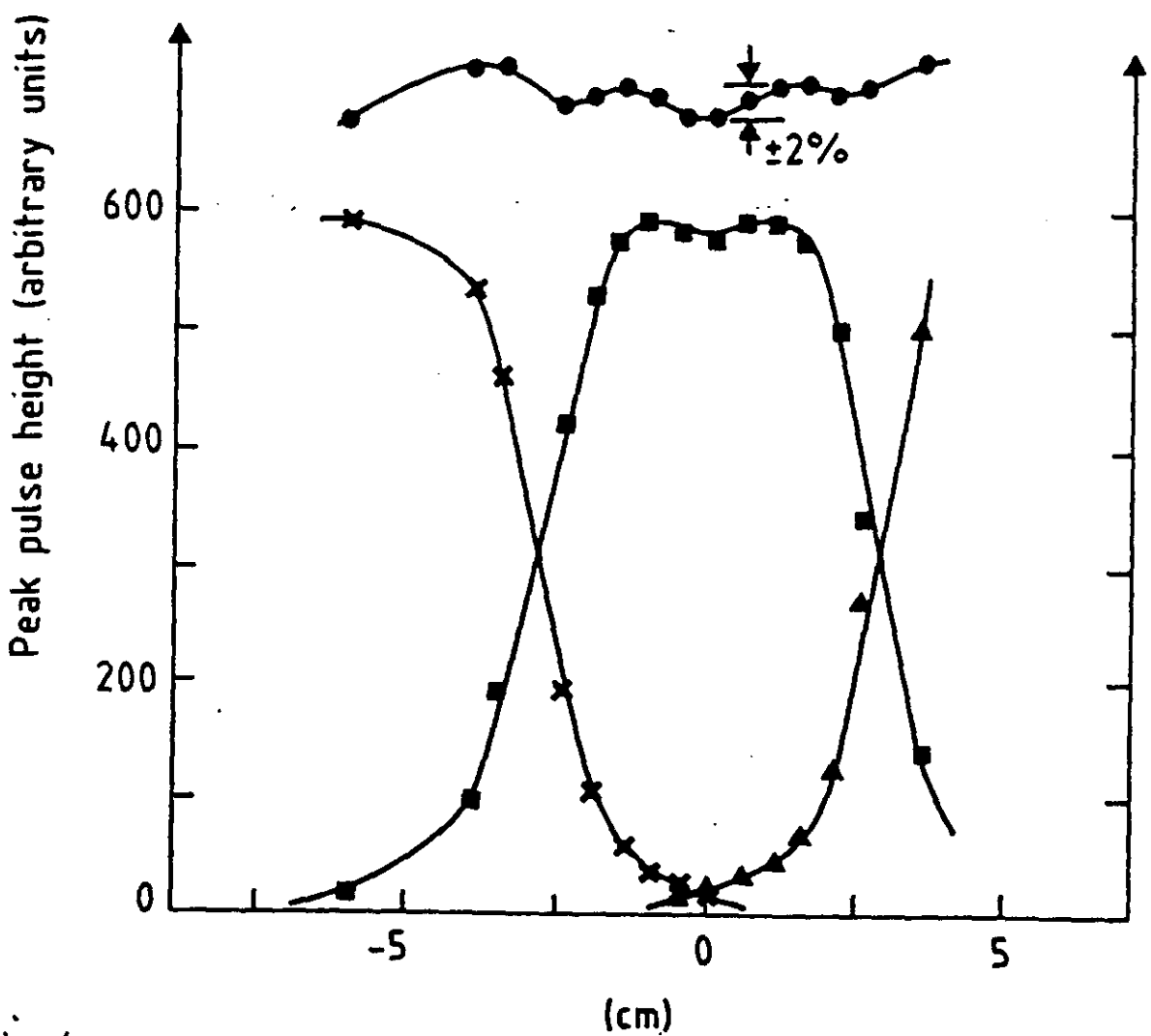
Peak pulse height (arbitrary units)
±2%
600
400
200
0
-5
0
5
(cm)

Fig. 4

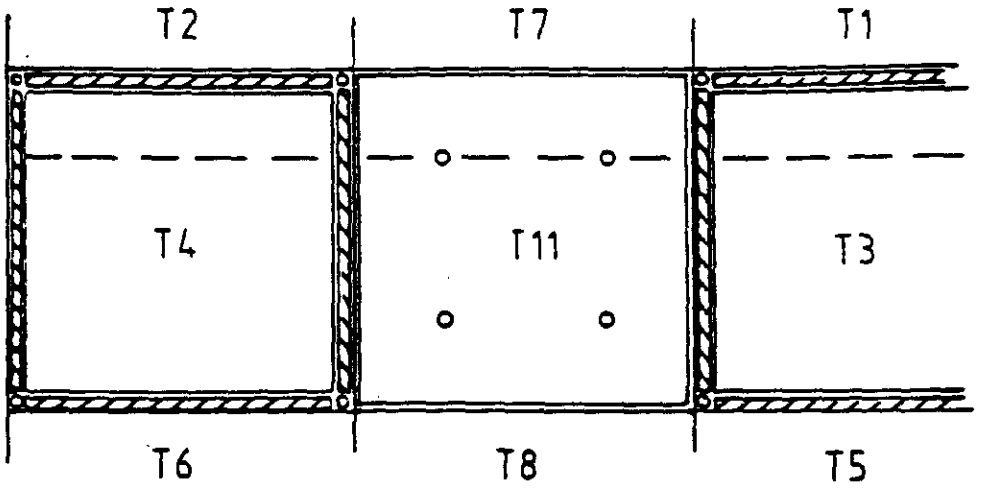
T2
T7
T1
T4
T11
T3
T6
T8
T5

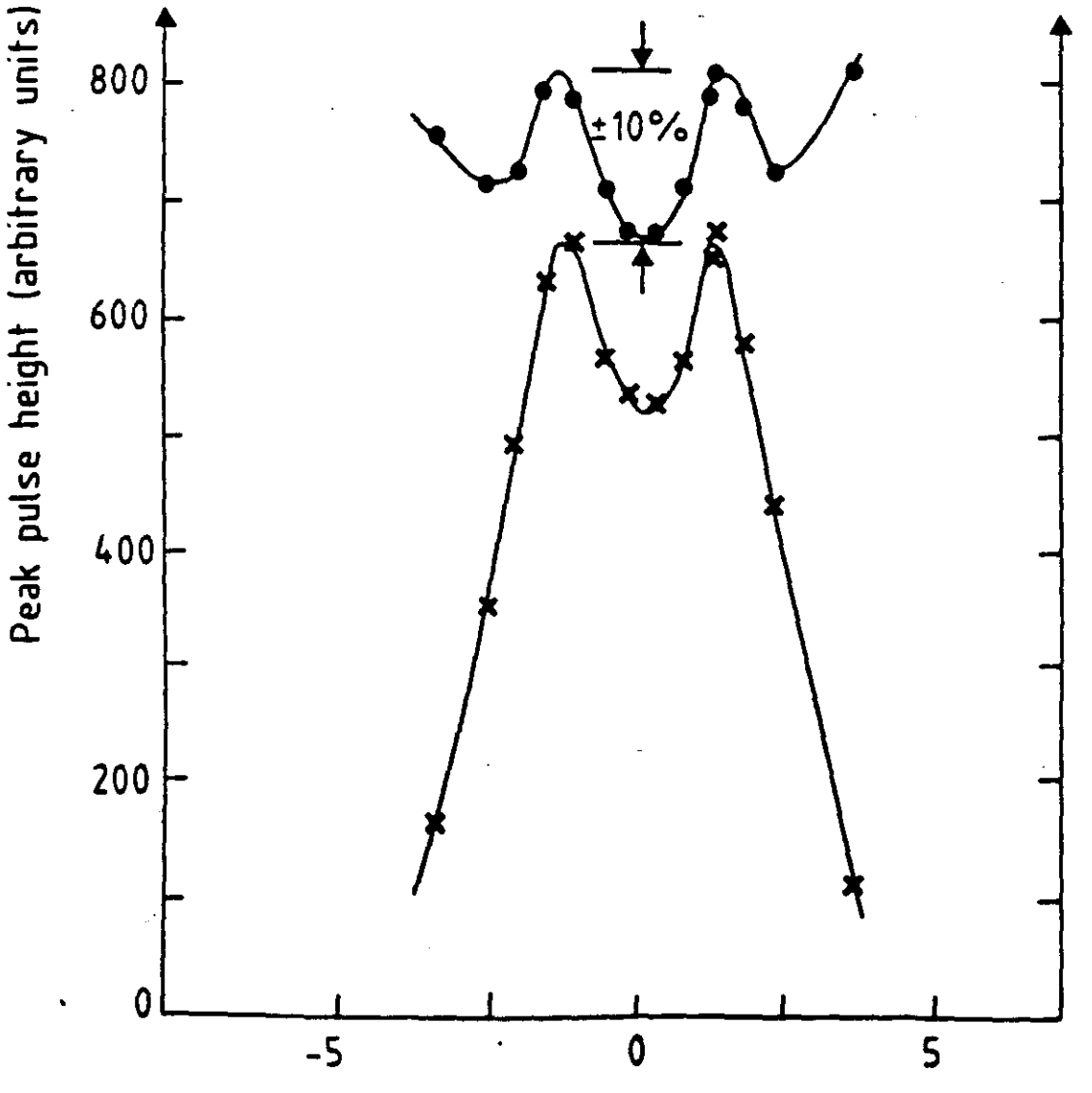
Peak pulse height (arbitrary units)
800
600
400
200
0
±10%
-5
0
5

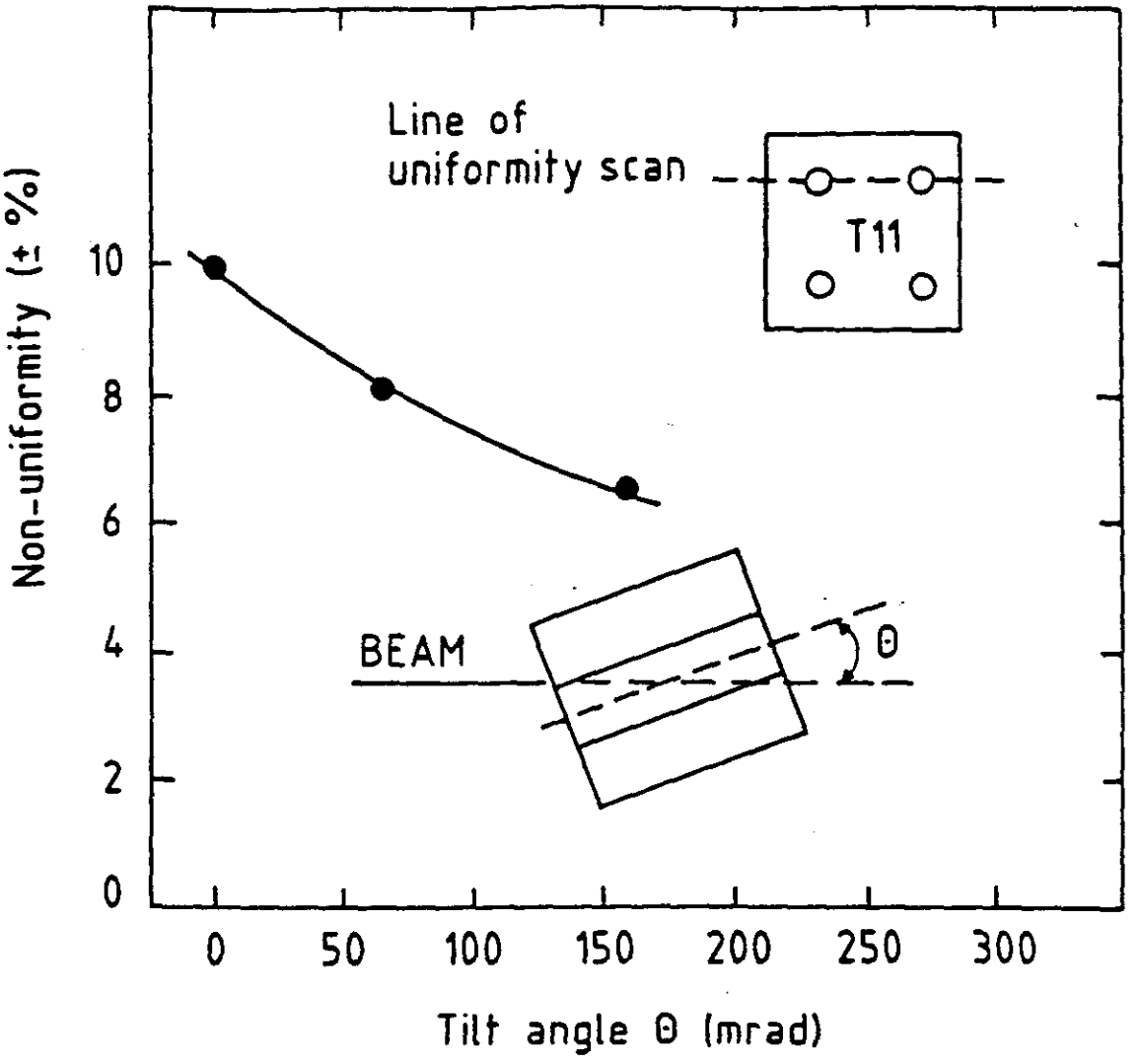
Line of
uniformity scan
T11
BEAM
θ
Non-uniformity (± %)
10
8
6
4
2
0
0
50
100
150
200
250
300
Tilt angle θ (mrad)

Fig. 6

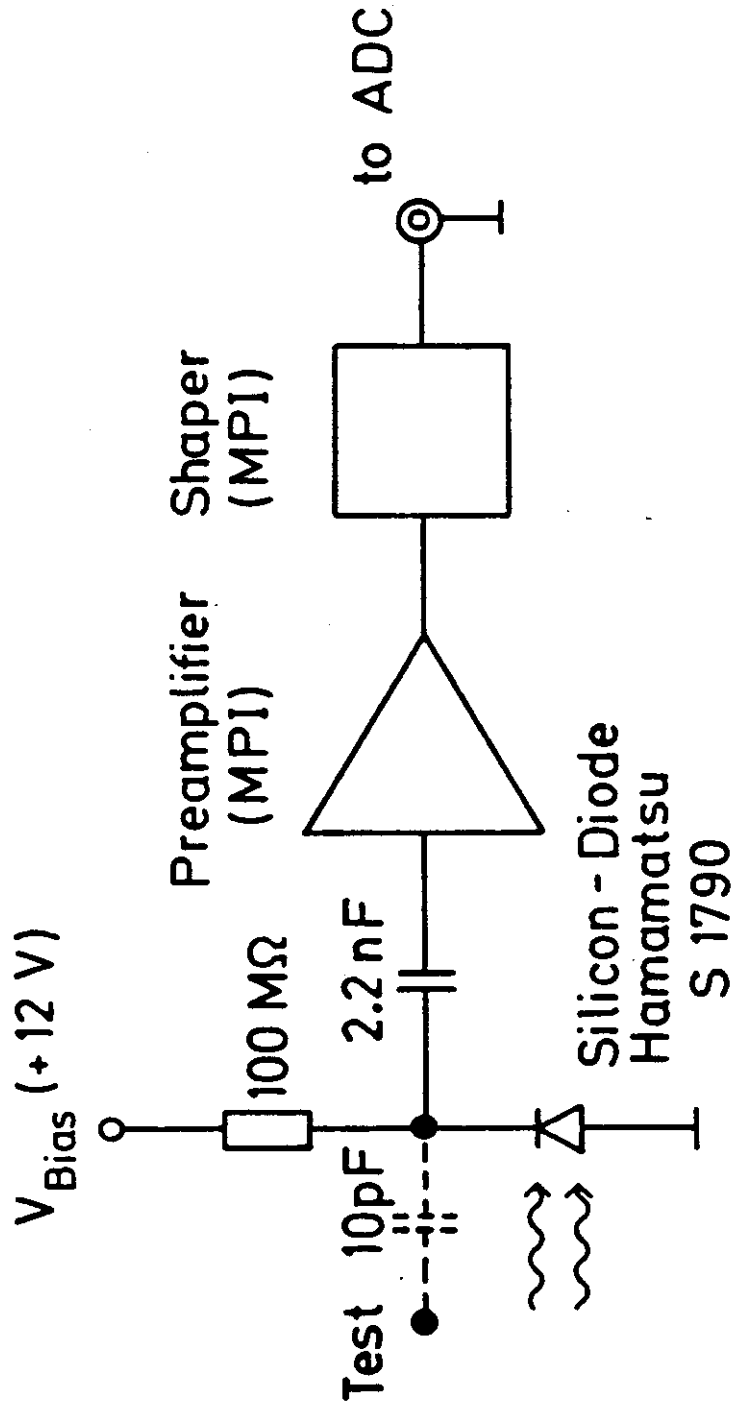
to ADC
Shaper (MPI)
Preamplifier (MPI)
V_{Bias} (+12 V)
100 MΩ
2.2 nF
Silicon - Diode Hamamatsu S 1790
Test 10pF

Fig. 7